GEORG-AUGUST-UNIVERSITÄT
GÖTTINGEN

GGNB

Receptive Field Characterization in MSTd Neurons

Dissertation for the award of the degree
Doctor rerum naturalium

submitted by

Amr Maamoun
from Damascus

Faculty of Biology
Georg-August-Universität Göttingen
Doctoral program *Neurosciences (MSc/PhD), IMPRS*
of the Georg-August University School of Science (GAUSS)

Göttingen, 2018

Thesis committee

Prof. Dr. Stefan Treue (Supervisor)
Cognitive Neuroscience Laboratory, German Primate Center, Göttingen

Prof. Dr. Melanie Wilke
Institute for Cognitive Neurology, University Medical Center, Göttingen

Prof. Dr. Tim Gollisch
Department of Ophthalmology, University Medical Center, Göttingen

Examination board

Referee: Prof. Dr. Stefan Treue (Supervisor)
Cognitive Neuroscience Laboratory, German Primate Center, Göttingen

Co-referee: Prof. Dr. Melanie Wilke
Institute for Cognitive Neurology, University Medical Center, Göttingen

Further members of the examination board:

Prof. Dr. Tim Gollisch
Department of Ophthalmology, University Medical Center, Göttingen

Prof. Dr. med. Hansjörg Scherberger
Neurobiology Laboratory, German Primate Center, Göttingen

Prof. Dr. Ralf Heinrich
Department of Cellular Neurobiology, Schwann-Schleiden Research Centre, Göttingen

Arezoo Pooresmaeili (MD, PhD)
Perception and Cognition Group, European Neuroscience Institute, Göttingen

Date of thesis defense: 09 January 2018

Declaration

I hereby declare that the content of this dissertation is original and results in its entirety from my own work, except as mentioned in the Acknowledgements.

Amr Maamoun
Göttingen, 2018

in the name of the nameless singular . . .

Acknowledgements

I would like to acknowledge the significant and extensive contributions of my supervisor Stefan Treue to this work, consisting of extensive feedback to the initial design phase of the project, troubleshooting design condsiderations, continuous feedback and comments regarding different stages of analysis, and feedback regarding this written work.

I also would like to acknowledge the support from the Ph.D. program "Neurosciences" – International Max Planck Research School at the Georg August University Göttingen. Specifically, I am grateful to Sandra Drube and the late Michael Hörner for their continuous support over the years of my stay in Germany. Michael took genuine interest in his students, and provided valuable feedback whenever approached. May he rest in peace.

Benedict Wild contributed to this project by collecting up to 68/181 (37.6%) of the non-pilot cells used in this thesis, and creating the illustration of the reverse correlation stimulus (p. 30). I thank Cliodhna Quigley for attending the early thesis committee meetings and providing valuable input and feedback.

I am grateful to Ralf Brockhausen for being there in the early stages of debugging and installing the stimulus that was used in this dissertation, for providing support in various technical challenges that were magically resolved in his presence, and for keeping an upbeat and joyful working atmosphere. I am glad to have had the pleasure to have him as a colleague.

Pablo Martinez and Suresh Krishna were always there to provide expertise when I was confronted with challenging conceptual problems, and of course to extend moral support.

This project would not have been possible without the excellent technical assistance of primarily Leonore Burchardt; in addition to Sina Plümer, Janine Henrici (aka *Astrid*), Janine Kunze, Klaus Heisig, and Beatrix Glaser. For a short period of time Antonio Calapai and Dana Pfefferle provided valuable help with monkey handling. Finally, Lydia Gibson and Michael Berger were helpful in setting up the Latex template for this thesis.

To my loved ones I owe more than can be conveyed in mere words. . . I am eternally grateful for your blissful presence in my life.

Abstract

The dorsal region of the medial superior temporal area (MSTd) in primate extrastriate visual cortex is reported to play a major role in the encoding and perception of optic flow stimuli, i.e. large-scale motion patterns on the retina created by the movement of the visual environment relative to the organism. Correspondingly, MSTd neurons show tuned responses to the direction of linear motion stimuli, as well as to the direction of *spiral space* motion stimuli (Graziano et al., 1994), i.e. complex motion patterns that include expansion, contraction, rotation, and their mixtures, arranged in a continuous circular dimension. In addition, MSTd cells have been reported to be position-invariant in their responses to spiral motion stimuli. Here we describe a study aimed at investigating the motion patterns MSTd neurons are most responsive to, unconstrained by the two limited sets of motion type dimensions mentioned above. We used reverse correlation, a linear method that has been successfully used to characterize receptive fields in V1 and MT. Our reverse correlation stimuli were large complex random dot patterns, formed by the smooth variation of local dot direction and speed between a virtual grid of positions in the stimulus where the local parameters were chosen randomly every 100ms from all possible linear directions and a large range of speeds. We investigated whether the reverse correlation method can be successfully used in MSTd to recover structured maps of receptive fields, and whether the motion patterns resulting from such analysis provide an appropriate description of the specific motion preferences of individual MSTd neurons, compared to the simple assumption of linear and/or spiral direction tuning. We also determined the position dependency of MSTd responses to spiral motion patterns. We recorded from 181 single MSTd cells in three rhesus monkeys, trained to foveate a fixation point. For around 25% of the 150 cells that underwent the reverse correlation task, analysis recovered in varying degrees significantly structured receptive field maps. The recovered maps show a dominance of preference to linear motion to varying degrees across cells, yet the neural responses to spiral and linear motion patterns was significantly correlated with their motion similarity to the reverse correlation maps in 54% to 68% of those cells. Almost all of the cells showed position invariant responses to spiral motion patterns. Our results

indicate that reverse correlation can be applied successfully in area MSTd, although the resulting maps might be better able to explain linear motion preferences of the cell rather than more complex motion patterns. Our findings of position invariance are in line with previous evidence from literature (Graziano et al., 1994), and suggest that more studies are needed to clarify how MSTd neurons can be position invariant to optic flow stimuli and still be able to individually encode heading direction (Duffy & Wurtz, 1995; Orban, 2008).[1]

[1]This abstract was submitted in part as a poster abstract to the Society of Neuroscience (SfN) conference, 2017.

Table of contents

Chapter 1

Introduction

1.1 Optic Flow

Suppose you sit in a dimly lit room watching footage of an athlete performing a jump from the top of a mountain relying for their safety on a jumpsuit. The athlete is equipped with a head-attached camera allowing the viewers to be subjected to almost the same visual stimulation that the athlete experiences. The fast succession of visual cues from the video delivers to the viewer a perception of visually expanding environment around the center of the main heading direction, a visual perception we associate with a terrifying fall from a height.
Such a perception of the environment during self-motion is an example of *optic flow* perception. Optic flow refers to the complex patterns of visual motion that are projected onto the retina during motion through the environment. The visual motion processing system in the brain responsible for encoding such patterns of complex visual motion spans several levels of processing stages starting with the simple receptive rod cells in the retina, and extending to several striate and extra-striate cortical areas. In this chapter, we will describe these processing centers and review the related literature, with a focus on neural electrophysiological experiments conducted in rhesus macaque (*Macaca mulatta*), the animal model mostly used in the last few decades to study the primate striate and extra-striate cortex.

1.2 Visual Information Processing Hierarchy

Starting in the retina, ganglion cells process neural signals from a number of rod cells and send their visual motion information to the magno-cellular layers of the lateral geniculate nucleus (LGN) of the thalamus, with subsequent projections leading up to

layer 4Cα of primary visual cortex (V1), and then in turn into layer 4β; for review see (Albright, 1993). The stream of visual information appears to diverge in V1 into two distinct pathways: the ventral 'color and shape' pathway, which originates from V1 and leads to cortical areas involved in color and shape processing along the ventral side of the brain such as V2, V4, and infero-temporal (IT) area; and the dorsal 'where' pathway, which originates in V1, passes through V2 and leads to other cortical areas along the dorsal side of the brain, such as medial temporal (MT) area, medial superior temporal (MST) and ventral intra-parietal (VIP) area. This pathway has been reported to be involved in visual motion processing (Maunsell & van Essen, 1983; Maunsell & Newsome, 1987; Mishkin et al., 1983).

1.2.1 Medial Temporal (MT) Area

According to physiological evidence, motion-sensitive cells in V1 (Hubel & Wiesel, 1968) project their fibers along the dorsal stream into several areas such as V2, an area that also contains strongly motion-tuned cells (Orban & Callens, 1977) and then eventually to MT (Maunsell & van Essen, 1983; Van Essen et al., 1981).
MT lies on the posterior walls of the superior temporal sulcus, where a retinotopic representation of the visual field – similar to V1 – is maintained (Gattass & Gross, 1981), and where receptive fields assume a larger size in comparison to V1 (Maunsell & Van Essen, 1983). Sizes of MT receptive fields increase positively in proportion to visual eccentricity (Britten & Heuer, 1999; Desimone & Ungerleider, 1986; Richert et al., 2013; Tanaka et al., 1986; Zeki, 1974), reflecting the same tendency as in V1 (Van Essen & Newsome, 1984). Most neurons are strongly tuned to the direction of simple linear motion and to its speed (Maunsell & Van Essen, 1983; Treue & Andersen, 1996). It is interesting to note however, that this simplistic classical view of MT being maximally tuned to only one linear motion direction has been recently challenged, Richert et al. (2013) found that 38% of cells showed different motion direction preferences in different spatial locations inside the receptive field.

1.2.2 Medial Superior Temporal (MST) Area

Besides the reciprocal connections of MT to several areas such as V1, V2, V3, and V4; MT projects to MST (Desimone & Ungerleider, 1986; Ungerleider & Desimone, 1986) and VIP as well (Maunsell & van Essen, 1983). MST lies on the superior and anterior banks of the superior temporal sulcus. However, we differentiate between MST and a more deep and ventrally lying area, FST (Ungerleider & Desimone, 1986).

FST is an area sensitive to visual motion and appears to be involved in visual analysis of actions (Nelissen, 2006).
A distinction has also been made between the dorsal part of MST (MSTd) and the ventral part (MSTv). A clear image has emerged that MSTv is responsive to small linear motion stimuli (Saito et al., 1986), with an involvement in visual trajectory analysis and eye pursuit (Ilg, 2008; Komatsu & Wurtz, 1988; Orban, 2008). MSTd on the other hand contains a cluster of neurons with large receptive fields that are selectively responsive to simple linear motion (similar to MT), and even more complex motion patterns such as radial and rotation motion, implying a role of MSTd in optic flow analysis (Duffy & Wurtz, 1995; Orban, 2008; Saito et al., 1986). The structure of the receptive fields of MSTd, and their various properties will be the focus of the present study.

1.3 Characteristics of MSTd Receptive Fields

Inspection of cortical connectivity reveals that MT lies on a lower level in the visual processing hierarchy in relation to MST and VIP (Maunsell & van Essen, 1983). As such, some of the characteristics of MT receptive fields are maintained in MSTd neurons, while others are not. Whereas MT contains a well-defined retinotopy, MSTd retains only a crude retinotopic representation of the visual field, with posterior parts favoring the central visual field, and anterior parts preferring the periphery (Desimone & Ungerleider, 1986). This notion of a retinotopy in MSTd is not supported by other studies (Saito et al., 1986), yet some degree of spatial clustering in the selectivity to visual stimuli is clearly present (Chen et al., 2008). Sizes of MSTd receptive fields can be large and they can cover a significant portion of the visual field (Desimone & Ungerleider, 1986), with an average of 41° (visual degrees - square root surface) (Tanaka et al., 1986). While on the periphery MT and MSTd receptive field sizes are similar, MSTd receptive field sizes do not have a clear relationship to eccentricity according to many articles (Raiguel et al., 1997; Saito et al., 1986; Tanaka et al., 1986; Tanaka & Saito, 1989). However one early article (Desimone & Ungerleider, 1986) found a clear correlation between size and eccentricity in a manner similar to MT, with MSTd receptive fields being larger than those of MT at any given eccentricity.
It was the seminal work of Saito et al. (1986) that made clear that MSTd neurons respond to even more complex motion patterns than MT, patterns such as radial (expansion and contraction) and rotation (clockwise and counter-clockwise) motion, and that some even do not selectively respond to simple linear motion stimuli (Lagae

et al., 1994; Saito et al., 1986; Tanaka et al., 1986). All that was suggestive of the potential role of MSTd in encoding optic flow (Saito et al., 1986). Additionally, it was clear that an individual MSTd neuron could be selective to more than one optic flow component (linear, expansion/contraction or rotation motion) (Graziano et al., 1994; Lagae et al., 1994; Tanaka & Saito, 1989), which was replicated using small and large visual stimuli (Duffy & Wurtz, 1991a,b). It is interesting to note that while responses to smaller stimuli maintained the neuron's selectivity to a given optic flow pattern that is present when using larger stimuli, responses to smaller stimuli were weaker in magnitude (Duffy & Wurtz, 1991b).
In order to stimulate MSTd neurons, the aforementioned studies used moving dot patterns stimuli. Several studies showed that the selectivity of MSTd neurons to radial, rotation or linear motion did not depend on the specific motion carrier, and that different motion patterns could be used to elicit the same responses from neurons, such as dots, squares (Geesaman & Andersen, 1996); stripe patterns, concentric rings for radial motion and windmills for rotation motion (Tanaka & Saito, 1989).

1.4 Experimental Methodology

It is relevant to note that in the early 90s, there was a shift in the methodology used to study the behavior of MSTd neurons in macaque monkeys. First, while many early studies used anaesthetized monkeys (Lagae et al., 1994; Maunsell & Van Essen, 1983; Saito et al., 1986; Tanaka et al., 1989), in a manner similar to early electrophysiology experiments done in cats in V1 (Hubel & Wiesel, 1968, 1959), many labs began to conduct experiments in awake behaving monkeys trained to sit in a monkey chair and to behaviorally participate in experiments (Andersen et al., 1990; Duffy & Wurtz, 1991a,b; Graziano et al., 1994).
Another development consisted in the technological advancement in methodology: Early experiments relied on using hand-manipulated stimuli with the aid of a slide-projector, similar to early experiments in V1 (Hubel & Wiesel, 1968, 1959; Saito et al., 1986; Tanaka et al., 1989), while other studies incorporated computerized controlled stimuli on a limited scale (Maunsell & Van Essen, 1983). However as experiments moved into the 90s, stimuli were displayed and fully controlled by computers (Andersen et al., 1990; Duffy & Wurtz, 1991a; Lagae et al., 1994).

1.5 Spiral Space Tuning

Graziano et al. (1994) suggested that the tuning of MSTd cells to multiple components of motion such as linear, radial and rotation motion (Duffy & Wurtz, 1991a,b) could result from MSTd neurons being tuned to intermediate forms of motion. They introduced the *spiral space* motion stimuli (Graziano et al., 1994), which combine radial motion (expansion and contraction), rotation (clockwise and counter-clockwise) and their intermediate forms (expansive clockwise spiral, contractive clockwise spiral, contractive counter-clockwise spiral, expansive counter-clockwise spiral) into a continuous one-dimensional circular space. Such a space is similar to a linear motion circular space, which contains the cardinal motion directions (upward, rightward, downward, and leftward) and their intermediate motion directions.

Up to 86% of MSTd neurons showed selective tuning to the spiral space stimuli (Graziano et al., 1994) (Fig. 1.1). The preferred motion direction of most cells showed a distinct bias towards the expansion direction, with smaller number of cells selectively preferring other motion directions. Curiously, many cells had spiral patterns (specifically expansive spirals) as their preferred motion directions. The bias towards expansion can be seen in other studies (Saito et al., 1986), as well as the bias towards radial motion in general (Duffy & Wurtz, 1991a).

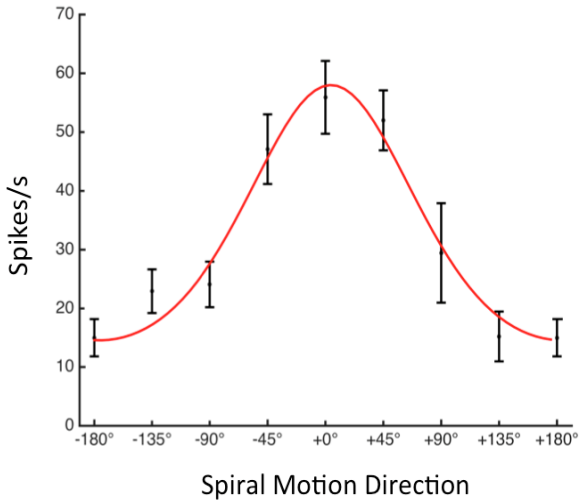

Fig. 1.1 Example of spiral space tuning in an MSTd neuron. The response of the neuron (spikes/s) is plotted against the different directions of the spiral space (0° corresponds to expansion, 45° to expansive clockwise spiral, 90° to clockwise spiral, 135° to contractive clockwise spiral, +180°/-180 to contraction, -135° to contractive counter-clockwise spiral, -90° to counter-clockwise rotation, -45° to expansive counter-clockwise spiral). Fitted to the data (red curve) is a von Mises (circular Gaussian) function. *Cell from recorded data: 20151126_sun_34.1.*

1.6 Heading Direction Tuning

In 1995 there was a shift in the way MSTd was viewed to be contributing to optic flow processing. It was shown that not only do MSTd neurons respond to linear and spiral space motion pattern, but that MSTd neurons were sensitive to shifting the center of the motion pattern along the fronto-parallel plane (Duffy & Wurtz, 1995). This ability of neurons to react to such information was indicative that they might be contributing to the encoding of the heading direction (Duffy & Wurtz, 1995; Lappe et al., 1996), with different cells preferring different heading directions. More elaborate investigation of such properties followed, where responses of MSTd neurons were mapped in response to different 3-D heading directions (Logan & Duffy, 2006).

The tuning to 3-D translational *self motion* in different heading directions was more comprehensively probed by Gu et al. (2006), and subsequently a comprehensive probing of tuning to 3-D rotation self motion in different heading directions was conducted (Takahashi et al., 2007). Worthy to note is that nearly all recorded cells showed a significant tuning to heading direction, and that rotational selectivity is plentiful in MSTd.

It is important to point out here that whereas Duffy & Wurtz (1995) found a larger percentage of cells with straight-forward heading direction as their preferred direction, and while Lappe et al. (1996) found a more homogenous distribution of encoded heading directions, in several following studies (Gu et al., 2006; Takahashi et al., 2007) there was a clear bias in encoding heading directions in favor of lateral motion directions (i.e. motion towards the left or right). Additionally, rotation self motion with laterally positioned heading centers/directions were preferred by disproportionally more cells than other directions (Takahashi et al., 2007).

Two points of discussion are relevant here: MSTd neurons seem to encode optic flow in an eye-centered frame of coordinates regardless of whether gaze is fixating or freely moving (Lee et al., 2011). Secondly, MSTd not only encodes optic flow resulting from self-motion, but also responds to optic flow resulting from the motion of objects in the visual field, which does not necessarily contradict the idea of MSTd encoding self-motion (Logan & Duffy, 2006).

Finally, it appears that depth of the visual field plays a big role in optic flow processing in area MSTd, where adding multiple planes of depth to optic flow stimuli leads to a significant increase in the response of up to 70% of the cells in comparison to no-depth stimuli (Upadhyay et al., 2007).

1.6.1 Evidence and Contradictions

Despite this large body of evidence, correlation between the activity of MSTd neurons and the behavior of the monkey in a discrimination task involving opposite heading directions was reported to be weak (Heuer & Britten, 2004), even though individual neurons maintained direction sensitivities more accurately than that of the monkey (Celebrini & Newsome, 1994), suggesting that the involvement of MSTd in estimating heading direction might not be as direct as thought (Heuer & Britten, 2004). Additionally, evidence emerged that micro-stimulation and chemical inactivation of MSTd area biases the performance of monkeys in a heading discrimination task negatively, suggesting a causal link between MSTd and heading perception (Britten & van Wezel, 1998; Britten & Van Wezel, 2002; Gu et al., 2012).
Other areas have been shown to be involved in optic flow processing, areas to which MSTd projects (Orban, 2008) such as 7a (Merchant et al., 2001; Siegel & Read, 1997), VIP (Chen et al., 2011), and STP (Anderson & Siegel, 2005). Additionally, area PEc has been found to selectively respond to optic flow patterns (Raffi et al., 2002).
This broad spectrum of evidence indicates the definite involvement of MSTd in heading direction perception together with other areas, but does not point to a necessary one-to-one relationship (Britten, 2008).

1.6.2 Heading Direction Discrimination

Studies conducted on humans reveal that subjects can discriminate heading direction differences of $\sim 1^\circ$ using visual optic flow information only (Warren & Hannon, 1990). Similarly, monkeys are able to discriminate differences of 1° – 2° with 75% performance levels (Britten & van Wezel, 1998). Additionally, human subjects are better able to accurately judge heading directions corresponding to straightforward self-motion through environment, but perform less accurately in the case of more eccentric heading directions (Crowell & Banks, 1993; Gu et al., 2010), similar results are replicated in Macaque monkeys (Gu et al., 2010).
These results seem to be contradictory to the finding that there is predominance for lateral motion encoding in MSTd (optic flow resulting from lateral motion to the left or right), rather than straightforward motion (Gu et al., 2006; Takahashi et al., 2007). However, recent work has demonstrated that these seeming discrepancies were successfully integrated in a comprehensive model that shows that neural responses can explain the psychophysical results yielding high accuracy in discriminating straightforward heading direction with sensitivity declining with more eccentric heading

directions (Gu et al., 2010), echoing results from both human and monkey studies as explained above.

1.7 Motion Speed Preferences

Motion direction is not the only variable to which MSTd neurons are tuned in a motion pattern. MSTd neurons are reported to be quite sensitive to the overall speed of a motion pattern (Duffy & Wurtz, 1997b; Duijnhouwer et al., 2013; Tanaka & Saito, 1989), with cells having an average speed preference (average speed is defined as speed of the pattern at halfway between the motion center and the edge of the stimulus) ranging from 10°/s to 80°/s for radial and rotation patterns. Several earlier studies used an average speed of 40°/s in their stimuli, a speed known to elicit a good response from MSTd neurons (Duffy & Wurtz, 1991a; Tanaka & Saito, 1989), while others used a much lower average speed of 4.4°/s (Graziano et al., 1994).
More importantly, the presence of a speed gradient in a radial or rotation motion pattern significantly influences the response of MSTd neurons, where stimuli with speed gradients elicit on average better neural responses in comparison to stimuli with no speed gradients (Duffy & Wurtz, 1997b; Tanaka et al., 1989). Similar sensitivity can be found in MT (Treue & Andersen, 1996).
Finally, there have been no studies dedicated to thoroughly investigate potential selective responses of MSTd to different motion speeds in combination with their heading direction responses (Orban, 2008).

1.8 Vestibular input to MSTd

Intriguingly, and in contrary to earlier visual areas involved in visual motion processing, MSTd area does not only receive visual information regarding self-motion, but also responds to vestibular signal alone and in combination with visual signal (Bremmer et al., 1999; Duffy, 1998; Gu et al., 2006; Page, 2002; Takahashi et al., 2007). Whereas visual information is encoded in an eye-centered coordinates frame, vestibular information appears to be encoded in a head-centered reference frame (Fetsch et al., 2007; Lee et al., 2011). However, in comparison to other cortical areas also involved in optic flow processing to which MSTd projects (e.g. VIP, VPs), MSTd receives significantly less vestibular input, suggesting that MSTd might only be first stage of self-motion processing (Chen et al., 2011).
It appears that the responses of *congruent cells* in MSTd, neurons that have similar

visual and vestibular preferred heading directions, show correlation with the monkey's perceptual decisions during a heading direction discrimination task (Fetsch et al., 2010; Gu et al., 2008). Finally, the vestibular input to MSTd seems to cluster and follow a crude topographic organization (Chen et al., 2008).

1.9 MSTd in Human Cortex

The aforementioned studies on MSTd area, are rich with accumulated experimental evidence gained from studying the brain of the Rhesus Macaque monkey. However, a wealth of fMRI and PET studies have investigated responses to optic flow and self-motion in human cortex. Here we mention a few: correlates of areas MT and MST (as identified in macaque brain) have been found inside the motion sensitive MT+ complex in the human brain (Zeki et al., 1991), using different criteria to identify MST such as sensitivity to radial motion, lack of retinotopy and response to stimuli in the ipsilateral visual (Huk et al., 2002). With more evidence pointing to the existence of an MSTd correlate specifically (Morrone et al., 2000).
As suggested in studies conducted in macaques, MST in human cortex is not the only area involved in self-motion perception (Kleinschmidt, 2002; Wall & Smith, 2008). In addition, human MST not only responds to optic flow resulting from self-motion but also responds to optic flow caused by the motion of objects in the environment (Kleinschmidt, 2002; Kourtzi et al., 2002).

1.10 Position Invariance

As early as 1990, it was reported that MSTd neurons are position invariant, i.e. the preferred motion direction of the neuron remains the same, unaffected/invariant to the location of the stimulus over the receptive field of the neuron (Andersen et al., 1990; Duffy & Wurtz, 1991b), where this is only relevant to complex motion stimuli such as radial, rotation or spiral motion patterns. Specifically, when presenting radial or rotation stimuli at five concentric locations (Fig. 1.2 A), a position invariant cell retains the preferred motion direction (e.g. clockwise rotation) across all tuning locations (Fig. 1.2 B), without any preference reversal. This indicates that the local motion preferences in the central tuning location cannot explain the responses to the stimuli in the other locations, highlighting non-linear encoding properties (Graziano et al., 1994).
Lagae et al. (1994) defined position invariance similiarly as a lack in reversal in

selective preference to radial or rotation motion direction when testing several locations of the receptive field, along other restrictions regarding stability in the directionality across locations. Interestingly, authors investigated the feature of position invariance in both MT and MSTd, and their work was useful to create two criteria to further differentiate MT from MSTd: First, the lack of MT selectivity to complex motion patterns such as radial and rotation motion, and second, the presence of position invariance to radial and rotation stimuli in MSTd and not in MT (Lagae et al., 1994). Graziano et al. (1994) took the analysis a step further to quantify position invariance across cells. They devised the following method: spiral space stimuli were presented at five concentric locations (Fig. 1.2), and the preferred and anti-preferred motion direction of the cell were defined as the preferred and anti-preferred motion direction at the central location, respectively. The *directionality index (DI)*, which quantifies how well a cell is tuned to the central preferred direction versus the central anti-preferred direction (DI = $1 - \frac{anti-preferredResponse}{preferredResponse}$), was measured for the peripheral locations ($DI_{surround}$), as well as for the central location (DI_{center}). Lastly, they defined a *Position Invariance Index (PI)* as (PI = $\frac{DI_{surround}}{DI_{center}}$), which was calculated for every peripheral location. All 4 PIs per cell were pooled across cells into one population distribution as can be seen in (Fig. 1.3). According to the authors, a value of PI = 1 in one location would indicate perfect position invariance, with negative values indicating a reversal in the preferred motion direction of the cell in that specific location. Considering that the pooled distribution of PIs peaks at value of 1, and that there were no negative PI values (indicating absence of preferred direction reversal across locations and across cells), authors conclusions were in support of position invariance in MSTd cells. Lagae et al. (1994) had a similar position invariance measure and defined a neuron to be position invariant if the average value of directionality indices (according to the preferred direction at the central location) across all tested locations exceeded a value of 0.5.

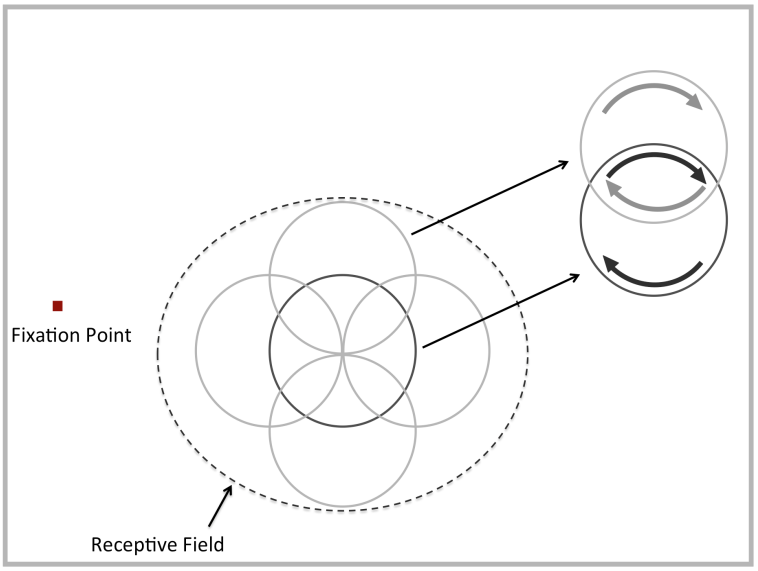

(a)

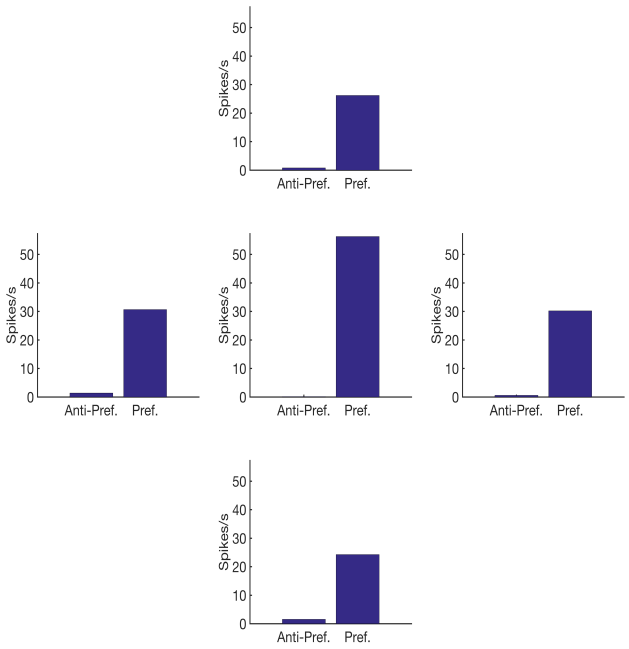

(b)

Fig. 1.2 Position Invariance testing. **a -** Spatial arrangement of tuning stimuli (Graziano et al., 1994). In order to test for position invariance, tuning stimuli are presented in one out of 5 possible concentric locations, which are arranged in a cloverleaf arrangement within the boundaries of the receptive field. In case of a position invariant neuron, local motion preference in the central location cannot explain the response of the neuron to stimuli in the peripheral locations. **b -** Position invariant response of a neuron to its preferred motion direction (Pref.) versus its response to the anti-preferred direction (Anti-Pref) across tuning locations; *example cell: 20170505_edg_33.1.*

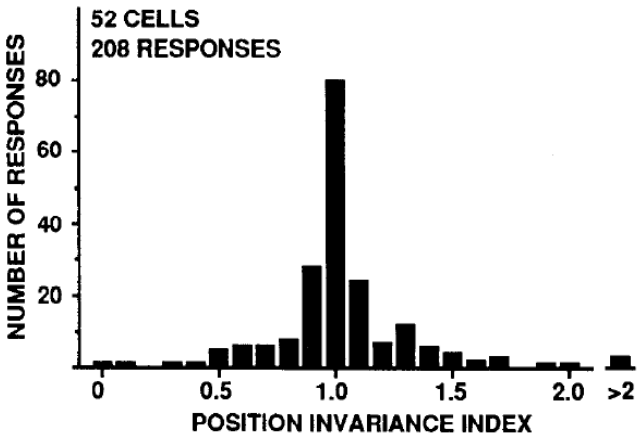

Fig. 1.3 Distribution of position invariance indices (PIs) across four tuning locations and across cells (Graziano et al., 1994). PI at a given location with a value of 1 indicates that the directionality index remained unaltered at that location and at the central location. Negative value indicate that there was a reversal in motion direction preference at the same location. The number of *Responses* indictates the total number of PIs across cells. *Adapted from* Graziano et al. (1994), *with permission from the first Author Michael S. Graziano.*

However, as indicated by the authors themselves, to say that MSTd neurons are mostly position invariant, rules out the possibility that MSTd cells can be involved individually in heading direction encoding (encoding the direction of self-motion through the environment), and only permits the possibility of population coding of heading direction (Graziano et al., 1994). This stands in contradiction to a wealth of literature pointing to the clear role of individual MSTd in heading direction tuning (Britten & van Wezel, 1998; Britten & Van Wezel, 2002; Duffy & Wurtz, 1995; Gu et al., 2012, 2006; Lappe et al., 1996; Lee et al., 2011; Logan & Duffy, 2006; Takahashi et al., 2007). Indeed, the first study to investigate heading direction tuning (Duffy & Wurtz, 1995), where 90% of cells were found to modulate responses to a preferred motion direction as its center of motion changed location spatially, addressed the topic of position invariance and the claim made by Graziano et al. (1994) to the inability of MSTd neurons to individually encode heading direction. Duffy & Wurtz (1995) attributed results of Graziano et al. (1994) to a *relative* position invariance, where the response of a neuron to the preferred direction versus its response to the anti-preferred direction changes depending on the chosen tuning location while retaining the same motion direction preference, in contrast to a theoretical *absolute* position invariance where the response of the neuron to the preferred direction versus the anti-preferred direction remain the same independent of the location while retaining the same motion direction preference.

We speculate that two factors were confused in the three above-mentioned studies (Duffy & Wurtz, 1995; Graziano et al., 1994; Lagae et al., 1994): motion direction preference invariance, and directionality invariance (DI = 1 – $\frac{anti-preferredResponse}{preferredResponse}$). A cell that is position invariant, should in theory retain the same motion direction preference across different locations within its receptive field. However, one cannot expect for a cell to retain the same directionality (response to the preferred direction versus response to the anti-preferred) over different locations within the receptive field as it is a common assumption that the response firing profile of a neuron reaches its peak at some parts of the receptive field, and slides into baseline firing rate at the outer edges of the receptive field. This change in firing rate across different regions of the receptive field should invariably affect strength of directionality.
We aim in the present article to dissociate these two variables, and quantify the extent of position invariance in MSTd neurons. This topic is relevant to the issue of linear/non-linear integration in the area of MSTd.

1.11 Linear/Non-Linear Integration

We are confronted with two conflicting scenarios: Firts, MSTd neurons integrate linearly input coming from an array of MT neurons with spatially distributed receptive fields, in a way similar to linear integration properties of V1 neurons (Deangelis et al., 1993). Thus, if a complex motion pattern is presented to an MSTd neuron, the response of the neuron to the global motion can be easily predicted from its responses to the isolated local motion directions in such a pattern (Fig. 1.4). Such a framework would preclude the ability of a cell to be position invariant, i.e. to be selectively responsive to the same motion direction over many locations within its receptive field. Second scenario assumes MSTd neurons as non-linear integrators: response of a neuron to the global motion cannot be easily predicted from its response to the local motion directions. This framework does lend itself for explaining position invariance in MSTd neurons.

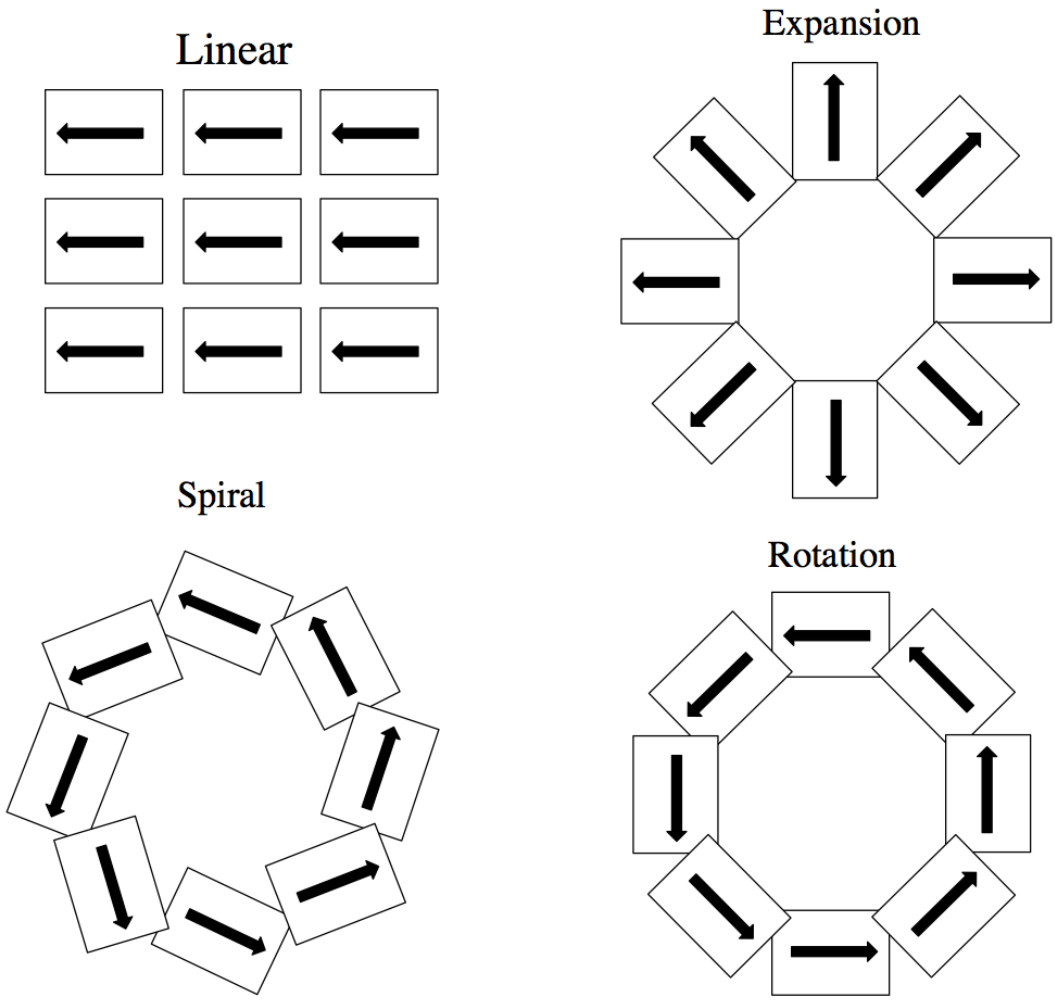

Fig. 1.4 Linear integration model of a neuron responsive to linear, radial (expansion/contraction), rotation and spiral motion (Tanaka et al., 1989). Every box corresponds to a theoretical optimally placed MT neuron, with signal from all MT neurons converging onto an MSTd neuron that sums its input linearly.

Whereas early studies provide some support to the linear integration framework (Saito et al., 1986; Tanaka et al., 1989), later findings offered evidence for the alternate view: Orban et al. (1992) overlaid the preferred motion direction (e.g. rotation) of MSTd cells on non-preferred motion direction (e.g. expansion), and reported their inability to detect responses to the smallest preferred/anti-preferred (rotation/expansion) ratio ($\frac{1}{4}$), concluding that a linear integration scenario does not describe the neural behavior of MSTd neurons (Orban et al., 1992).
More thorough investigations of MSTd non-linearity followed: Although the response of the neuron to the global motion pattern can be predicted from its responses to the local motion patterns in a substantial subpopulation of MSTd neurons, this statement cannot be generalized to the entire population (Yu et al., 2010). In a large subpopula-

tion it was found that the inclusion of a parameter describing the interaction between the neuron's responses to separate patches of local motion was necessary to improve the ability of a local motion response summation model to predict response of the neuron to global motion, and that the responses of the neuron to a combination of several patches of local motion patterns were better able to explain the neuron's behavior than responses to individual location patterns.

Similarly, Mineault et al. (2012) concluded that although a linear or *hierarchical* model of neural responses can account for the behavior of many MSTd neurons, it responds too strongly to linear motion and too weakly to more complex motion patterns. The addition of a non-linear integration component to their model enhanced its responses to complex motion patterns such as rotation and radial motion, while retaining ability to encode linear motion. This idea is echoed in several other studies (Duffy & Wurtz, 1991b; Graziano et al., 1994; Sugihara et al., 2002). In addition to non-linear integration, recurrent interactions within MSTd seem to play a role in stabilizing and providing accurate estimates of heading direction (Layton & Fajen, 2016).

An additional indication to the non-linear nature of MSTd neurons is the observation that no straightforward relationship between the linear translational direction preference of a neuron and its spiral motion direction could be observed, suggesting that MSTd neurons are encoding a high-dimensional complex motion pattern, and that tuning properties to such a stimulus could explain the various known motion selectivities of MSTd neurons to linear and spiral motion (Graziano et al., 1994; Mineault et al., 2012). It is interesting to note however, that Lappe et al. (1996) did find a strong correlation between the reversal direction and linear direction preferences. In this study, linear motion direction was correlated with the direction along which the cell changes its preference from contraction to expansion motion (with an average of 180° of angular distance between correlated directions). Linear direction was also correlated with the direction along which the cell changes its preference from counter-clockwise motion to clockwise motion (with an average of 90° of angular distance between correlated directions).

Finally, a potential source of non-linearity in MSTd neurons could arrise from their ability to integrate motion input over time (second order motion processing), where MSTd neurons respond to a specific optic flow motion direction only if it was part of a particular path through the environment (Froehler & Duffy, 2002; Page et al., 2015). This was reported despite earlier evidence against second order integration (Paolini et al., 2000).

1.12 Reverse Correlation as Mapping Method

Do MSTd neurons encode only heading direction? How does that explain their selectivity to spiral space motion stimuli? How does the selectivity of MSTd neurons to simple linear and shearing deformation motion (Mineault et al., 2012) fit into the puzzle? To accurately answer these questions, we need to study the fine spatial and directional preferences structure of an MSTd receptive field. Such a detailed investigation of the receptive field of a neuron has been conducted many times in several striate, extra-striate, and even non-visual areas using a multitude of methods.
A common approach has been to use white noise stimuli to calculate a spike-triggered average or a reverse correlation, which consists of conducting a correlation between the neural spike stream and the input signal while considering either a fixed (in case of spike triggered average), or a range of neuronal delays (in case of reverse correlation), with the later case allowing the experimenter the added advantage to study the temporal properties of the receptive field (Ringach & Shapley, 2004). This a method could be useful in uncovering the motion pattern which maximally drives MSTd neuron (Britten, 2008), and has been successfully applied in cochlear nucleus and in primary auditory cortex (a.M. van Gisbergen et al., 1975; Eggermont et al., 1983; Klein et al., 2006), LGN and V1 in cat and macaque monkey (De Valois et al., 2000; DeAngelis et al., 1995; Jones & Palmer, 1987; Reid & Shapley, 2002), and even in MT in macaque monkey (Borghuis et al., 2003; Livingstone et al., 2001; Richert et al., 2013). This method was helpful to suggest a new controversial view of MT neurons, where 40% of MT neurons encode several different motion directions within different parts of their receptive fields rather than encoding one simple linear motion direction over the excitatory receptive field area (Richert et al., 2013).
To our knowledge, reverse correlation has been applied once in MSTd area (Chen et al., 2008), to determine how well crude selectivity to visual and vestibular input cluster within area MSTd, without any emphasis on the fine spatial and directional tuning structure of the receptive field. In that study, a large $90° \times 90°$ stimulus was divided into a 4×4 grid of subfields, where different directions of motion were randomly displayed in every subfield/segment for 100ms each. It is important to note, that the authors reported 64% of all cells successfully mapped with the reverse correlation method, with statistically significant receptive field structures recovered.
At the heart of this approach is the assumption that MSTd neurons integrate input linearly, and that different signal parameters do not interact in non-linear fashion. Thus, this method may not to be able to recover statistically significant and structured receptive field maps in those cells that integrate incoming input in a non-linear fashion.

According to the literature, such cells are abundant in MSTd (Mineault et al., 2012; Yu et al., 2010). As we suggest in the Discussion chapter, it might then be useful to use more advanced adaptive sampling methods in order to recover receptive fields of such non-linear behaving neurons.

1.13 Goals of Investigation

In the present study we first aimed to establish whether the method of reverse correlation can be used to study the detailed structure of the receptive fields of MSTd neurons. We created a novel and complex motion white noise stimulus, with dimensions of $45° \times 30°$, and divided by a grid into 15×10 segments or subfields, where motion direction and speed in every subfield is drawn randomly and independently from other segments. We recorded from a large number of MSTd neurons, which were presented with several thousands of samples of this stimulus in a rapid serial succession (every 100ms), with the stimulus located optimally to cover the receptive field. We then correlated the response of the neurons to the random motion directions in every segment. Due to the linear nature of the method, it is not clear whether such an approach can be successfully used in an area that is reported to contain many neurons that integrate their input in a non-linear fashion (Mineault et al., 2012; Yu et al., 2010).
Therefore we quantify how successfully the method recovers statistically significant structured receptive fields in MSTd cells, and whether some methodological variables (such as total number of stimulus samples that were presented) or different properties of the investigated neurons (such as strength of directionality) could have any influence on the success of the method. Additionally, we assessed whether the local directional preferences, as recovered in receptive field map, could be used to explain the behavior of the neurons in response to the tuning stimuli that were placed in several locations across the receptive field. In other words, we investigated whether the responses of the neurons to the local motion patterns can be used to explain the behavior of the neuron in response to a global motion pattern.
Secondly, we studied the resulting directional motion pattern of those receptive fields successfully mapped by the reverse correlation approach and we attempted to observe any consistent trend across those patterns. A question here is whether we would be able to recover complex motion patterns such as expansion and rotation, or whether our chosen method would only map those receptive fields with a simple homogenous linear motion preferences.
Thirdly, we addressed the issue of position invariance. We quantified precisely how

well MSTd neurons maintain selectivity to the same spiral motion direction over several locations in the receptive field, and whether we could replicate previous findings regarding position invariance (Graziano et al., 1994).

Chapter 2

Materials and Methods

2.1 Subjects

Three adult male macaque monkeys (*macaca mulatta*) named Sunny (to be referred to as S), Eddy (to be referred to as E) and Iggy (to be referred to as I) were used in this experiment; had an age of 16, 12 and 11 years and weigh approximately 12, 8 and 11 kg, respectively. Monkeys had undergone previous experiments with acute electrophysiology recordings from the left visual cortex (where medial temporal (MT) area was targeted in monkey S and E, and dorsal medial superior temporal (MSTd) area in monkey I). As such, they entered the experiment equipped with implanted custom-made titanium head-posts, which are useful in fixating the head of the animal during experiment. They also were equipped with recording chambers, which were centered over the left superior temporal sulcus and allowed access to areas MSTd and MT. Recording chambers are cylindrical in shape (19mm in diameter) and allow access to the brain tissue unhindered by the skull bone, they are kept sterile through regular cleaning, and can be opened and sealed by a cap. After a period of recording on monkey I, he underwent an explantation procedure, removing the recording chamber from the left side of the skull, and implanting a new chamber targeting MSTd in the right hemisphere. The placement accuracy of the recording chambers was confirmed using structural MRI images, which allowed accurate identification of the area of interest MSTd relative to the chamber position (Fig. 2.1). The author did not participate in any of the medical procedures or operations conducted on the animals.
Experiments were conducted in accordance with institutional, national and international regulations and guidelines, and they were approved by the regional governmental office in Lower Saxony, Germany (Niedersächsisches Landesamt für Verbraucher-

schutz und Lebensmittelsicherheit [LAVES]), under the permit numbers: 33.9-42502-04-13/1100 and 33.19-42502-04-13/1100.

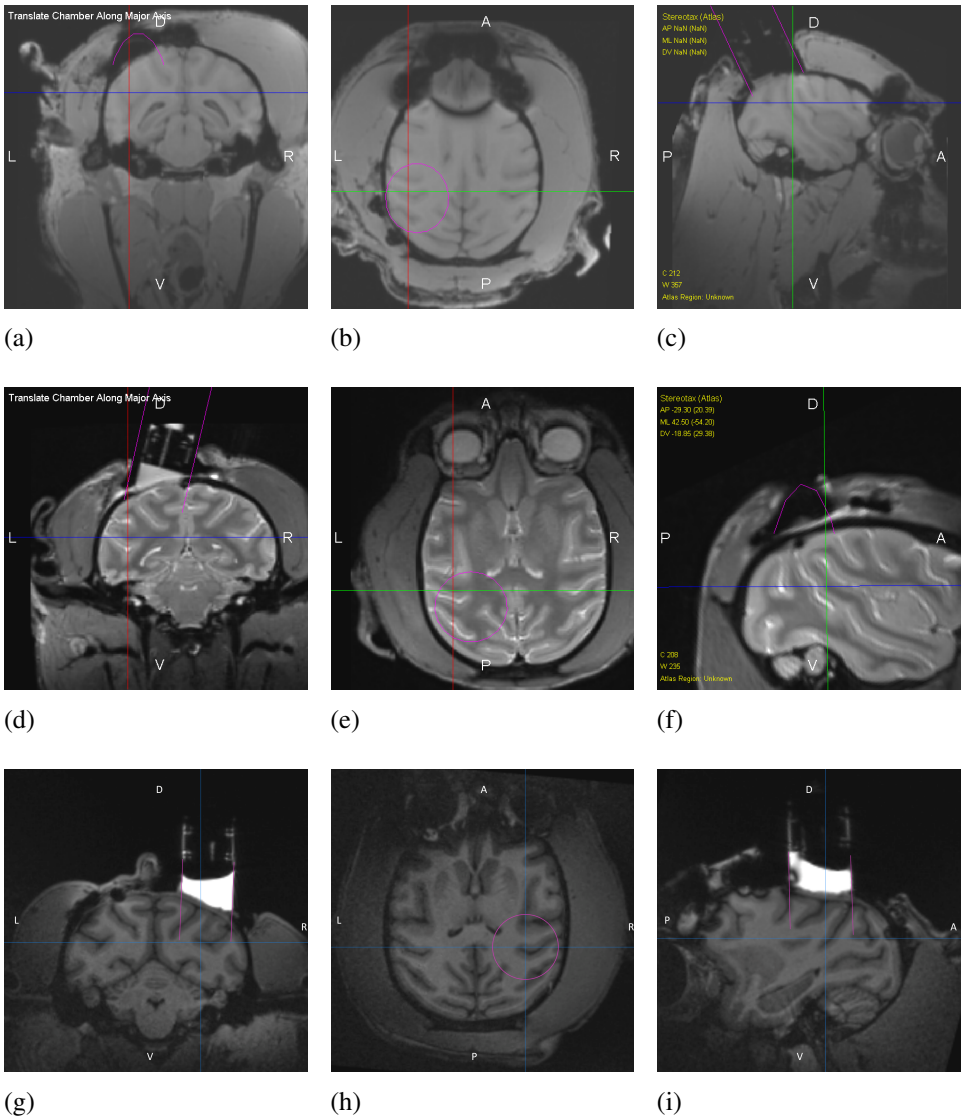

(a) (b) (c)

(d) (e) (f)

(g) (h) (i)

Fig. 2.1 MRI images showing the placement of recording chambers in monkey S (Images **a**, **b**, and **c**), in monkey I - left hemisphere (Images **d**, **e**, and **f**), and in monkey I - right hemisphere (Images **g**, **h**, and **i**). Purple cylinder and ellipse indicate the position of the chamber, with crosshairs indicating the position of the target area MSTd.

2.2 Experimental Setup

2.2.1 Setup A

Setup A was used to conduct the experiment on monkey S and E. While seated in a primate chair, and with the head fixated to the chair, the monkey viewed a computer monitor from a fixed distance of 57 cm in a dark room. The monitor had a resolution of 1920×1080 pixels, covered $60^\circ \times 30^\circ$ of visual field and had a refresh rate of 120Hz. Eyes position was monitored using an Eyelink 1000 plus system (SR-Research Canada) at a sampling rate of 500 Hz. Stimuli were of white color (luminance = 82.7 cd/m^2) displayed on a grey background (luminance = 17.3 cd/m^2). The Fixation square alternated between white color (luminance = 82.7 cd/m^2), red in a light shade (luminance = 13.4 cd/m^2), and a darker shade of red (luminance = 8.9 cd/m^2). An open source software MWorks 0.5.1 (mworks-project.org) running on an Apple Mac pro computer controlled the presentation of stimuli.

2.2.2 Setup B

Setup B was used to conduct the experiment on monkey I-left hemisphere (to be referred to as I-left), and most of the cells in Monkey I-right hemisphere (to be referred to as I-right), as outlined in the Appendix. While seated in a primate chair, and with the head fixated to the chair, the monkey viewed a back projection screen from a fixed distance of 102 cm in a dark room. A projector was used to display stimuli on the screen with a resolution of 1920×1200 pixels, covered $60^\circ \times 40^\circ$ of visual angle, and had a refresh rate of 60Hz. Eyes position was monitored using an Eyelink 1000 plus system (SR-Research Canada) at a sampling rate of 500 Hz. Stimuli were of white color (luminance of 31.33 cd/m^2) displayed on a grey background (luminance $\sim$ 1 cd/m^2). The Fixation square alternated between white color (luminance = 82.7 cd/m^2), red in a light shade (luminance = 1.9 cd/m^2), and a darker shade of red (luminance = 0.6 cd/m^2). An open source software MWorks 0.6.0 (mworks-project.org) running on an Apple Mac pro computer controlled the presentation of stimuli.

2.2.3 Setup C

Setup C was used to collect some of the cells in Monkey I-right, as outlined in the Appendix. While seated in a primate chair, the monkey viewed a computer monitor from a fixed distance of 57 cm in a dark room. A projector was used to display stimuli on the screen with a resolution of 1920×1080 pixels, covered $58^\circ \times 28^\circ$ of visual

angle, and had a refresh rate of 60Hz. Eyes position was monitored using an Eyelink 1000 plus system (SR-Research Canada) at a sampling rate of 500 Hz. Luminance values are equivalent to the values in Setup A. An open source software MWorks 0.6.0 (mworks-project.org) running on an Apple Mac pro computer controlled the presentation of stimuli.

2.2.4 Recording systems

Two slightly different recording systems were used in the different setups. Monkey S, E, I-right, and I-left and underwent acute electrophysiology recordings using a Mini-Matrix system (Thomas Recording, Germany), a multi-electrode driving device, which was mounted daily on the recording chamber, where stainless steel guide tubes penetrate the dura allowing an easy passage of electrodes (Thomas Recording, Germany, impedance between 1-2MΩ) into the brain tissue. Using the Mini Matrix, we could simultaneously insert up to 3 electrodes targeting our brain area of interest MSTd. Broadband signal from the electrodes was amplified and recorded using an Omniplex MAP system (Plexon, USA, sampling at 40kHz, 16bit) in Setup A, and an Omniplex acquisition system (Plexon, USA, sampling at 40kHz, 16bit) in Setup B & C.
A subset of cells in monkey I-left were recorded in setup B using a Kopf-drive system (David Kopf Instruments, California, USA), (All cells collected from monkey I between the 26.07.2016 and the 06.04.2017, 28 files, 22cells). This is a single-electrode driving device, which was mounted daily on the recording chamber, where one single stainless-steel guide tube penetrates the layers of dura in a location specified by a physical grid that is mounted on the chamber before electrodes are driven into the brain tissue. The guide tube allowed an easy passage of one electrode (Thomas Recording, Germany, impedance between 1-2MΩ) into the brain tissue. Signal from recording electrodes was amplified and recorded using an Omniplex acquisition system (Plexon, USA, sampling at 40kHz, 16bit).

2.2.5 Single unit recordings

As the experiment focuses on studying the receptive field of a single MSTd neuron at a time, we normally recorded data from only one electrode that received signal from the most stable unit (neuron). However it happened several times that on a given day more than one unit were recorded concurrently using the same electrode.
Waveforms of collected neural units were sorted online and offline. Selecting a unit for

recording relied on online sorting, where selection criteria included stability over time, good isolation from other surrounding units (as judged by visual inspection of the signal) and passing a threshold that clearly separates the unit from noise. Online sorting was necessary to guide suitable placement of visual stimuli during all experimental tasks.
After each session, we performed offline sorting of neural data using OfflineSorter V4 software (Plexon USA). We processed the raw signal with a 6-poles Bessel high-pass filter to detect the occurence of spikes, and we defined a sufficient threshold for seperating spike waveforms from background noise. A PCA analysis was conducted on the collected spikes, and waveform clusters were then sorted manually, where waveforms of a given unit were included only if well isolated and clearly separate from noise and surrounding units. Analysis and results included in this work relied exclusively on offline sorting.

2.3 Procedure and Tasks

Embedded in all the experimental tasks (except for the first task of Hand Mapping) was a luminance-change detection task. A red fixation point ($0.2° \times 0.2°$) appears at the start of the trial on the monitor, where the monkey is required to fixate his gaze throughout the trial. Once fixated, the monkey can initiate a trial by a press of a button and subsequent release (as in the case of monkey S and E), or by pressing and then holding the button down (as in the case of monkey I). After a waiting period of 200ms, stimuli are shown on the screen. The monkey then waits for the luminance change of the fixation dot, which occurs within 3 - 4.6s of the trial's start, and responds to the change by pressing the button again (as in the case of monkey S and E), or simply releasing the pressed button (as in the case of monkey I), within a response window of 600ms. Upon successful completion of the trial, the monkey receives a reward in the form of a drop of fluid, and is then shown a blank screen for 200ms before a new trial begins. In case the monkey fails to respond to the luminance change in the correct time window, the trial ends without rewarding the animal, a blank screen is shown for 200ms before a new trial begins, and the trial is labeled as a failure trial. If he responds prematurely before there was a luminance change, the trial ends without rewarding the animal, a blank screen is shown for 200ms before a new trial begins, and the trial is labeled as a failure trial as well. If the monkey breaks fixation at any point during the trial, the trial is terminated without rewarding the animal, a blank screen is shown for 200ms before a new trial begins, and the trial is labeled as a fixation break trial.

First task of Hand Mapping did not involve a luminance detection task, monkeys only needed to fixate gaze on the fixation point throughout the trial of 1.8 seconds to receive the reward.

2.3.1 Hand Mapping task

On a given recording day, after electrodes are driven into the brain tissue targeting MSTd, and a signal from a neural unit is present and stable over a few minutes, well isolated from surrounding units and easily crossing a threshold differentiating it from noise, we ran a hand mapping task to establish whether the neuron in question is sensitive to visual motion and determine the rough location of the receptive field relative to the fixation point.

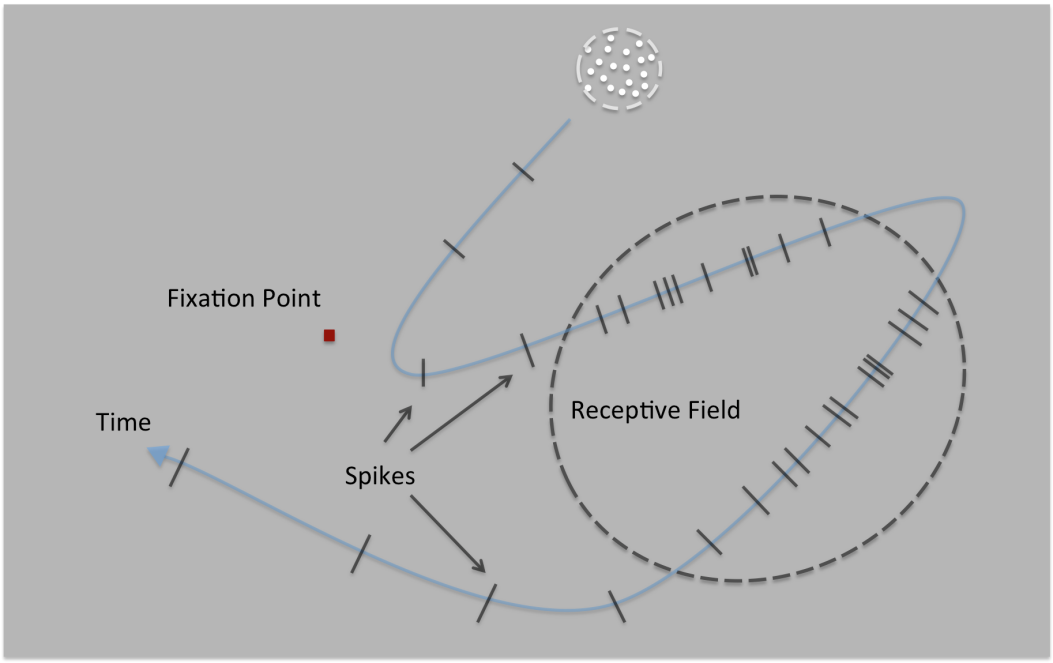

Fig. 2.2 Illustration of the Hand Mapping task. In a given trial a small RDP of 2° radius is moved across the monitor. As it crosses into the receptive field of a neuron, the spiking rate of the neuron increases. This task helps to identify whether a neuron is sensitive to visual motion, and determine the rough location of the receptive field on the monitor relative to the fixation point.

After successful trial initiation (monkey initiates trial by fixating gaze on the fixation point), a circular RDP (random dot pattern) would appear on the screen. The RDP of 2° (visual degrees) radius had a density of 1 dot/[visual degrees]^2, with a dot radius of 0.15°. The physical location of the RDP on the monitor can be manually controlled

using a computer mouse. Moving the RDP over the monitor to different locations in the visual field, in different directions and different speeds yields a response from a motion sensitive neuron (as an increase of the firing rate from baseline) if the RDP crosses into its receptive field at any time point (Fig. 2.2), in a manner similar to mapping done using hand-held stimuli in early electrophysiological experiment in V1, MT and MST (Hubel & Wiesel, 1959; Maunsell & Van Essen, 1983; Saito et al., 1986; Tanaka et al., 1989).
Such neural response can be visually detected when observing the incoming waveforms that are sorted automatically online, more easily it can be discerned over a speaker where every spike is converted into an audible 'click' sound, and finally it can be clearly visible using an online Matlab analysis routine which correlates every emitted spike with the location of the RDP at the time of emission while assuming a neural processing latency of 70ms. All three methods have been used in different cells to estimate the rough location of the receptive field relative to the fixation point. A trial lasts 1.8s and ends in dispensing a fluid reward to the monkey if gaze fixation is maintained successfully throughout the trial.
After a few trials of Hand Mapping, we can then change the location of the fixation point to bring as much as possible of the receptive field of the neuron in question onto the monitor. In this step we aim at an optimal placement of our stimuli in the receptive field. If however a neuron appeared to be not a motion-sensitive cell, we would start searching for a new unit.
Neural data from hand mapping task were never recorded. A more in-depth analysis of the receptive field of the neuron is conducted using the following Automatic Mapping task.

2.3.2 Automatic Mapping Task

Following a Hand Mapping task, we have information whether the neuron in question is motion sensitive, and we would have the fixation point located optimally on the screen to allow as much as possible of its receptive field to be covered by the monitor. We then ran an Automatic Mapping task. After successful trial initiation, one circular RDP appears on the monitor with a radius of 1.5°, a dots density of 4 dots/[visual degrees]^2 with a dot radius of 0.2°, and with the dots taking random different simple translational motion directions. Dots that cross the edge of the RDP are extinguished and placed in a new random location inside the RDP.
The RDP serially and without breaks changes location between a set of pre-defined grid-like spaced locations. These locations span the entire screen, evenly spaced with

2° of vertical or horizontal distance between any two locations. The RDP stays only for 50ms in one location, constituting one presentation. This short presentation time was chosen as it allows the presentation of a large number of samples within a short period of time, while still efficiently mapping the receptive field. One trial contains between 60 - 70 presentation samples, and lasts between 3 - 3.5s. Each location was sampled between 5 - 10 times on average. On a few occasions where the isolation of the cell was not completely clear during the experiment, or perhaps when sptial response of the cell was not clear, more Automatic Mapping trials were conducted. Every time the RDP changes location, a motion speed for the RDP is randomly drawn from a speed interval of [4 - 24 visual degrees/s].
In 76 cells, 10% of the sample presentations were blank and did not show any stimulus on the screen. The purpose of these 'blank presentations' is to calculate the baseline firing-rate of the cell in this task and estimate the spill-over effect generated by the random and quick location changing of the RDP, i.e. a carried-over increase of firing rate related to the previous sample presentations. However an analysis of those blank presentations is not included in this manuscript.
This task was analyzed online and offline. Online analysis was helpful to generate an online map of the motion-sensitive receptive field of the neuron at a pre-determined plausible biological neural latency of 70 ms. Such a map was then helpful to guide the placement of stimuli in the Tuning and Reverse Correlation tasks during the experiment.

2.3.3 Tuning Task

A map of the motion-sensitive receptive field of the neuron as generated online by the Automatic Mapping task was helpful to decide on the optimal placement and size of the tuning stimuli in this task. In this task, tuning stimuli consist of an RDP (random dot pattern) placed in one of 5 different concentric locations following a cloverleaf arrangement, as discussed earlier in the Intoduction chapter (Fig. 1.2), which is positioned optimally over the receptive field of the neuron, except for 31 cells where tuning stimuli were placed in different locations in the receptive field following no predetermined arrangment, or even outside of the receptive field misguided by an erroneous online Automatic Mapping (Cells with the proper placement are outlined in the Appendix). Radius of tuning RDP was usually 5° - 10° and determined at the end of the Automatic Mapping task, and was set to fit all the presented stimuli within the boundaries the receptive field. Radius remained constant thereafter across locations, across different directions and across trials. Tuning RDP had a dot density

of 2 dots/[visual degrees]^2 with a dot radius of 0.2°. If dots happen to cross the edge of the RDP, they are extinguished and they re-appear in a new location inside the RDP randomly chosen to maintain a uniform dot density across the pattern.
Dots in a single presentation of the tuning RDP moved coherently either in a linear motion direction (16.6% of tuning sample presentations and only presented in the central location), drawn from 8 possible linear motion directions [upward 0° direction, upward and rightward 45°, rightward 90°, downward and rightward 135°, downward 180°, downward and leftward 225°, leftward 270° and upward, and leftward 315°]; or in a spiral direction (83.3% of tuning sample presentations and in all possible tuning locations), drawn from 8 possible spiral motion directions [expansion 0° direction, expansive clockwise spiral 45°, clockwise rotation 90°, contractive clockwise spiral 135°, contraction 180°, contractive counter-clockwise spiral 225°, counter-clockwise rotation 270°, and expansive counter-clockwise spiral 315°].
Dot speed for linear RDPs was constant and randomly drawn for every presentation sample from a set of 6 discrete values [4, 8, 12, 16, 20, 24 visual degrees/s]. Speed for spiral RDP at a distance of 1° from the center of the pattern (angular speed for all dots within pattern remains constant for an individual presentation) was held constant, and was randomly drawn for every sample from a set of 6 discrete values [4, 8, 12, 16, 20, 24 visual degrees/s].
The RDP serially and without breaks takes on different configurations (6 possible configuration: one configuration as linear motion in central location, and 5 configurations corresponding to spiral motion presented in 5 different possible locations) in different directions and speeds. The RDP stays for 100ms in one configuration with a given direction and speed constituting one presentation sample before the stimulus is removed from the display, and a new sample with a random new configuration, direction, and speed is abruptly presented. This short presentation time was chosen as it allows the presentation of a large number of samples within a short period of time, while still efficiently mapping the directionality of the receptive field. Specifically, 100ms of presentation time seems to allow the perception of complex motion of spiral space stimuli. No seperate study has been conducted to confirm this methodologically. One trial contains between 36 - 46 presentation samples, and thus can last between 3.6 - 4.6s. Each configuration was sampled between 20 - 30 times on average for every direction and speed value. On a few occasions where the isolation of the cell was not completely clear during the experiment, or perhaps when tuning response of the cell was not clear, more Tuning trials were conducted.
In 76 cells, 10% of the sample presentations were blank and did not show any stimulus on the screen. The purpose of these ‘blank presentations’ was to calculate the baseline

firing-rate of the cell in this task and estimate the spill-over effect generated by the random and quick location changing of the RDP. However, as in the Automatic Mapping task, an analysis of those blank presentations is not included in this manuscript.

2.3.4 Reverse Correlation Task

After the Tuning task is completed, the monkey is presented with the last task of Reverse Correlation. For this task I created a *reverse correlation RDP (RC stimulus)*, a large rectangular RDP which contains 10×15 square segments of motion (In 47 cells in monkey I, a smaller RDP with 6×9 segments was used), set as grid where horizontal or vertical distances from center of one segment to another equals 3 visual degrees (Fig. 2.3). This arrangement yields an overall RDP size of $30° \times 45°$ for the 10×15 segments arrangement, or $18° \times 27°$ for the 6×9 segments arrangement. Linear motion direction designated for every segment was drawn randomly from an interval of [0 - 360°]. Speed of the motion for every segment was also drawn randomly from an interval of [0 - 20°/s]. At the center of each segment the dot direction and speed is influenced mainly by the motion direction and speed designated to that segment. However off-center dots are prone to be influenced in their motion by neighboring 3×3 segments: the center of each segment yields a *gravitational Gaussian weighting field* which grows weaker away from the center of a given segment to reach weak levels at the center of a neighboring segment (with standard deviation = 1.2°); thus every dot, which is not directly positioned at the center of a segment, has a motion direction and speed that is a Guassian-distance weighted average of the direction and speed of the 3×3 surrounding segments, with the variance of the Gaussian filter set to minimize the influence of an individual segment center over a dot residing at the center of a neighboring segment. The function determining direction or speed is given here:

$$f(x,y) = \frac{1}{n} \cdot \frac{\sum_i^n . p_i . e^{-\left(\frac{(x-x_i)^2}{2\cdot\sigma_1^2} + \frac{(y-y_i)^2}{2\cdot\sigma_2^2}\right)}}{\sum_i^n . e^{-\left(\frac{(x-x_i)^2}{2\cdot\sigma_1^2} + \frac{(y-y_i)^2}{2\cdot\sigma_2^2}\right)}} \tag{1}$$

where:

n = number of neighboring segments ranging from 3 to 9
p_i = is the parameter (direction or speed) in question of segment i
x, y = coordinates of the dot in visual degress relative to the fixation point
$x_\mathrm{i}, y_\mathrm{i}$ = coordinates of center of segment i relative to the fixation point
σ_1 = Standard deviation of the Gaussian surface filter along its first axis
σ_2 = Standard deviation of the Gaussian surface filter along its second axis

The standard deviations of the Gaussian filter σ_1 and σ_2 were set to a value of 1.2°. This yields smooth water-like motion in-between centers of segments. Such smoothening effect was chosen based on findings from literature, where withdrawal of direction and speed gradient in a stimulus, i.e. segmenting the stimulus, led to a decrease of neural response of MSTd neurons (Tanaka et al., 1989).

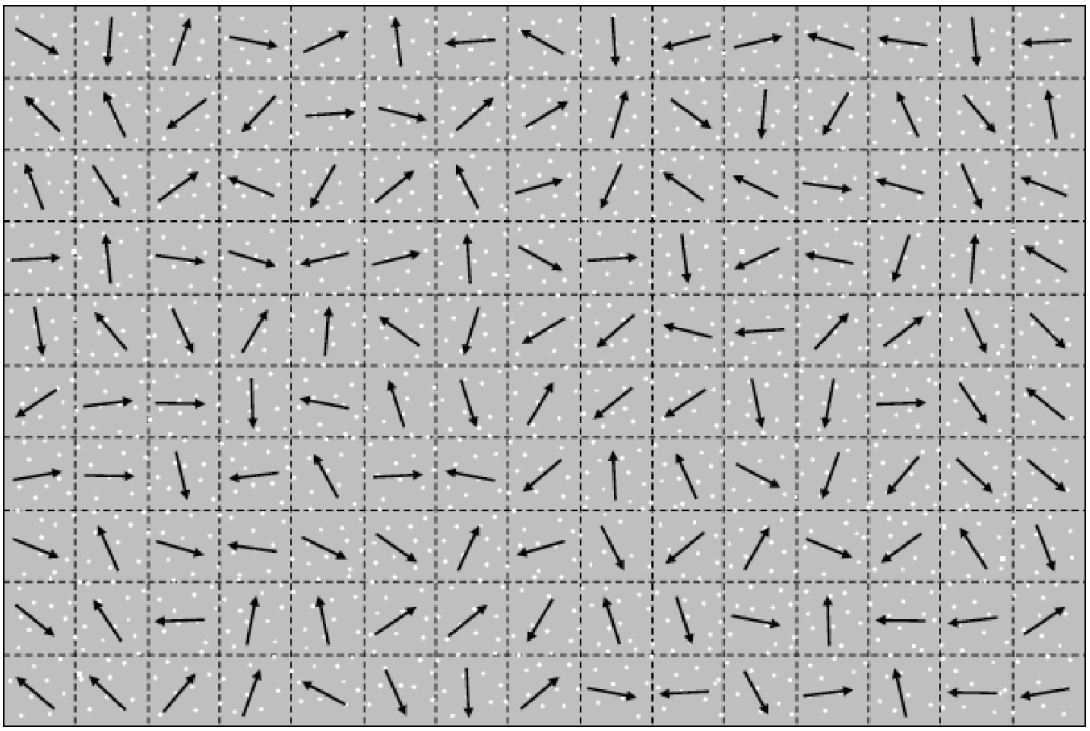

Fig. 2.3 Illustration of the Reverse Correlation stimulus. Arrows indicate the direction that dots follow at the center of every segment. Every dot has a motion direction and speed that is an average of the direction and speed of the 3×3 neighboring segments, weighted by the dot's distance from the respective segment center. Frame boundaries, dotted boundaries and arrows are only for illustration and are not visible on the monitor. *Figure courtesy of Benedict Wild.*

As dots move, the local dots densities of the pattern are kept constant by a dots-re-distribution algorithm, which removes dots from high dots-density regions and inserts

them in low dot-density regions at every frame. Number of dots is held constant at 10 dots/segment, corresponding to 1.11 [dots/visual degree], yielding a total number of 1500 dots for the 10×15 segments arrangement, or 540 dots for the 6×9 segments arrangement.
The RC stimulus is positioned optimally to cover the most responsive parts of the receptive field according to the map generated by the online analysis of the Automatic Mapping task. The stimulus is shown for 100ms constituting one presentation sample, and every 100ms a new sample is presented without an interruption in the dots display, with a new set of motion direction and speed parameters controlling the motion in every segment of the RDP. One Trial contains between 36 - 46 presentation samples and lasts between 3.6 - 4.6s. Monkey keeps performing this task until the end of the recording session, until the unit becomes unstable or until the monkey stops working. As such the total number of trials in this task was variable across cells.

2.4 Data Analysis

During offline analysis of the Automatic Mapping, Tuning and Reverse Correlation tasks, we used not only the correctly completed trials, but also the failure and fixation break trials, beacuse we were interested in the individual stimulus sample presentations where the monkey was correctly performing fixation, irrespective of the trail's outcome. Thus, we discarded data from the last incomplete sample presentation which preceded a fixation break, as was done by a similiar study (Borghuis et al., 2003). We also discarded the incomplete sample presentation which directly preceded a pre-mature response leading to a failure trial.

2.4.1 Automatic Mapping Task

The design of the Automatic Mapping task facilitates the construction of a detailed spatial and temporal map of the receptive field, where the temporal dimension illustrates how the spatial information of the map evolve over 250ms preceding the emission of a spike. Every location on the screen was sampled 5-15 times on average. We counted the number of spikes that occurred within an analysis time window that matched in time-length the length of a sample presentation (50 ms), which was then offset from the onset time of the sample presentation by a range of latencies [0, 1, 2, 3..., 250 ms] (Fig. 2.4). We then averaged across all presentations in that specific location, in every specific latency at a time. In this way, every location was assigned an average firing-rate at every latency. We assumed for our purposes that the response

latency of the neuron is constant across the receptive field.

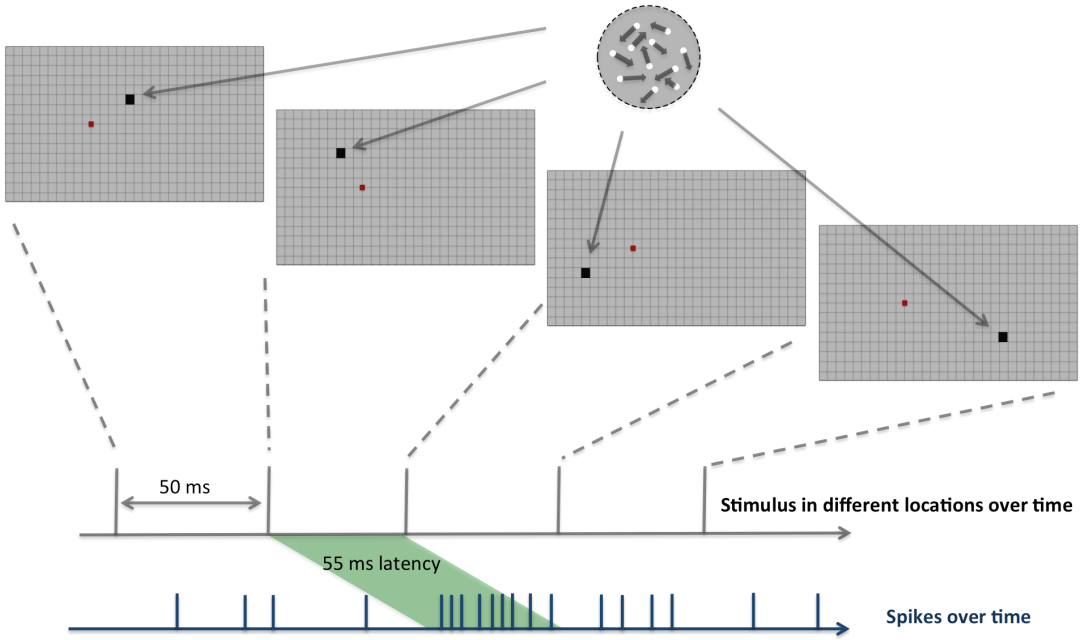

Fig. 2.4 Illustration of Automatic Mapping task analysis. As the Automatic Mapping RDP changes location every 50ms, spike stream is recorded. Spikes after every sample are counted within a window length that matches the time length of the sample presentation (50 ms), which however is offset using a range of investigated latencies. Here is shown an example case where the occurrence of a stimulus in a specific location on the screen produces a 55 ms latent increased response from the neuron.

We searched across investigated latencies for the one latency where the spatial map had the highest variance in averaged firing rates across all locations, which enabled us to calculate an optimal latency for every cell (Fig. 2.5), i.e. some time delay after the occurrence of a stimulus where the neuron would have had time to integrate and process input and produce its maximum spatial response (Fig. 2.6 a).

Using one map at every latency as a video frame, we were able to generate a video which illustrates the evolution of the receptive field within the 250ms following the presentation of a stimulus. These temporal properties of the MSTd receptive fields were not investigated further in this study.

Online analysis of this task involved carrying out the above-mentioned analysis at the end of every trial at a latency pre-set to 70ms. Searching online through latencies to look for the optimal latency at the end of every trial would not have been

computationally feasible. Such an online map enabled us to roughly determine the location and size of the receptive field (as the online sorting of cells is not as accurate as that of offline sorting, it can contain considerable amount of noise and poor unit isolation), and it guided our placement of the Tuning and Reverse correlation task stimuli.

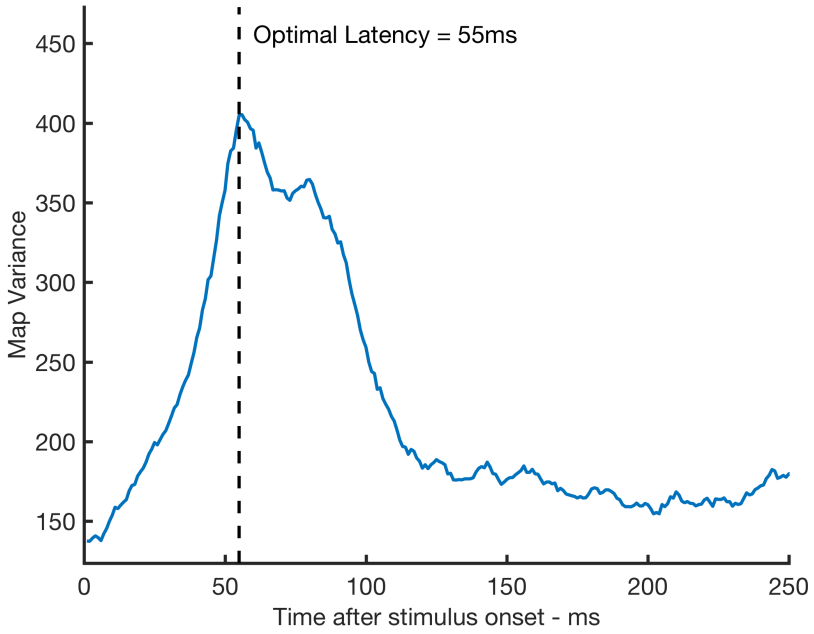

Fig. 2.5 Optimal latency calculation in the Automatic Mapping task. One example cell with map variance plotted against time after stimulus onset (at t = 0). Optimal Latency is chosen at the peak of the variance evolution over time. *Example cell: 20151126_sun_34.1*

The edge pixels, i.e. the outmost peripheral locations of the map, were cut out as a preparation step for next step in offline analysis, where edge pixels contained firing rates of the cell in response to a partial presentation of the Automatic Mapping stimulus (stimulus partially occluded by the edge of the monitor), and thus were cut out from further analysis.

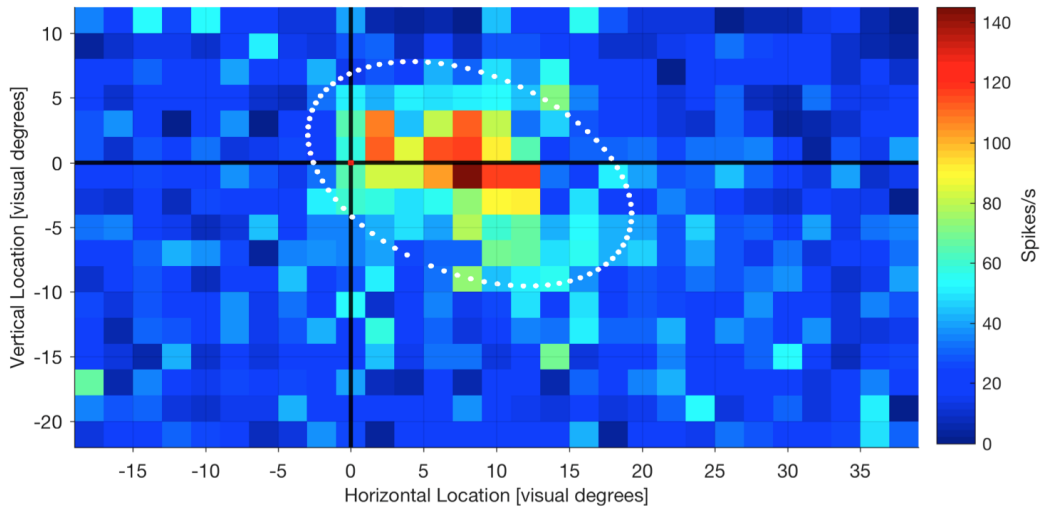

(a)

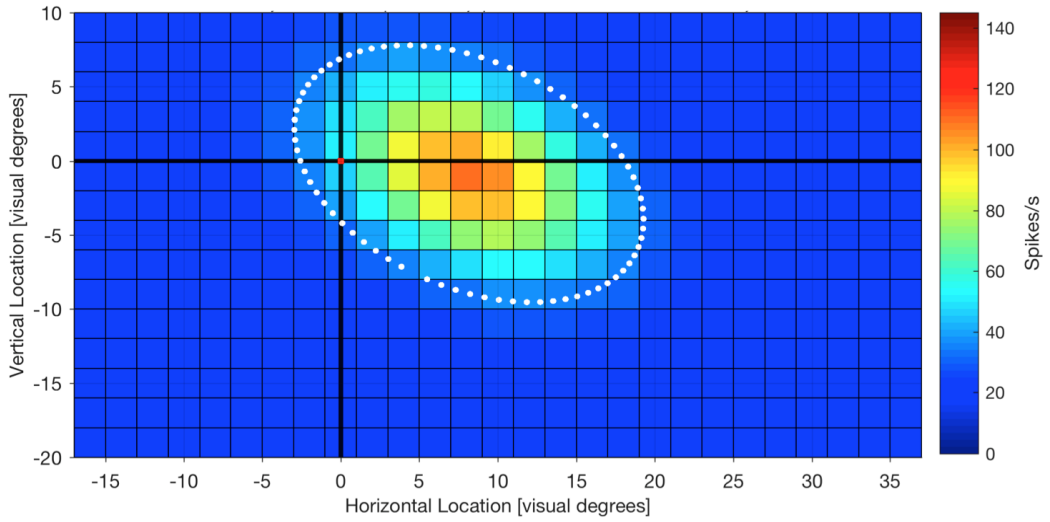

(b)

Fig. 2.6 Automatic Mapping Data from an example neuron. Intersection of black horizontal and vertical lines denotes the position of the fixation point, which is variable across cells and is determined in the preceding Hand Mapping task. Horizontal and vertical location coordinates denote the distance from the fixation point in visual degrees. **a -** Receptive field map at an optimal latency of 55ms. Color code indicates the intensity of response of the neuron (spikes/s) to the occurrence of a stimulus at that specific location by a delay of 55ms. White doted ellipse denotes the boundaries of the fitted receptive field (area within 2 standards deviations from estimated center, see text). **b -** Fitted Gaussian surface to the same receptive field at latency 55ms. r-square = 0.63, size = 290 [visual degrees]^2, eccentricity = 8°. White dotted ellipse denotes the boundaries of the receptive field. As mentioned in the text, the edge pixels containing the firing rates in probed locations on the monitor's edge were not included in generating the fitted map. *Example cell: 20151126_sun_34.1*, collected in setup A.

Next, maps from the optimal latency were fitted with a Gaussian surface to facilitate measuring size and eccentricity of the receptive field (Fig. 2.6 b). The MATLAB *fit* function was used, using a method of non-linear least squares. The surface is described by the following equation:

$$f(x,y) = \alpha + \beta . e^{-\left(\frac{((x-x_0).cos\theta+(y-y_0).sin\theta)^2}{2\cdot\sigma_1^2}+\frac{(-(x-x_0).sin\theta+(y-y_0).cos\theta)^2}{2\cdot\sigma_2^2}\right)} \quad (2)$$

where:

x, y = coordinates in visual degress relative to the fixation point
α = baseline
β = amplitude
x_0, y_0 = Coordinates of center of surface
θ = Rotation angle of the surface, i.e. between first axis and horizontal orientation
σ_1 = Standard deviation of the Gaussian surface along its first axis
σ_2 = Standard deviation of the Gaussian surface along its second axis

Starting values for the different parameters to be fitted were selected as follows: as an approximation, the initial value of β was set as the median (across locations) firing rate of the map at the optimal latency; the initial value of α was set as the maximum (across locations) firing rate of the map a the optimal latency minus β; the initial value of x_0, y_0 were set as the spatial average of all locations weighted by the neural response at each location of the map at the optimal latency; θ was set arbitrarly to an initial value of 0; and σ_1, σ_2 were each set arbitrarly to a value of 5°. Fitted surfaces with an R squared less than 0.2 (corresponding to maps where a receptive field could not be visually discerned), or with an estimated location of the receptive field's center falling more than 10° outside of the monitor were deemed unsatisfactory, and thus were not included in any further analysis invloving this task. The later criterion was set up to avoid exaggerated over-fitting for receptive fields which were too large to be accommodated on the monitor in the experimental setup, and so were present on the boundary of the monitor and only partially simulated by our stimuli. Size of the receptive field is defined as the area of the Gaussian surface that lies within 2 standard deviations (σ_1 along first axis, and σ_2 along the second axis) form the center of the receptive field.
Such measurements were helpful to extract the relationship between size and eccentricity of receptive fields across the entire population of recorded neurons.

2.4.2 Tuning Task

The analysis of the tuning task followed closely that of the Automatic Mapping task. Every motion direction in every configuration of parameters (as mentioned above, 6 possible configurations: one linear motion configuration in central location, and 5 different spiral configurations in all 5 possible locations) was sampled 20-30 times on average for every sampled speed. We counted the number of spikes that occurred within an analysis time window that matched in time length that of a sample presentation (100ms), which was then offset from the onset time of the sample presentation by a range of latencies [0, 1, 2, 3..., 250 ms] (Fig. 2.7). We then averaged across all repetitions of a given direction and speed of a specific configuration yielding an average firing-rate, at every latency at a time. Searching across investigated latencies for the one latency where all configurations and across speeds had their highest variance in firing rates concurrently enabled us to calculate an optimal latency for every cell.

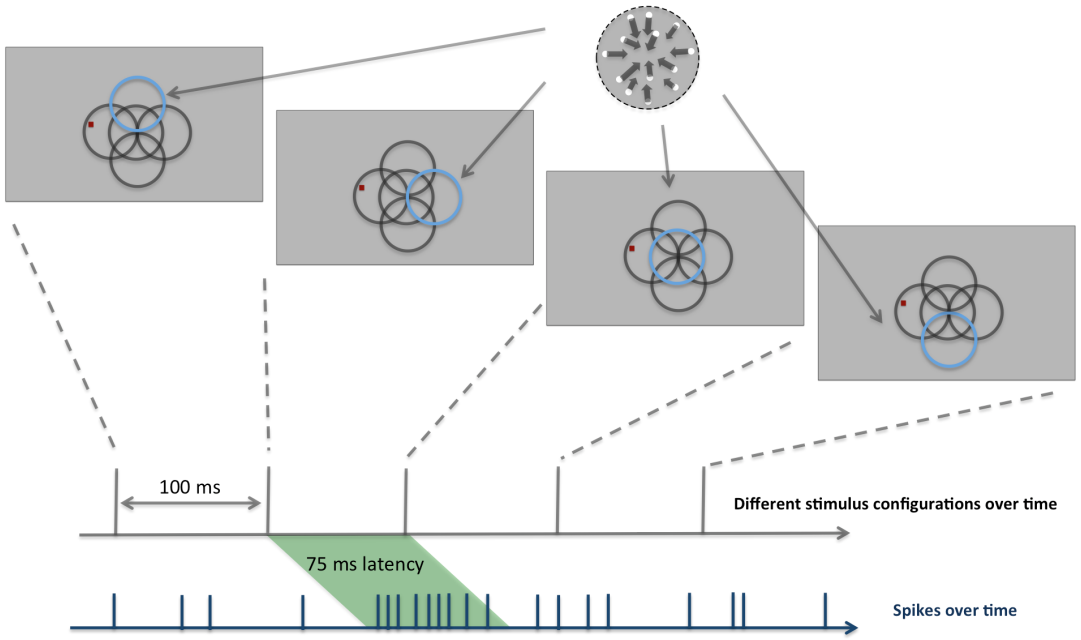

Fig. 2.7 Illustration of Tuning Task analysis. As the tuning RDP changes configuration every 100ms, spike stream from one neuron is recorded. Spikes after every sample are counted within a window length that matches the time length of the sample presentation (100ms), which however is offset in accordance with a range of investigated latencies. Here is shown an example case where the occurrence of a stimulus in a specific configuration on the screen produces a 75ms latent increased response from the neuron.

Data for different speeds for different configurations at the optimal latency are fitted with von Mises (circular normal distribution) curves to facilitate extracting directional tuning parameters (Batschelet, 1981). The curve is described by the following equation:

$$f(x) = \frac{\alpha}{I_0(\kappa)} \cdot e^{\kappa \cdot cos(x-\mu)} \tag{3}$$

where:

x = motion direction
α = amplitude
κ = measure of concentration, where $1/\kappa$ is analogous to σ^2 of a normal distribution
$I_0(\kappa)$ = modified Bessel function of order 0
μ = preferred direction

Starting values for the different parameters to be fitted were selected as follows: as an approximation the initial value of α was set as the maximum average firing rate across directions at the given speed, κ was set arbitrarly at a value of 2, and μ was set to the direction at which the maximum average firing rate across directions at the given speed occured. Data that had a fitting R squared of less than 0.2 were deemed unsatisfactory, and were not further analyzed (Fig. 2.8).

Further more, we assessed significance of directional tuning at every speed for every configuration at the optimal latency using a multiple comparison ANOVA, and accepted a data set if it passed the ANOVA test with a p-value < 0.05.

For every cell, and for all configurations we estimated a preferred speed. To estimate the preferred speed at a given configuration, we determined the speed, which generated the highest average firing rate given all individual directions, provided an acceptable von Mises fit was present at the found preferred speed, and provided the directional tuning was significant using the ANOVA test.

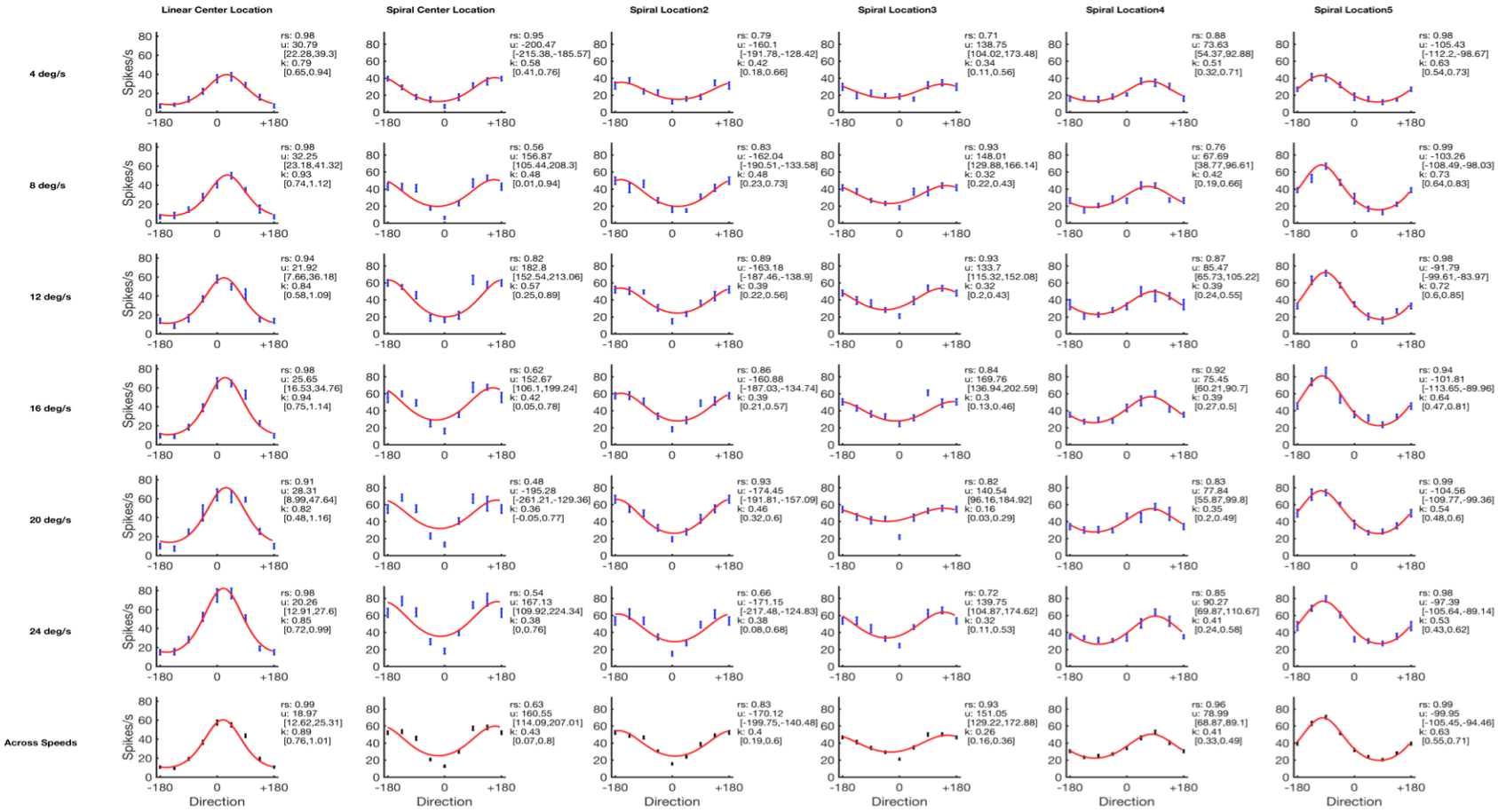

Fig. 2.8 Fitted tuning data of an example neuron. Column 1 contains data from linear motion configuration of different speeds and directions presented at the central location. Columns 2 – 6 contain data from spiral motion configurations of different speeds and directions presented at the central and the rest of tuning locations. Rows 1 – 6 contain data gathered with the indicated speed, and row 7 contains data averaged across speeds. In every plot a neuron's response (spikes/s) is plotted against the motion direction (in degrees). Parameters showing to right of plots are: rs = R squared, u = preferred direction (in degrees) with the associated confidence 95% interval below it, and k as a measure of concentration with the associated confidence interval below it. *Example cell: 20160503_sun_34.1*

A measure of *directionality index (DI)* was calculated for every configuration and for every speed. It is defined as:

$$DI = 1 - \frac{anti - preferredResponse}{preferredResponse} \tag{4}$$

DI captures the difference in firing rates of the neuron in response to a preferred direction (the peak value of the von Mises fit at a certain direction a) versus the response to the anti-preferred direction stimulus (the value of the von Mises fit at the opposite direction a + 180°), highlighting the strength of directionality of the neuron. For example, for a linear motion pattern at the central location with a linear speed of 4°/s, a DI of value close to 0 means that the response to the anti-preferred direction was very similar to the response to the preferred direction (very weak linear tuning at that specific speed in our example), whereas values closer to 1 mean that the response to preferred direction was significantly higher than response to anti-preferred direction (very strong linear tuning at that specific speed in our example).

Another measure of *response index (RI)* was calculated as follows:

$$RI = \frac{Response_{PreferredSpiral} - Response_{PreferredLinear}}{Response_{PreferredSpiral} + Response_{PreferredLinear}} \tag{5}$$

RI indicates whether a cell is more responsive to its preferred spiral motion direction and speed, or to its preferred linear motion direction and speed both at the central tuning location. A cell that is more responsive to linear motion has an RI value closer to -1, whereas a cell that is more responsive to spiral motion has an RI value closer to 1.

Finally a measure of *goodness of placement (GP)* was calculated for every tuning location for every cell, which captures how well tuning stimuli were placed within the boundaries of the receptive field as measured by the Automatic Mapping task, and is defined as follows:

$$GP = \frac{1}{n_i} \cdot \sum_{j}^{n_i} .r_{ij}/max(r) \tag{6}$$

where:

i = index of tuning location
j = index of an Automatic Mapping map pixel
n_i = number of mapping pixels that fall within a tuning location i
r_{ij} = response of the automatic mapping map at pixel j (spike/s)
$max(r)$ = the highest pixel response at the optimal latency (spike/s) of that map

Thus GP simply compares the average of responses of Automatic Mapping pixels that fall within the boundaries of a tuning RDP, to the maximum response of the Automatic Mapping map. We assume that stimuli that are well placed within the receptive field (and thus cover more Automatic Mapping pixels that have relatively higher responses) should have a value of GP closer to 1 and those that are poorly placed to have a value close to 0.

2.4.3 Reverse correlation task

As the name of the task implies, this task was analyzed using the classical method of reverse correlation: Reverse correlation analysis is in essence a spike-triggered average done in a range of latencies. In our analysis, latencies ranged from -400ms before to +200ms after the occurrence of a spike. As every sample of a Reverse Correlation stimulus extend to 100ms in temporal length, the correlation between a spike and a stimulus can extend past the time point of the occurence of the spike, therefore we opted to extend the analysis window to +200ms. For example, taking an l latency, we go to every spike emitted during the task and extract the direction parameters (set of directions assigned to all segments within the RC stimulus) at l ms prior to the occurrence of that spike. If we were to focus on segment i, we compile a distribution D_{li} that contains every motion direction that was assigned to that specific segment at l ms before the occurrence of all spikes. Assuming a circular Gaussian distribution of D_{li}, the direction of the mean resultant vector ($\vec{r}_{li}$) of D_{li} indicates the direction of motion that most likely was present at the center of segment i at l ms before the occurrence of a spike, i.e. preferred direction at a given location at a given latency. The magnitude of $\vec{r}_{li}$ (R) is taken as a measure of directionality's strength to the preferred direction at latency l (Fig. 2.9).

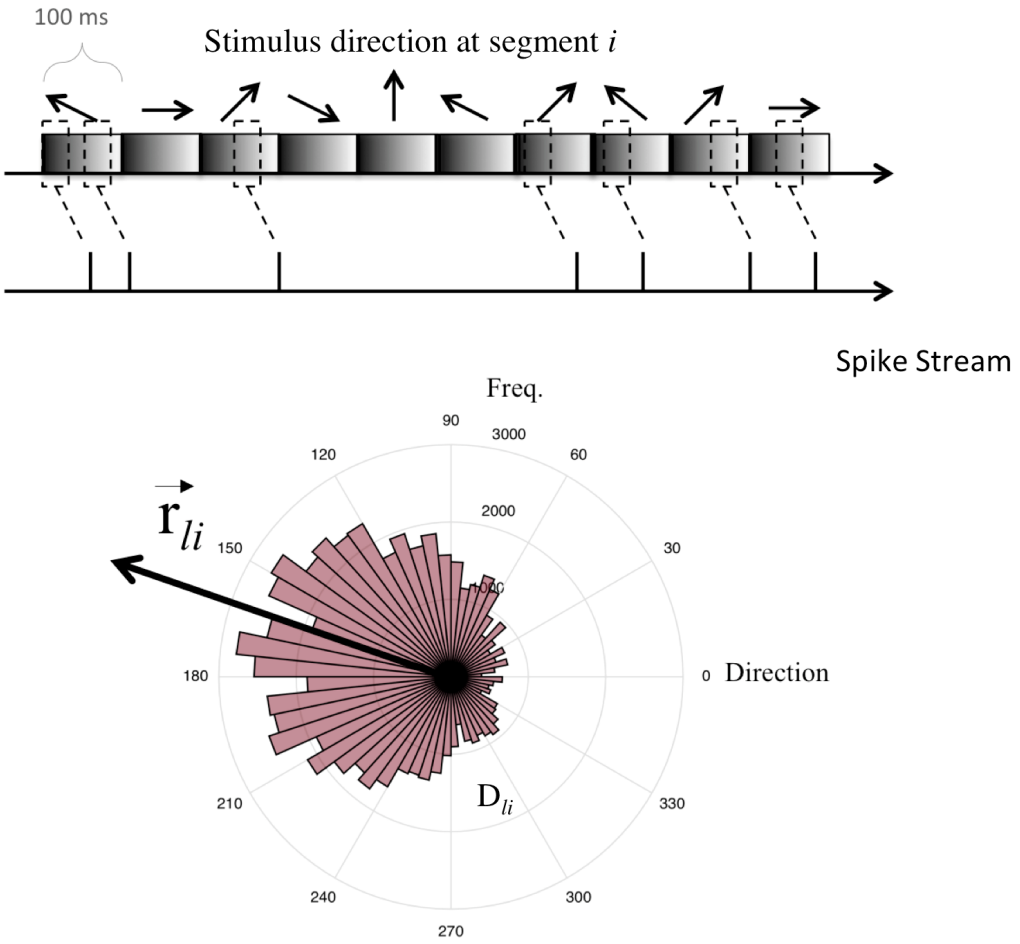

Fig. 2.9 Illustration of the principle of reverse correlation analysis. Taking the direction of motion at segment i at l latency before the occurrence of a spike for every spike generates a circular distribution of motion directions D_{li}. The direction of the mean resultant vector ($\vec{r}_{li}$) of such a distribution indicates the most likely direction of motion to be showing in segment i at latency l before the occurrence of a spike.

Conducting this analysis for all 15×10 segments that are part of the RC stimulus for a given latency generates a spatial-directional tuning map (To be referred to as an *RC map*) (Fig. 2.10). Conducting the analysis over all investigated latencies from -400 to +200ms in steps of 5ms produces 121 maps, these maps can then be used one frame at a time in a video that shows the evolution of the spatial-directional tuning over time. The temporal evolution of tuning properties in this task was not investigated further in this study.

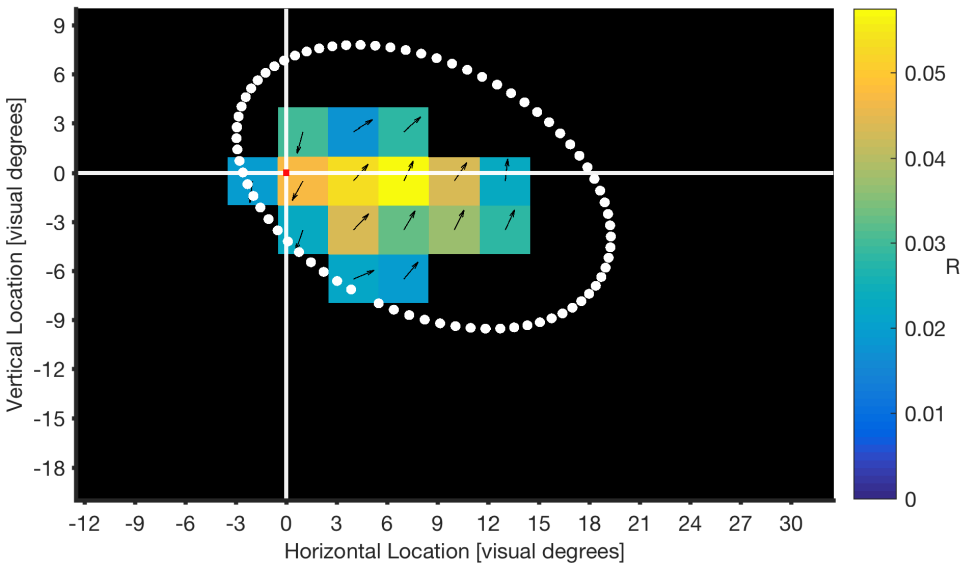

Fig. 2.10 RC map of an example MSTd neuron at an optimal latency of $l = 70$ms. In every segment i, a distribution D_{li} of all motion directions that were present 70ms before the occurrence of spikes is created. The direction of the mean resultant vector of such a distribution is indicated by the orientation of the arrow in its respective segment. The color code indicates the magnitude of the mean resultant vector $\vec{r}_{li}$ (R), where warmer color segments indicate a higher magnitude in mean resultant vectors in those segments, i.e. a stronger deviation from uniformity and thus a stronger directionality at the respective segments. The white intersecting lines indicate the location of the fixation point. Here in this map, we see a spatial cluster of significant directional tuning of almost $12° \times 18°$ in dimensions, that resides to the right of the fixation point. *Example cell: 20151126_sun_34.1.*

The following method was used to estimate whether the directional tuning of a given segment was significant: FIrst, for every latency l and for every segment i, we conducted the circular uniformity omnibus test or Hodges-Ajne test [using Matlab Circular Statistics toolbox (Berens, 2009)] to confirm whether distribution D_{li} is significantly deviant from circular uniformity in a unimodal or multimodal fashion. Starting with a p-value of 0.001, we corrected for the multiple tests that are done (one test for each of the 15×10 segments) by applying the Šidák correction:

$$\alpha = 1 - (1 - \alpha_0)^{\frac{1}{m}} \tag{7}$$

where:

α = p-value after correction
α_0 = p-value before correction
m = number of different null hypotheses

This yielded a p-value of $6.67x10^{-6}$. Thus, for tuning in a given i segment at a given latency l to be significantly different from noise, the p-value of the Rayleigh test conducted on D_{li} should be $< \alpha = 6.67x10^{-6}$.
Secondly, a further significance measure is put in place, where segments that are significantly directionally tuned for only one latency are deemed insignificant and likely to be the result of noise. We considered directional tuning which appears suddenly and last for only one latency improbable to be different from noise. An example of tuning evolution in one segment can be seen in (Fig. 2.11, A) as compared to simulated noise (where a reverse correlation analysis was applied using a randomly shuffled motion directions stream) in one example neuron (Fig. 2.11, B).
Thirdly, an additional significance measure was implemented, where every significant segment is required to cluster with at least 2 neighboring significant segments at any given latency. Any segment which does not meet all of the previous significance measures was deemed not significantly different from noise. Finally, a thresholding value of 0.0174 was used to deem any mean resultant vector with a smaller length as likely resulting from noise. The value of 0.0174 is the mean resultant vector's length below which fall 95% of the mean resultant vectors' magnitudes of 10000 randomely generated circular distributions. Then, any cell with any significant segments at any latency is then deemed to have been successfully mapped by reverse correlation.
Segments that do not contain significant directional tuning at a given latency are masked with a black square as can be seen in (Fig. 2.10), and are not included in further analysis.
Searching for the latency where the sum of the magnitudes of mean resultant vectors of D_{li} of all significant segments was maximal yields the optimal latency for a given neuron in this task, i.e. latency at which the tuning strength of all the significant segments was maximal concurrently.

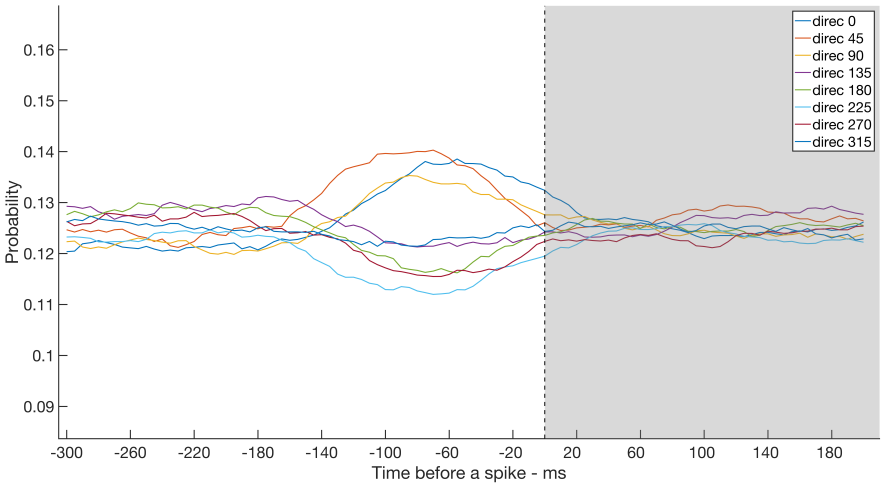

(a)

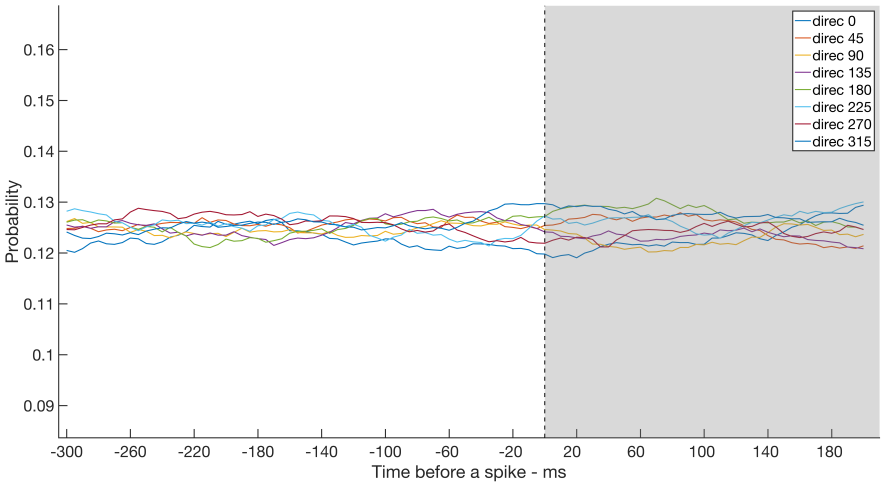

(b)

Fig. 2.11 An Example of temporal evolution of tuning in an example segment (the segment with the strongest tuning, i.e. strongest R value, in figure (Fig. 2.10)). Along the x axis time is plotted relative to the occurence time of a spike, along the y axis is the probablity that a given binned direction would be shown in the segment in question at a given latency before a spike. Grey shaded area highlights part of the analysis window that extend after the occurence of a spike, where probablities of the different motion direction should become homogenous. **A -** Direction distribution D_{li} is binned into 8 directions at each latency l. Tuning strength, or the deviance of a distribution from circular uniformity , can be observed over latencies preceeding a spike. Tuning reaches its maximum around 70ms before the spike to go back to noise at 100ms after a spike (because of temporal smoothening caused by the length of the stimulus sample (100ms). **B -** Temporal evolution of tuning in response to noise. Using randomely shuffled vector of all the motion directions presented to the same segment as in **A**, we conduct the same analysis. *Example cell: 20151126_sun_34.1*

An RC map at the optimal latency in principle illustrates the motion direction pattern of a hypothetical *optimal stimulus* for a given neuron. Should one reproduce a stimulus with motion direction pattern matching that of this optimal RC map, maximal response from the neuron is expected.
If this caveat holds true, then one would expect that by presenting stimuli that are of varying degrees of motion direction similarities to that optimal RC map, the responses of the neuron should positively correlate with these motion similarities.
As the recorded neurons were presented a high number of stimuli samples in the Tuning task, we tested for a correlation between the responses to these stimuli, and the motion similarity of the stimuli to the optimal RC map as recovered by the Reverse Correlation task analysis.
Therefore we created a *similarity index (SI)* measure, which aims at estimating the degree to which a Tuning stimulus was similar in motion to the optimal RC map. Formula for SI for a given tuning stimulus is defined as following:

$$SI = \sum_{i}^{n} R_i(1 - 2|(M_i^{os} - M_i^{ts})/\pi|) \tag{8}$$

where:

i = index of segment in the RC map
n = total number of segments that fall within a tuning location
R_i = magnitude of $\vec{r}_{li}$ of D_{li} where l is the optimal latency
M_i^{os} = motion direction of the optimal RC map in radians at the center of segment i
M_i^{ts} = motion direction in the Tuning stimulus in radians at the center of segment i

As we can see, a similarity value of motion in every segment lies between a value of -1 (in case direction of the optimal RC map and direction of dots in the tuning stimulus at the center of the given segment is 180° different) and value of 1 (in case direction of the optimal RC map and direction of dots in the tuning stimulus at the center of the given segment is 0° different). That similarity value is then weighted by the magnitude of mean resultant vector (R_i) of D_{li} in each individual segment (at the optimal latency) of the optimal RC map, which is a measure of the strength of directionality in that specific segment. This weighting procedure is based on the assumption that parts of the receptive field that have a stronger directionality play a bigger role in determining the response of the neuron to different stimuli presented in it. Of course this analysis was only possible in those cells that were successfully mapped by reverse correlation, and it was only applied to those spiral tuning configurations (and at the preferred speed) that

overlapped spatially with the recovered RC map, irrespective whether they generated a significant tuning. The response of the neuron to the Tuning samples is plotted against their individual motion similarity indices, and checked for correlation using Spearman's rank correlation coefficient. An example for similarity index analysis can be seen in (Fig. 2.12).

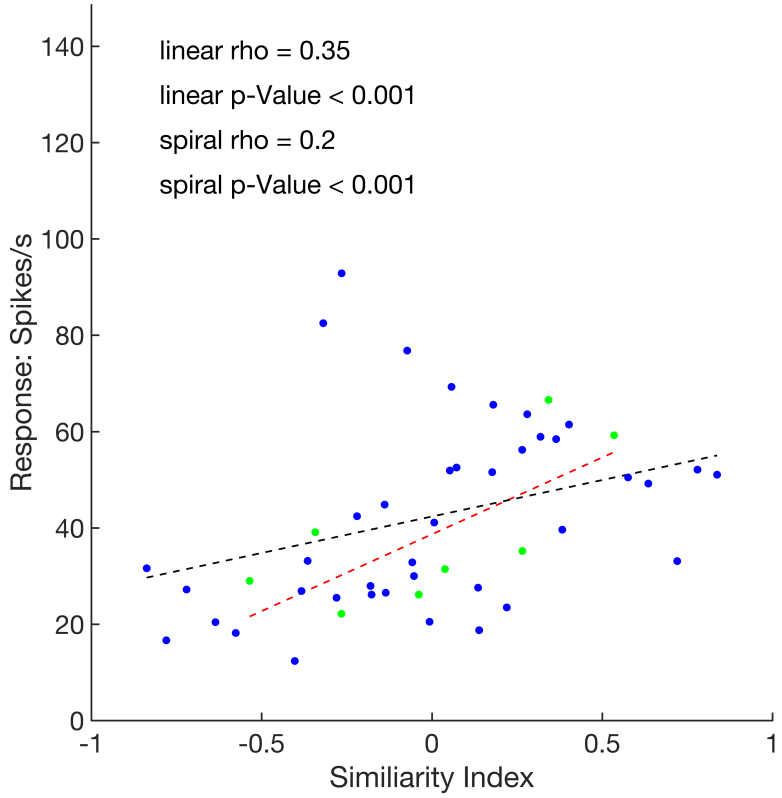

Fig. 2.12 An Example of similiarity index analysis. The response of the cell to individual spiral and linear tuning stimuli samples is correlated with the motion similiarity between the tuning stimuli and the optimal stimulus as recovered by the RC analysis. Spearmann's rank correlation test is conducted on linear and spiral stimuli samples, with the respective correlation coefficient (rho), and respective p-value indicated. Linear regression model was fitted to the data (red dotted line fitted to linear motion data, black dotted line fitted to spiral motion data). *Example cell: 20151126_sun_34.1*

Chapter 3

Results

3.1 Overview

In total 181 single units underwent the experiment outlined in the Methods section. We collected 116 cells from monkey S, 26 cells from monkey I-left, 37 cells from monkey I-right and 2 cells from monkey E. As outlined in the Appendix, We did not collect a complete data set (Automatic Mapping + Tuning + Reverse Correlation task) from all of the recorded cells: it was often the case that a cell did not remain stable past the first task. It also happened that while recording a unit *a* on the experiment, a second unit *b* appears during the second (Tuning) or third (Reverse Correlation) task. Unit *b* is then included in the analysis of second and third tasks, but excluded from any analysis involving the first task.

3.2 Automatic Mapping Task

In total 175 cells underwent the Automatic Mapping (112 from monkey S, 26 from monkey I-left, 35 from monkey I-right and 2 from monkey E), with a minimum number of spikes of 100 in this task. Spatial maps generated by analyzing the response of a given neuron to the Automatic Mapping stimulus at different latencies revealed an estimation of the spatial extent of the motion-sensitive regions of its receptive field.

3.2.1 Inclusion Criteria

Taking the spatial map of the receptive field at the calculated optimal latency, we were able to satisfactorily fit a Gaussian surface to 100 cells. Such fitted maps generated two key estimated values: square-root size and eccentricity of the receptive field.

Several criteria were used to qualify the goodness of fit. First we required for an acceptable fit an R squared > 0.2. Second we turned to the estimated eccentricity value: some receptive fields that were too large to be fully accommodated on the monitor in the experimental setup, were present on the boundary of the monitor and were only partially stimulated by our stimuli. To avoid exaggerated over-fitting data for such receptive fields, we did not include in any further Automatic Mapping analysis those cells with fits that placed the estimated center of the receptive field more than 10° outside the boundaries of the experimental monitor on either the horizontal or vertical spatial dimension (see Appendix). Finally, 6 cells were hand-picked and removed from the analysis, as they had a low number of spikes feeding into the Automatic Mapping analysis which resulted in an over-fitting problem where a high R-square would result from a fit to a noisy map (a fit could estimate a size of the receptive field to be as small as one pixel), even when a visual receptive field was not clear from visual inspection of the spatial maps (see Appendix).

3.2.2 Spatial Properties of Receptive Fields

As mentioned above, the selection criteria yielded a total number of 100 cells with acceptable fits. Using Spearmann's rank correlation test we investigated any relationship between sizes of the receptive fields (measured as square root of fitted surface area in visual degrees) and eccentricities (distance between center of fitted surface and fixation point in visual degrees) across the cells. Sizes of the receptive fields are positively correlated with their eccentricities (Spearman's rank correlation test; coefficient = 0.58; p value < 0.001) (Fig. 3.1).

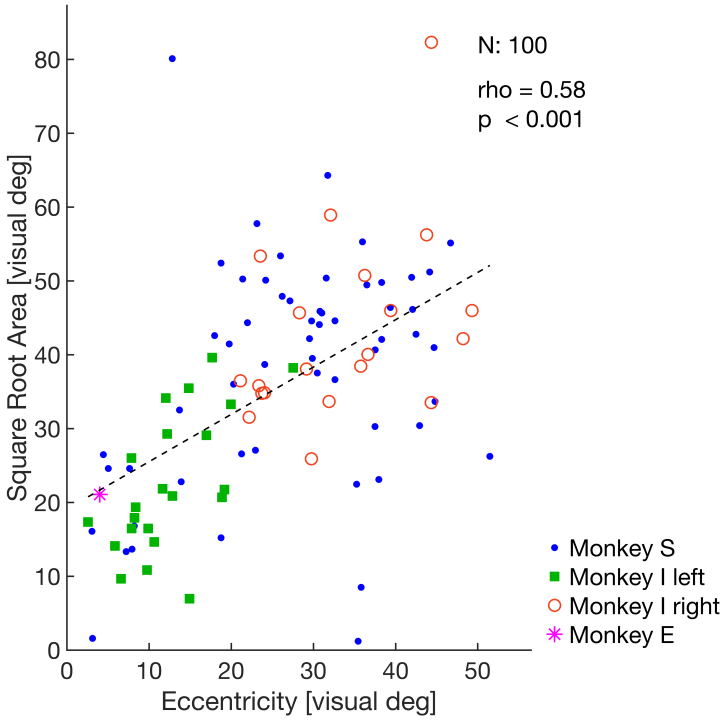

Fig. 3.1 Size and eccentricity of fitted receptive fields. Across the population, the receptive fields of 100 cells from all 4 hemispheres were fitted acceptably with a Gaussian surface. Such fits allowed estimated measurements of size and eccentricity of receptive fields. A significant correlation exists between the sizes of the receptive field (measured as square root of fitted surface area in visual degrees, as defined in methods section) and their eccentricities (distance between center of fitted surface and fixation point in visual degrees) (Spearman's rank correlation test; coefficient = 0.58, p-value < 0.001). Linear regression model was fitted to the data (dotted line) to illustrate correlation.

To further look at the spatial distribution of the recorded receptive fields, we created a spatial map, where we overlaid all of the receptive fields with acceptable fits (with their boundaries defined as stated in the methods section) while taking into consideration their corresponding spatial locations (Fig. 3.2).

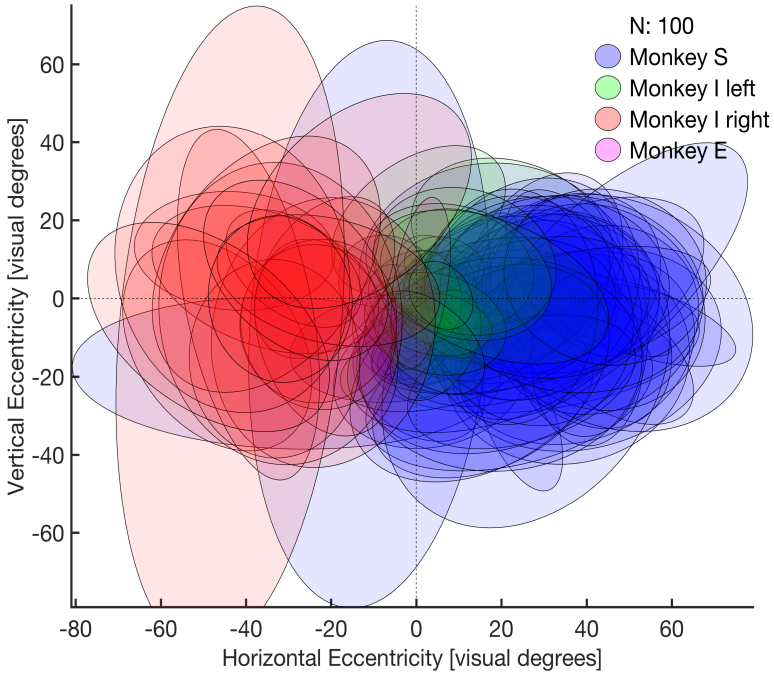

Fig. 3.2 Superimposed fitted receptive fields for all recorded cells. We overlapped all receptive fields (57 cells from monkey S, 22 from monkey I-left, 20 from monkey I-right, and 1 from monkey E) on one single map.

To clarify the spatial distribution of the receptive fields further, we created a map for each hemisphere, where for every pixel we calculated a percentage of coverage: percentage of acceptably fitted receptive fields that included that pixel within their spatial boundaries (Fig. 3.3). We can observe a map that contains superimposed receptive fields from 57 MSTd cells from monkey S (Fig. 3.3 a), a map that contains superimposed receptive fields from 22 MSTd cells from monkey I-left (Fig. 3.3 b), and a map that contains superimposed receptive fields from 20 MSTd cells from monkey I-right (Fig. 3.3 c).
Note that in this analysis we included only those receptive fields with an estimated fitted center not residing more than 10 degrees outside of the monitor in either the horizontal or vertical direction. This means that there's an underestimation of the coverage of the receptive field with horizontal eccentricity exceeding an absolute value 40°, or vertical eccentricity exceeding an absolute value of 25° in monkey S, and 30° in monkey I-left and monkey I-right.

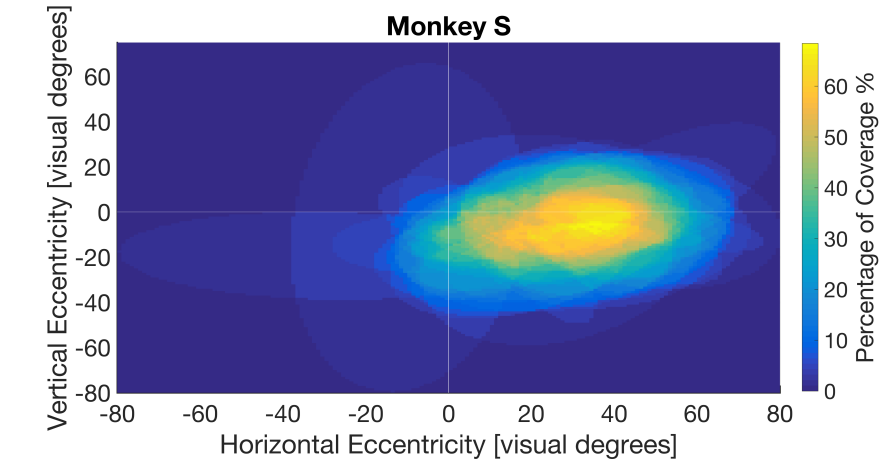

(a)

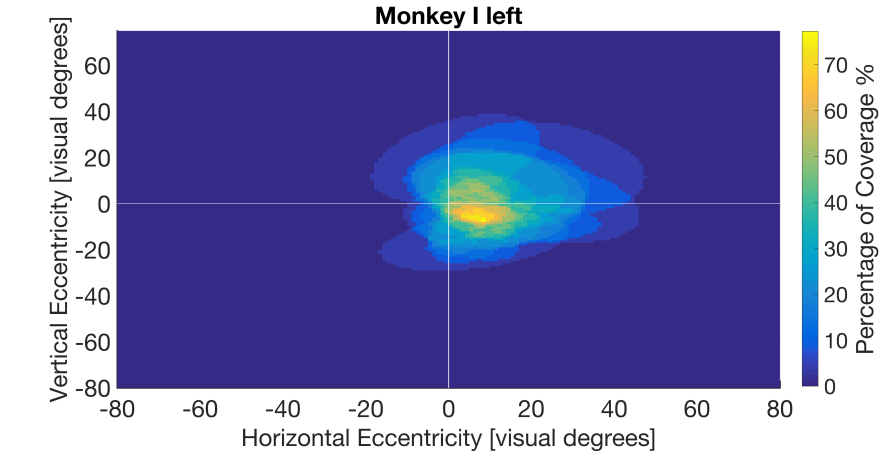

(b)

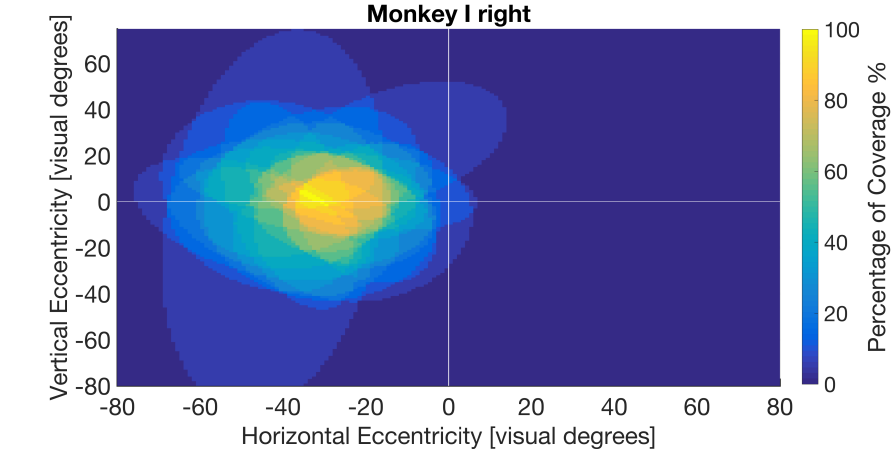

(c)

Fig. 3.3 Percentage of visual field coverage by the fitted receptive fields. Warmer colors in a given pixel of the visual field indicate higher percentage of coverage, i.e. percentage of fitted receptive fields that include that given pixel within their spatial boundaries. Intersection of white lines indicates the center of the visual field. **a -** Visual field coverage by the fitted receptive fields (of 57 cells) in monkey S. **b -** Visual field coverage by the fitted receptive fields (of 22 cells) in monkey I-left. **c -** Visual field coverage by the fitted receptive fields (of 20 cells) in monkey I-right.

3.2.3 Miscellaneous Measurements

We investigated whether the total number of spikes that a cell produced in response to the Automatic Mapping stimulus influences the goodness of fit of the fitting procedure to the receptive field as defined by R squared. The R squared is correlated significantly with the total number of spikes (Spearmann's rank correlation test, rho = 0.23, $p < 0.05$) (Fig. 3.4 a).

We also studied whether the total number of samples of Automatic Mapping stimuli shown to a given cell influences the goodness of fit of that cell's receptive field as defined by R-square (Fig. 3.4 b). A relationship does not seem to exist between the goodness of fit and the number of Automatic Mapping samples (Spearmann's rank correlation test, rho = 0.14, $p > 0.05$). Note that in this plot, we observe visually two somehow seperable columns as a result of the fact, that many cells that did not produce a visually discernible receptive field with 5 samples on average per locations, and so the task was continued until 10 average samples per locations were achieved, and some cells underwent a 15 average samples per locations. In addition, partial trials where monkey broke gaze fixation were included (with presented samples not counted online), leading to a variable number of samples for every cell.

Finally to better learn if there was a relationship between size of the surface of the receptive field and the physical recording-chamber location from which a cell was recorded, we created a spatial map of recording sites relative to the center of each recording chamber facilitate observing any such correlation (Fig. 3.5). Such a map serves to learn better about the relationship of topography in the area MSTd and functional spatial properties of the cells. We have not conducted any further analysis analysis regarding these maps.

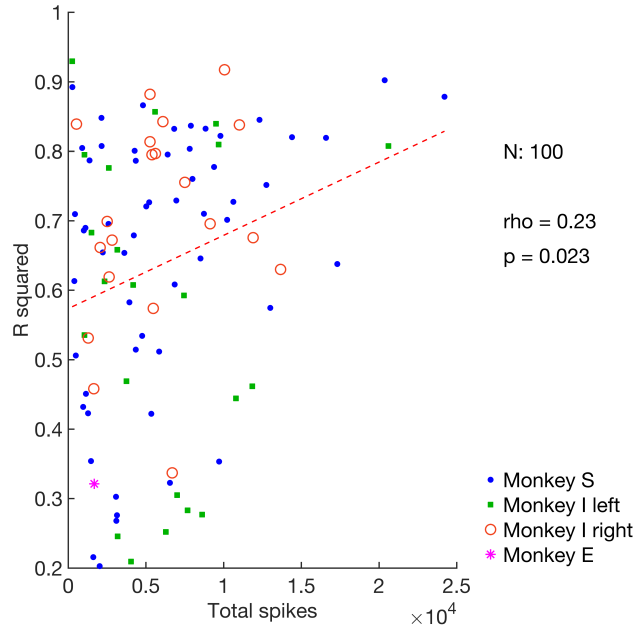

(a)

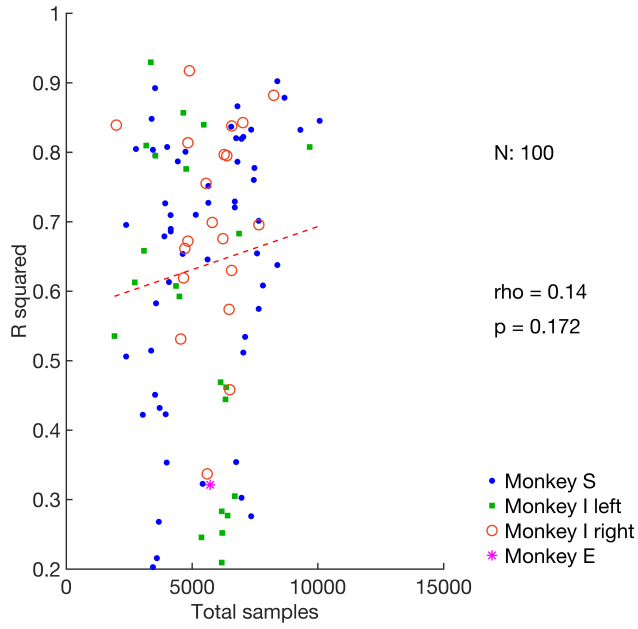

(b)

Fig. 3.4 Interaction of spike and sample number with the goodnness of fit as defined as r-square. **a -** The goodness of fit as defined as R squared is plotted against the total number of spikes which entered the Automatic Mapping task. **b -** The goodness of fit as defined as R squared is plotted against the total number of samples which were presented to a cell during the Automatic Mapping task. Dotted line is a linear regression model fitted to the data.

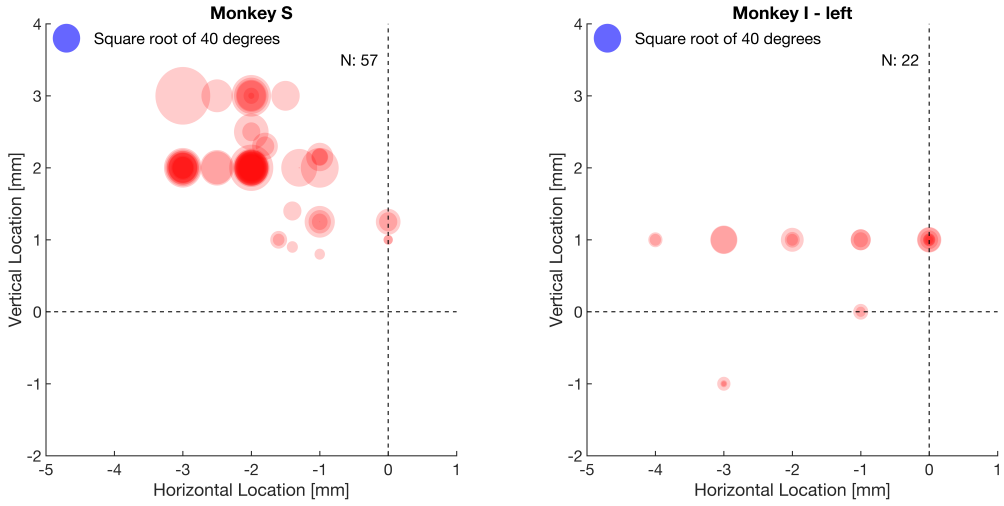

(a)

(b)

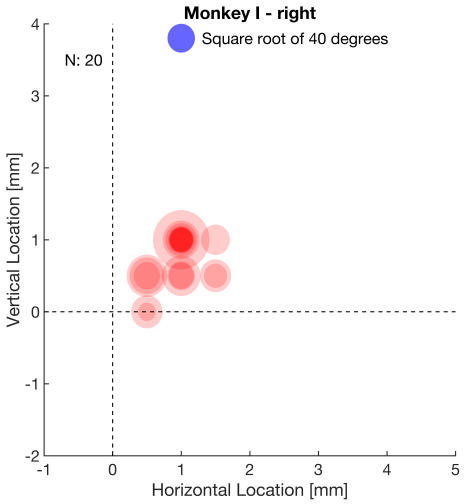

(c)

Fig. 3.5 Recording sites in monkey S, I left, and I right. This map outlines the physical locations of recording sites in relation to the center of the recording chamber. Circles of different sizes indicate the square root area of the receptive field (as extracted from the fitting procedure) in those locations. Note here that only those receptive fields which were successfully fitted are included here. On many locations circles overlap. **a -** Recording sites in monkey S. **b -** Recording sites in monkey I-left. **c -** Recording sites in monkey-I right.

3.3 Tuning Task

In total 169 cells underwent the Tuning task (108 from monkey S, 24 from monkey I-left, 35 from monkey I-right, and 2 from monkey E), with a minimum total number of spikes of 800 in this task.

3.3.1 Spiral and Linear Tuning

Not all cells had a significant spiral and linear tuning that is also acceptably fitted with Gaussian curves. We define here a satisfactory tuning if it was significantly different from noise (using an ANOVA test, p value < 0.05) and if the R squared resulting from a Gaussian curve fitted to the data was > 0.2. Accordingly, in all 169 cells there was a satisfactoy linear or spiral tuning in at least one tested location. 156 cells did have satisfactory spiral tuning in at least one tested location, versus 116 cells with satisfactory linear tuning in the central location. Of those, 107 cells had both satisfactory linear tuning in the central location and a satisfactory spiral tuning in at least one location. Of these, 82 cells had both satisfactory linear and spiral tuning in the central location. And finally, only 73 cells contained satisfactory spiral motion tuning in at least one tuning location in addition to the central location. Important to note here that we used a further requirement that was relevant in quantifying position invariance across cells, that is, for those 73 cells we only investigated tuning at the peripheral locations at the same speed as the optimal speed of the central spiral configuration.

As defined in the Methods section in equation nr. 3, we calculated *Directionality Index (DI)* for all cells (Fig. 3.6), in every configuration and in every tested speed. DI serves as a measure of tuning strength in different cells. Taking the highest spiral DI value for every cell across spiral configurations and at optimal speed (at the spiral configuration generating the highest DI), we arrived at a population mean = 0.6 (Fig. 3.6 A). Additionally, we took the linear DI at the one linear configuration and at the optimal speed, pooling across cells into one distribution (mean = 0.6) (Fig. 3.6 B).

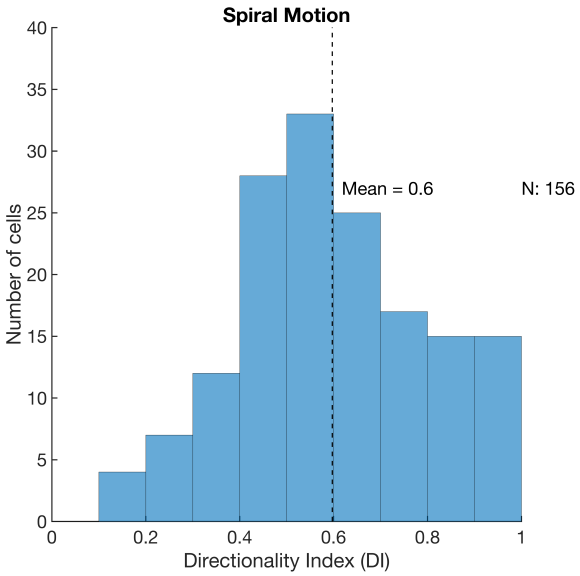

(a)

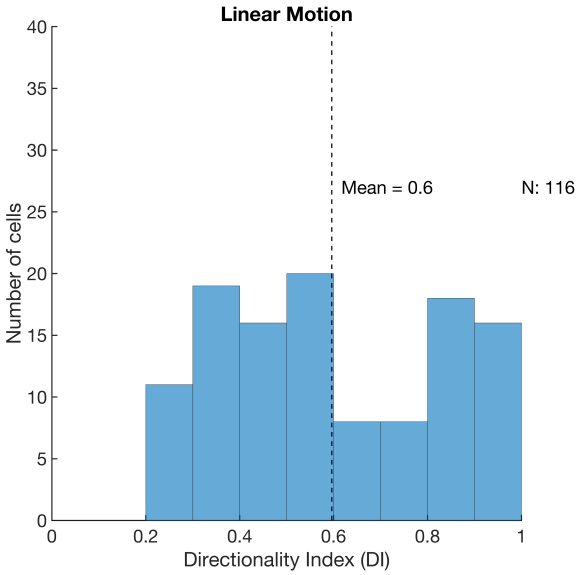

(b)

Fig. 3.6 Population distribution of Directionality Index (DI) for Spiral and Linear motion. **a -** Spiral motion DI across cells. **b -** Linear motion DI across cells.

To evaluate whether our cells are more strongly tuned to spiral or linear motion we evaluated a *Response Index (RI)* as outlined in equation nr. 4 for those 82 cells that had both satisfactory linear and spiral tuning at the central location (Fig. 3.7). The distribution of RIs across the population had a mean of 0.012, and was not significantly different from 0 (single sample t-test, p-value $>$ 0.05). This indicated that at the

population level, there was no preference for linear or spiral motion over the other motion type.

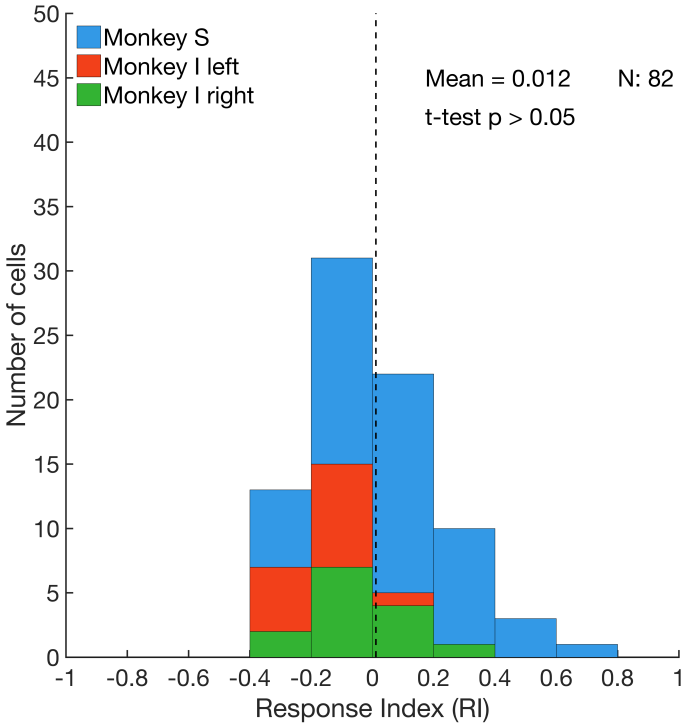

Fig. 3.7 Response Index (RI) across cells. Mean = 0.012 not significantly different from 0 (single sample t-test; p-value > 0.05).

To estimate whether MSTd neurons are more responsive to specific spiral or linear motion direction, we pooled the preferred spiral motion directions (across locations) at the optimal speed from every cell into one distribution, and the preferred linear motion directions at the optimal speed for every cell into another distribution (Fig. 3.8). As one can see from the figure, across the population there's a pronounced preference for 0° and 180° spiral motion directions which correspond to expansion and contraction respectively. This is an observation that was also found in a previous study using the spiral space stimuli (Graziano et al., 1994). No trend can be noticed in the linear motion direction preference.

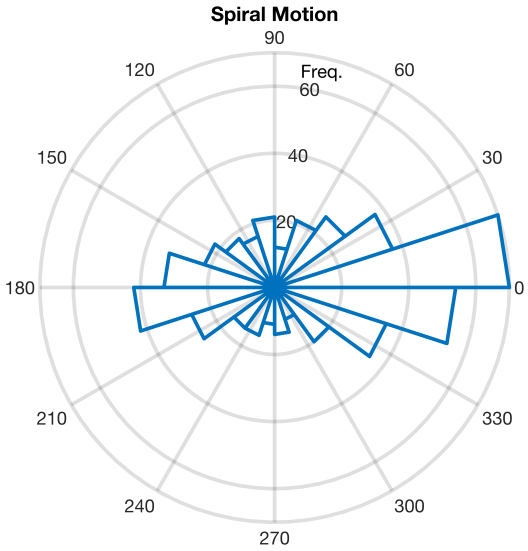

(a)

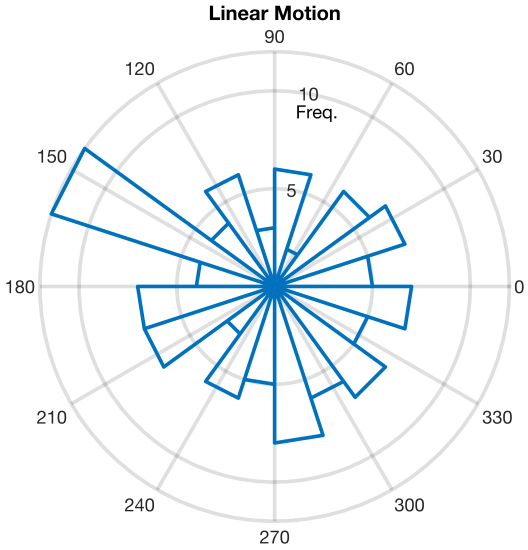

(b)

Fig. 3.8 Distribution of preferred directions for spiral and linear motion across neurons. **a -** Angular distance indicates spiral motion direction [expansion 0° direction, expansive clockwise spiral 45°, clockwise rotation 90°, contractive clockwise spiral 135°, contraction 180°, contractive counter-clockwise spiral 225°, counter-clockwise rotation 270° and expansive counter-clockwise spiral 315°]. **b -** Angular distance indicates linear motion direction [upward 0° direction, upward rightward 45°, rightward 90°, downward rightward 135°, downward 180°, downward leftward 225°, leftward 270° and upward leftward 315°].

3.3.2 Goodness of Placement

We calculated a *Goodness of Placement (GP)* measure as outlined in equation 5 for every tuning location: we expected that a better placement of a tuning stimulus within the receptive field yields a higher response of the cell to the stimulus, and a more pronounced tuning to the different motion directions presented within that stimulus at that location. In (Fig. 3.9 a) we plotted on the y-axis the maximal firing rate the cell generated in every spiral configuration (at the optimal speed and across directions), and the maximal firing rate the cell generated in the only linear configuration (at the optimal speed and across directions). On the x-axis we plotted GP for the corresponding tuning locations. Conducting a Spearman's rank correlation test we observed as expected positive correlation between DI and GP (coefficient = 0.32, p value < 0.001).

We then studied whether there was an interaction between strength of directionality and the goodness of placement. We plotted in (Fig. 3.9 b) on the y-axis the several DI measures for every cell, one for every spiral configuration (at the optimal speed) and one DI for the one linear configuration (at the optimal speed); and on the x-axis we plotted the GP for each corresponding tuning configuration. Conducting a Spearman's rank correlation test we observed a negative correlation between DI and GP (coefficient = -0.41, p value < 0.001). This suggests that the better a stimulus is placed within the receptive field the higher the response, however a better placement of the tuning stimuli yielded a response of the cell that is less well directional to linear and spiral space motion.

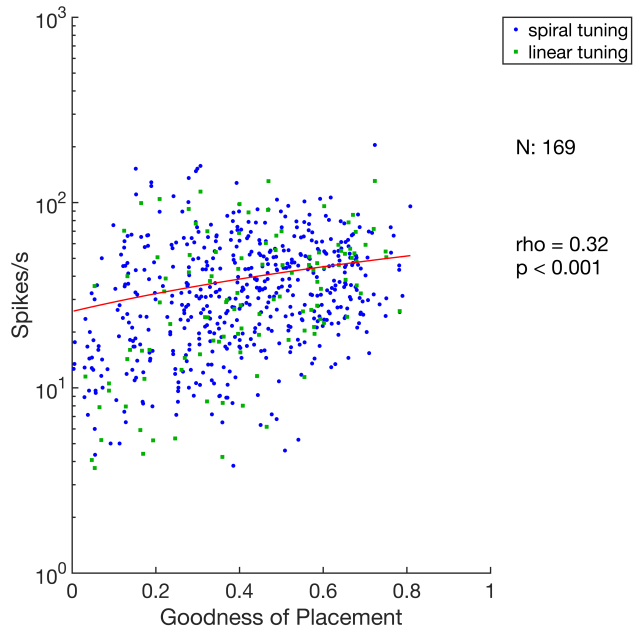

(a)

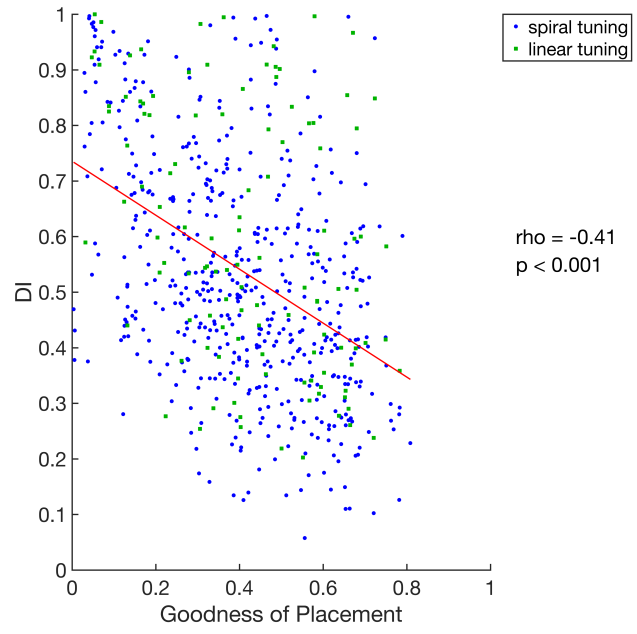

(b)

Fig. 3.9 Goodness of Placement and its influence on neural response across cells. **a -** Interaction between Goodness of Placement and the highest firing rate generated in a given tuning location. Linear regression model was fitted to the data (red line). **b -** Interaction between Goodness of Placement and the linear and mean spiral directionality index in a given tuning location. Linear regression model was fitted to the data (red line)

3.3.3 Position Invariance

To investigate the property of position invariance for spiral motion across cells, we employed several measurements: We aimed first to reproduce the results from (Graziano et al., 1994) as outlined in the introduction. First DI was calculated for the central tuning location (DIcenter), and for all peripheral locations (DIsurround) where there was significant and acceptable tuning present. Then we calculated a Position Invariance Index (PI) as ($PI = DI_{surround} / DI_{center}$) for every peripheral location. All PIs were then pooled into one population distribution as can be see in (Fig. 3.10). Remarkably, this distribution bears a great resemblance to the data from the study of Graziano et al. (1994) (Fig. 3.11): Not only does the distribution peak at the value of 1 indicating a large invariance in the directionality across tuning locations, but also there were few PIs with values less than 0. This indicates that there are few preferred direction selectivity reversals across cells.

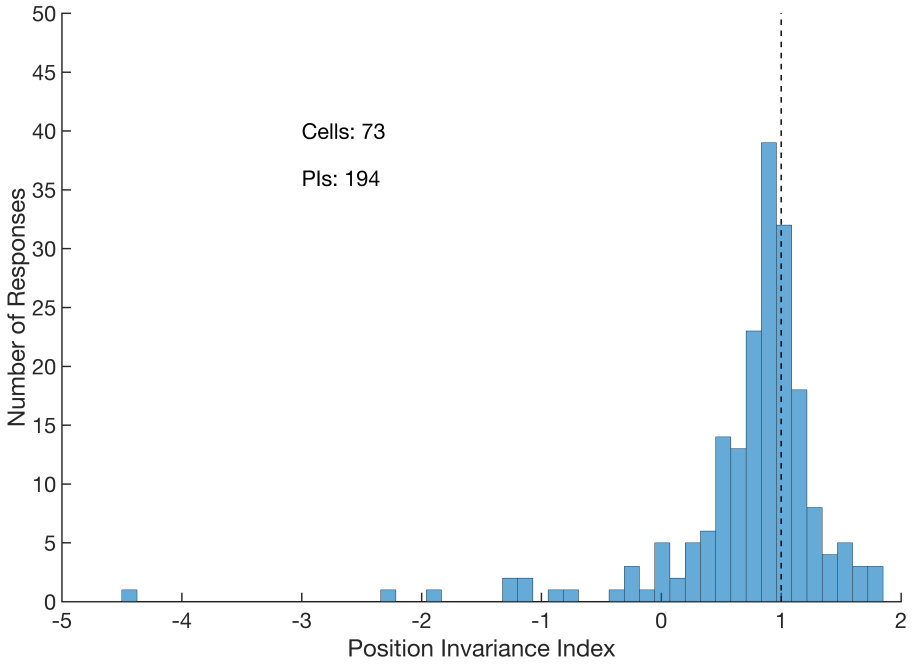

Fig. 3.10 Distribution of pooled PI across cells. The peak at value 1 and scarcity of negative values indicate a mostly position invariant profile of MSTd neurons.

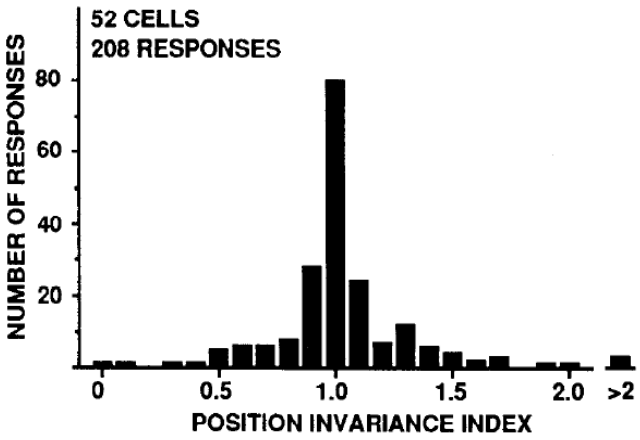

Fig. 3.11 Distribution of position invariance indices (PIs) across four tuning locations and across cells (Graziano et al., 1994). PI at a given location with a value of 1 indicates that the directionality index remained unaltered at that location and at the central location. Negative value indicate that there was a reversal in motion direction preference at the same location. The number of *Responses* indictates the total number of PIs across cells. *Adapted from* Graziano et al. (1994), *with permission from the first Author Michael S. Graziano.*

To better quantify position invariance, and to address the issue that we raised in the introduction chapter that the selectivity of a neuron to a given motion direction should be addressed separately from its directionality, we looked at the percentage of tuning locations where there was no reversal in spiral motion direction selectivity. After extracting the preferred spiral motion direction at the central location at the optimal speed, we extracted the preferred spiral motion direction at the peripheral locations at the optimal speed of the central location. We defined a reversal in the direction selectivity if there was an angle difference > 90° between any peripheral preferred direction and the central preferred direction (for example, the angle difference between a motion of expansion and that of rotation = 90°) (Fig. 3.12).

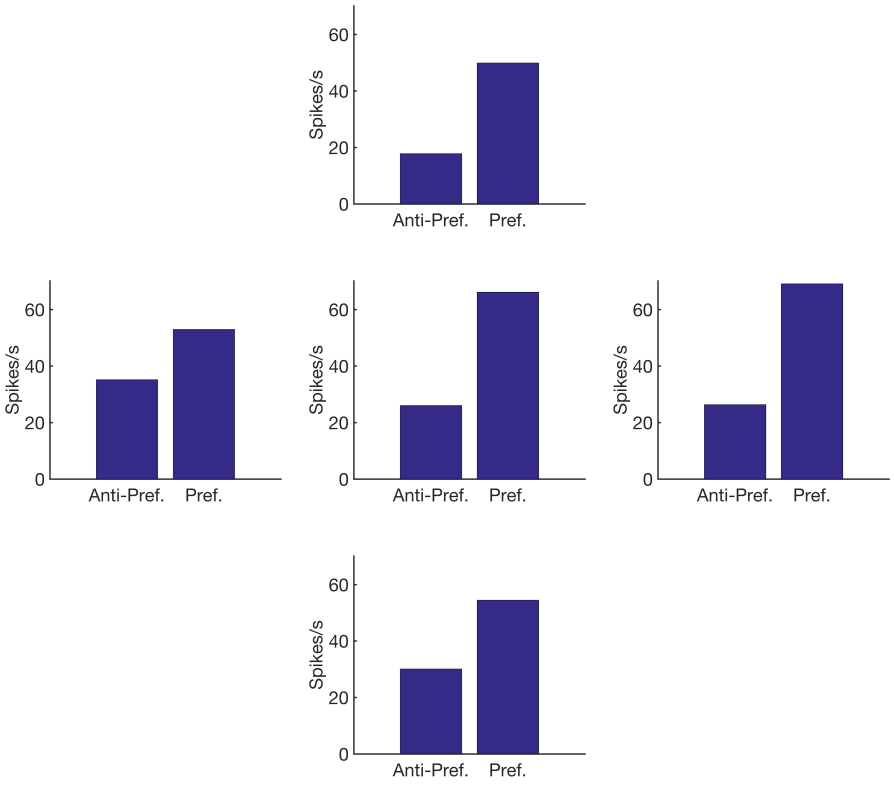

Fig. 3.12 Position invariance in an example neuron. We plotted the fitted response of the neuron to the preferred and anti-preferred spiral motion direction in all tuning locations. The lack of reversal in the response profile in any location indicates position invariance. *Example cell: 20170203_sun_34.1.*

Out of 73 cells that contained satisfactory spiral motion tuning in at least one tuning location in addition to the central location, we found no reversal in selectivity to the preferred motion direction in 58 cells (80%) (Fig. 3.13 a), here we calculated a *Percentage of Invariance* as (100 X number of locations with direction reversal/total number of peripheral locations with a significant tuning). Further analysis showed that in 77% of the cells had their preferred direction varying across locations within a range of 90°, reflecting a strong invariance in the spiral motion direction preference across tuning locations (Fig. 3.13 b). As control, the same analysis was conducted with randomely generated preferred directions replacing every significant preferred direction for every cell. This control analysis was conducted a 100 times, and was plotted in (Fig. 3.13 b) in red lines.

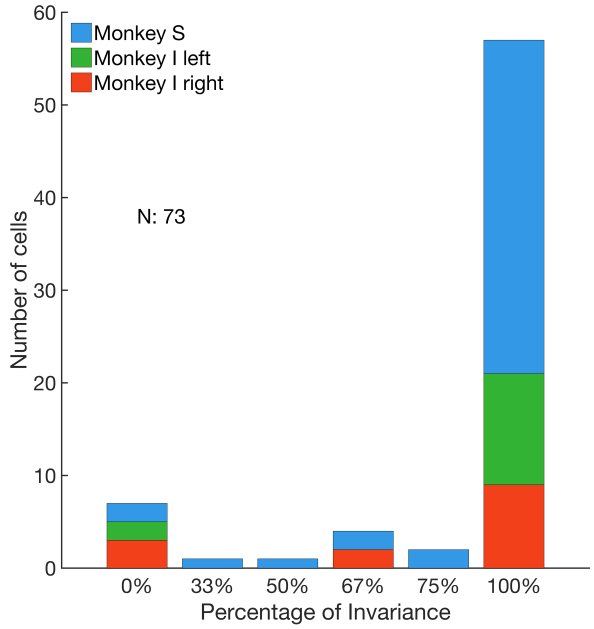

(a)

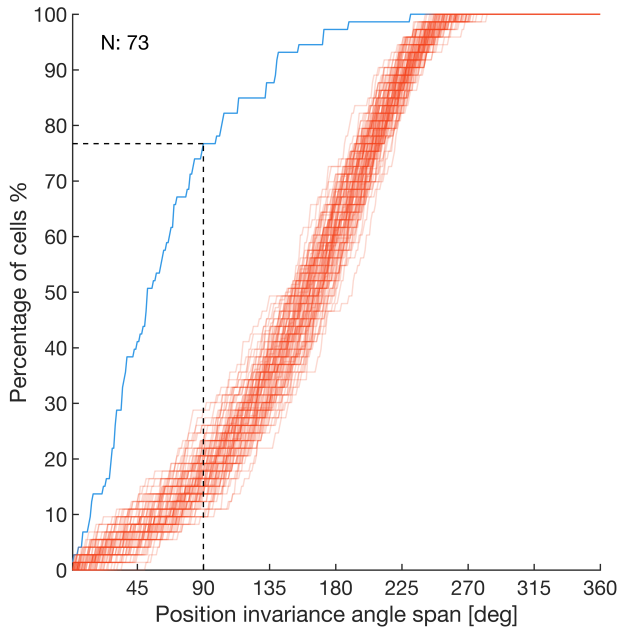

(b)

Fig. 3.13 Position invariance across cells. **a -** the percentage of peripheral tuning locations where a reversal in spiral motion direction selectivity was not observable. In total, 58 cells did not have motion direction selectivity reversal in any tuning location, with few cells having reversal in selectivity in one or more locations. **b-** A cumulative histogram of the angle span within which the preferred directions in all tuning locations are found across all cells. The figure shows for example that 77% of cells retain all their preferred motion directions within an interval of 90°. Red curves are the same analysis conducted on randomely generated data-sets.

Finally, we addressed the issue whether there is the feature of position invariance is stronger in those cells that are more stongly directional to spiral tuning stimuli. Indeed as we can see in (Fig. 3.14), there is a significant negative correlation between DI, the directionality index of a cell towards spiral space stimuli at the central tuning location, and the angle span of position invariance within which all the preferred directions of a cell can be found (Spearmann's rank correlation test, rho = -0.28, $p < 0.05$). This indicates that better directional cells are more likely to be increasingly position invariant.

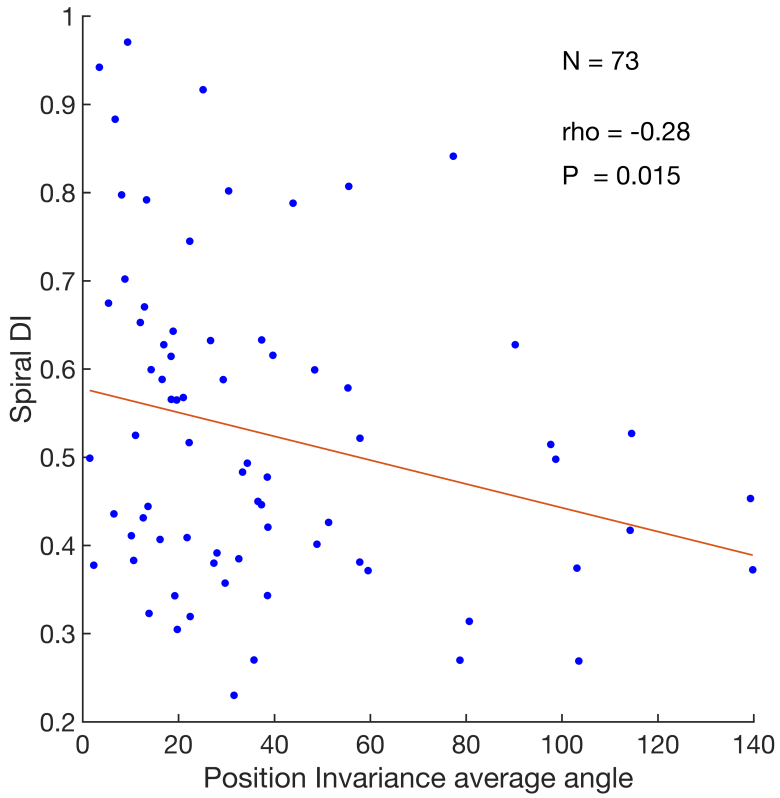

Fig. 3.14 Spiral directionality in relation to Position invariance. Negative significant correlation between how well directional a cell is to spiral space stimuli and how well position invariance it is (Spearmann's rank correlation test, rho = -0.28, $p < 0.05$). Linear regression model is fitted to data as a red line.

3.4 Reverse Correlation Task

In total 160 cells underwent in the Reverse Correlation Task (109 from monkey S, 12 from monkey I-left, 37 from monkey I-right, and 2 from monkey E). We imposed two selection criteria on these cells: We defined a criterion of a *minimal spike number* to

be equal to the lowest spike number that was produced by a cell that was successfully mapped in this task (as will be explained here below). All cells with total spike numbers lower than the minimal spike number (< 658 spikes) were removed from further analysis. Further more, we defined a criterion of a *minimal sample number* to be equal to the lowest total sample number that was presented to a cell that was successfully mapped in this task. All cells that were presented with a lower total sample number than the minimal sample number (< 2430 samples) were removed from further analysis. Thus, we were left with 150 cells (101 from monkey S, 11 from monkey I-left, 36 from monkey I-right, and 2 from monkey E).

3.4.1 Recovering Receptive Field Maps

The method of reverse correlation as applied in this study was successful in recovering partial receptive field maps for 38 out of 150 cells (25%) (Fig. 3.15, 3.16, 3.17, 3.18, 3.19). As defined in the Methods section, a map for a cell is successfully recovered if it contains a cluster of at least 3 neighboring segments, that are each significantly different from uniformity for at least 2 consecutive analysis time frames (one analysis time frame = 5 ms).

In (Fig. 3.20) we plot the number of significant segments that were recovered for all the 38 cells. In (Fig. 3.21 a) we created a histogram of the number of significant segments across cells (population median = 6 significant segments/cell). We compared the spatial extent of the recovered Reverse Correlation (RC) maps to the spatial maps acquired during the Automatic Mapping task, and we calculated a coverage percentage: the percentage of the receptive field recovered through Automatic Mapping that was also recovered in the RC map (Fig. 3.21 b). Across cells where both Automatic Mapping and Reverse Correlation tasks were run successfully (25 cells), RC maps had a median of only 6 % of the Automatic Mapping receptive field successfully mapped. Indicating that reverse correlation analysis recovered the directional and spatial structure of only partial regions of the receptive fields.

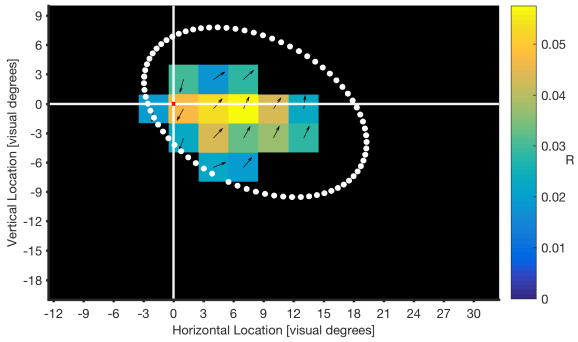

(a) Cell nr.1: 20151126_sun_34.1, Monkey S

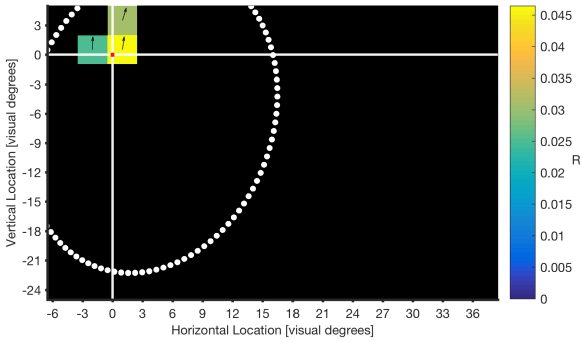

(b) Cell nr.3: 20160112_sun_35.1, Monkey S

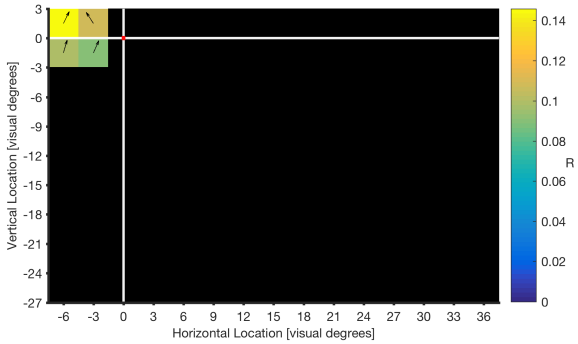

(c) Cell nr.10: 20160115_sun_36.5, Monkey S

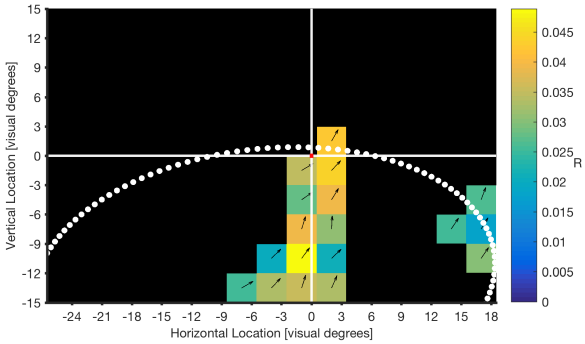

(d) Cell nr.11: 20160119_sun_35.1, Monkey S

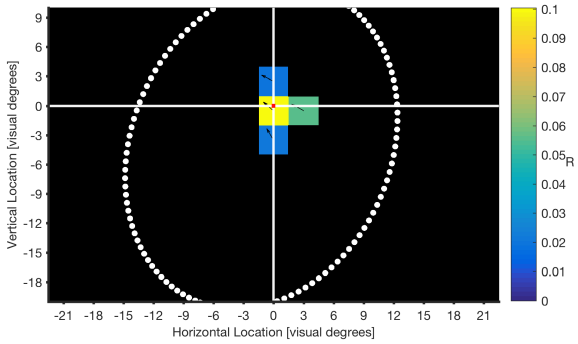

(e) Cell nr.14: 20160202_sun_34.1, Monkey S

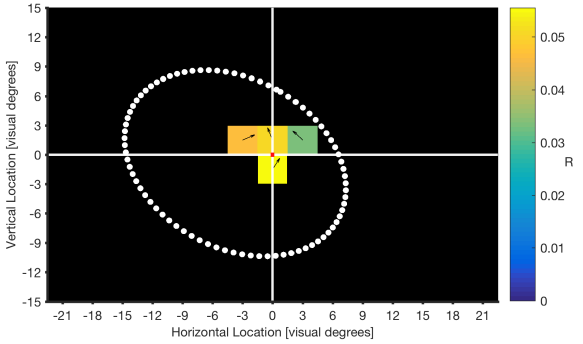

(f) Cell nr.16: 20160204_sun_35.1, Monkey S

Fig. 3.15 Compilation of all recovered Reverse Correlation maps. Dotted white line indicate the fitted receptive field's borders as outlined in the Method chapter. Intersection of horizontal and vertical white lines indicate the location of the fixation point. We note however that some cells did not generate an acceptable fit in the Automatic Mapping task and their borders were not indicated here. Compilation - part 1.

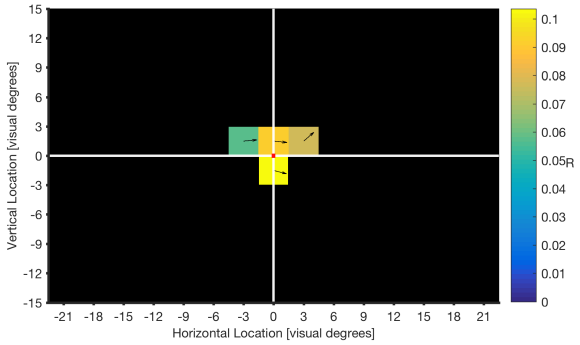

(a) Cell nr.17: 20160204_sun_35.2, Monkey S

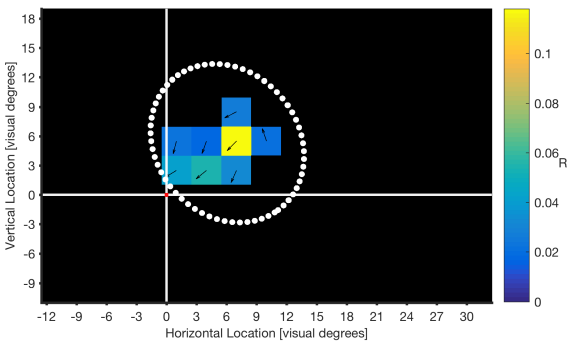

(b) Cell nr.19: 20160218_sun_33.1, Monkey S

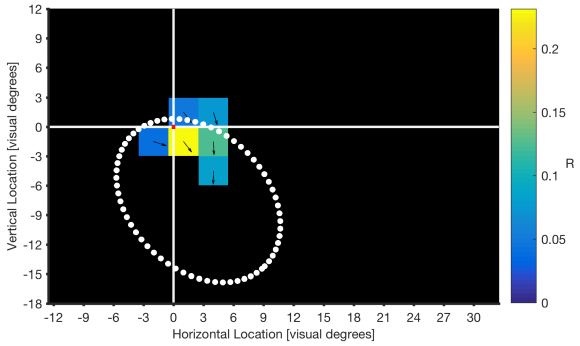

(c) Cell nr.20: 20160219_sun_35.1, Monkey S

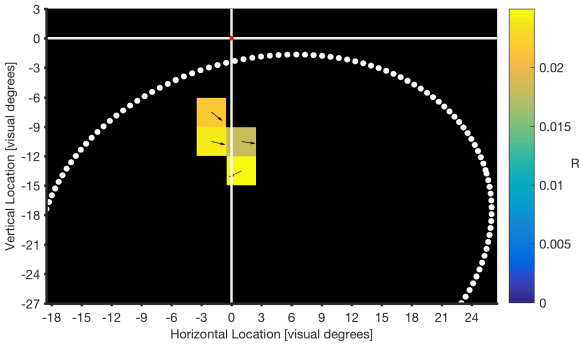

(d) Cell nr.22: 20160309_sun_34.2, Monkey S

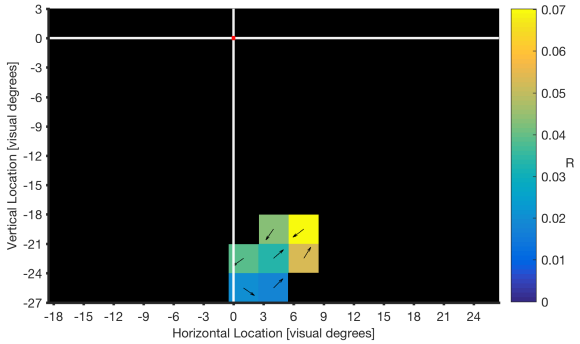

(e) Cell nr.23: 20160309_sun_34.3, Monkey S

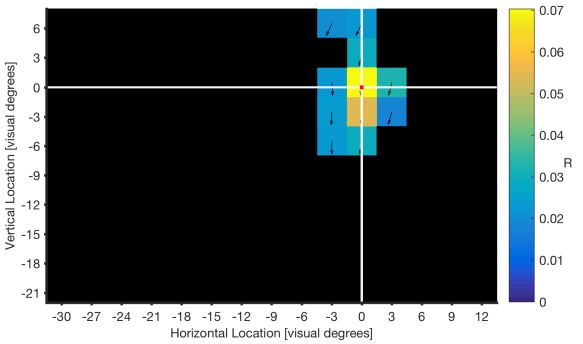

(f) Cell nr.27: 20160421_sun_34.1, Monkey S

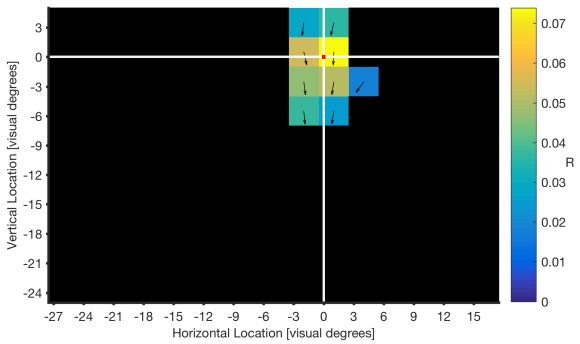

(g) Cell nr.30: 20160426_sun_34.1, Monkey S

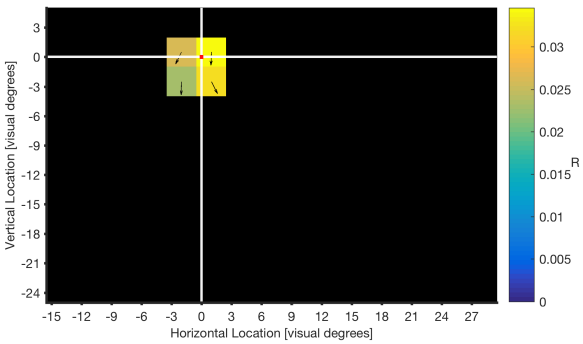

(h) Cell nr.32: 20160428_sun_34.2, Monkey S

Fig. 3.16 Compilation of all Reverse Correlation maps - part 2.

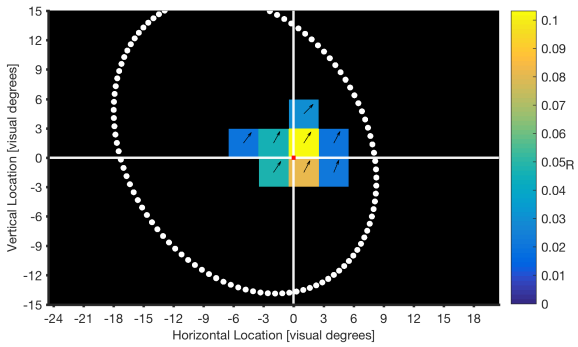

(a) Cell nr.34: 20160503_sun_34.1, Monkey S

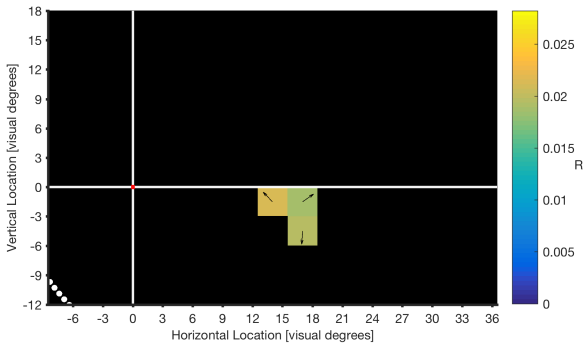

(b) Cell nr.38: 20160602_sun_34.1, Monkey S

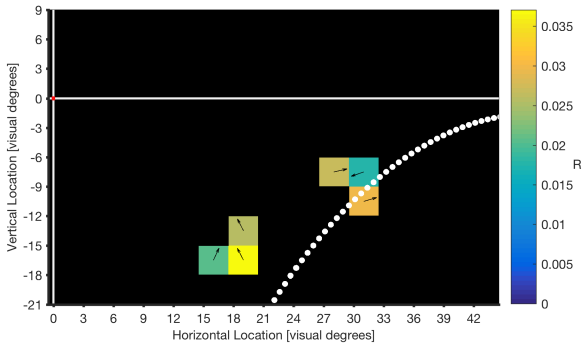

(c) Cell nr.45: 20160630_sun_33.1, Monkey S

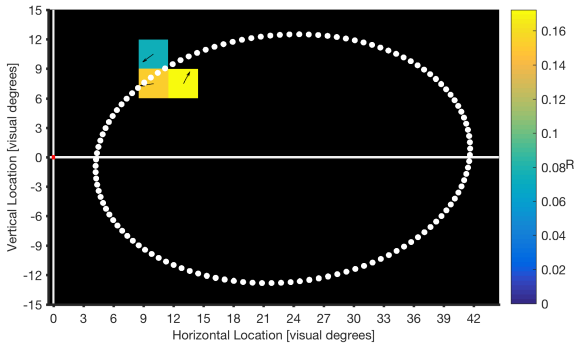

(d) Cell nr.51: 20160707_sun_33.2, Monkey S

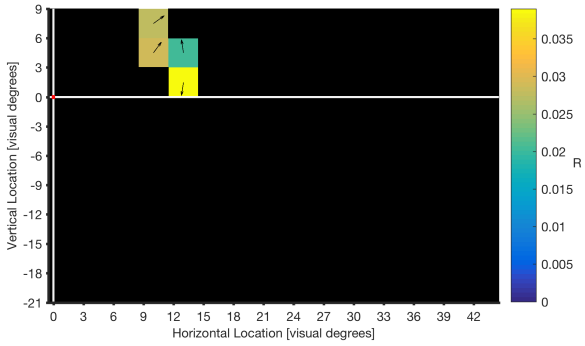

(e) Cell nr.53: 20160712_sun_33.1, Monkey S

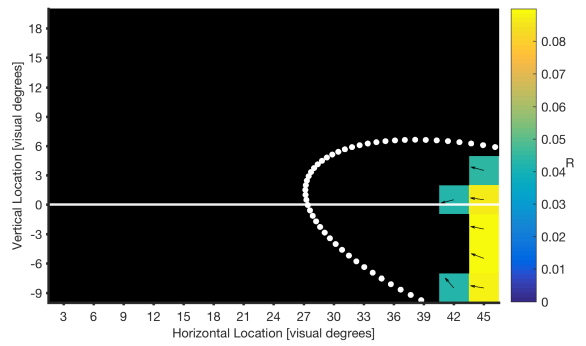

(f) Cell nr.56: 20160714_sun_33.1, Monkey S

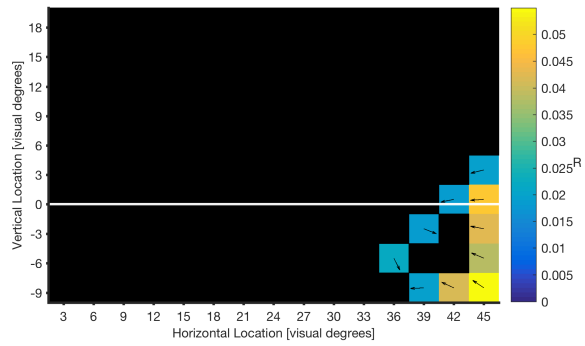

(g) Cell nr.57: 20160714_sun_33.2, Monkey S

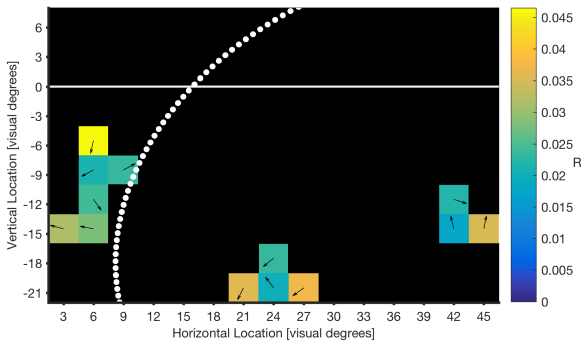

(h) Cell nr.58: 20160715_sun_33.1, Monkey S

Fig. 3.17 Compilation of all Reverse Correlation maps - part 3.

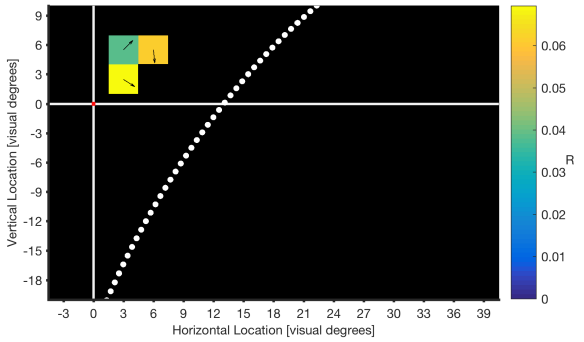

(a) Cell nr.59: 20160720_sun_33.1, Monkey S

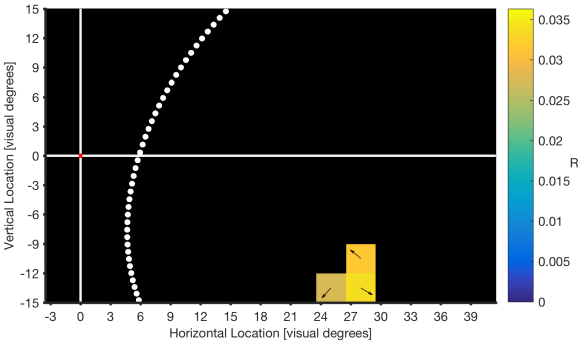

(b) Cell nr.72: 20160811_sun_34.1, Monkey S

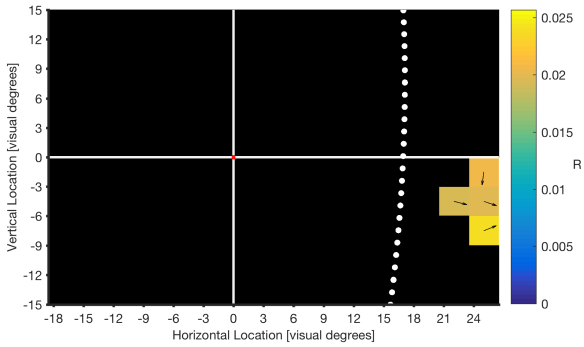

(c) Cell nr.85: 20161115_sun_34.1, Monkey S

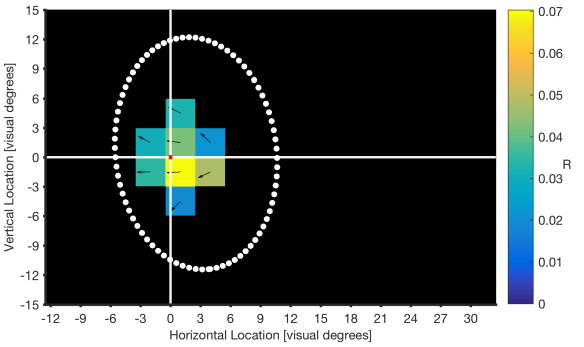

(d) Cell nr.133: 20170302_sun_97.1, Monkey I-left

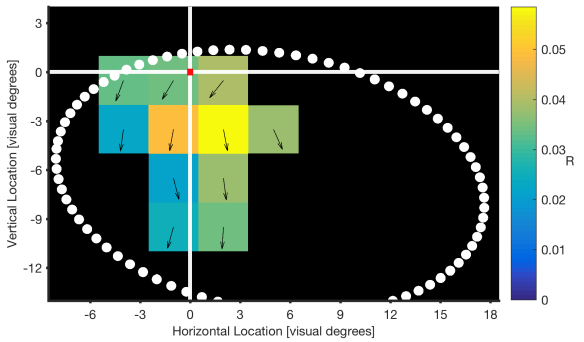

(e) Cell nr.135: 20170315_sun_97.1, Monkey I-left

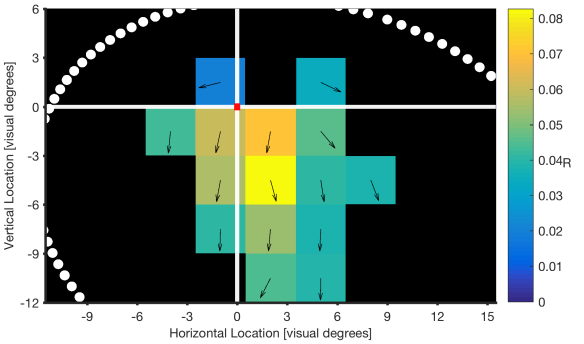

(f) Cell nr.136: 20170316_sun_97.1, Monkey I-left

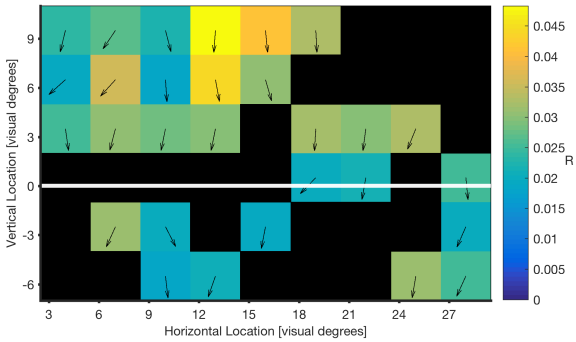

(g) Cell nr.141: 20170726_sun_117.1, Monkey I-left

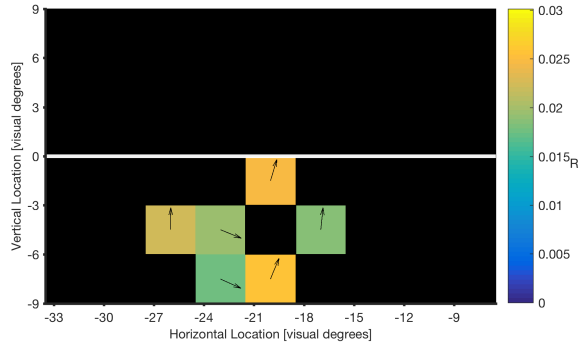

(h) Cell nr.145: 20180621_sun_121.1, Monkey I-right

Fig. 3.18 Compilation of all Reverse Correlation maps - part 4. Starting from (e), the small configuration (6 X 9 segments) of the RC stimulus is used throughout the rest of the cells.

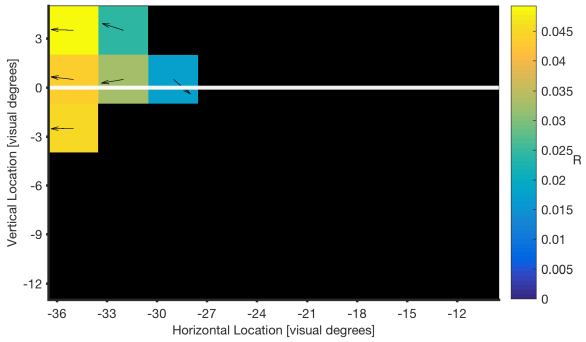

(a) Cell nr.152: 20180725_sun_131.1, Monkey I-right

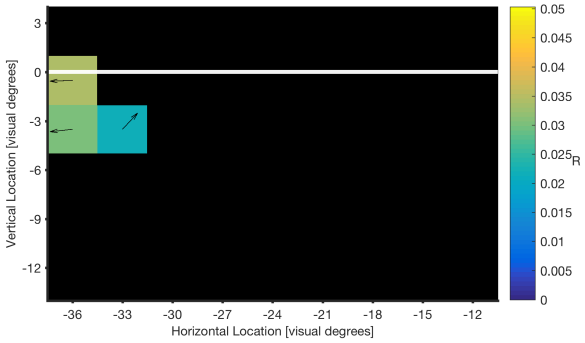

(b) Cell nr.154: 20180730_sun_131.1, Monkey I-right

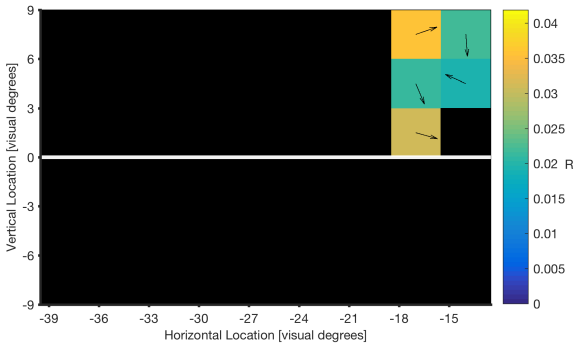

(c) Cell nr.155: 20180829_sun_129.1, Monkey I-right

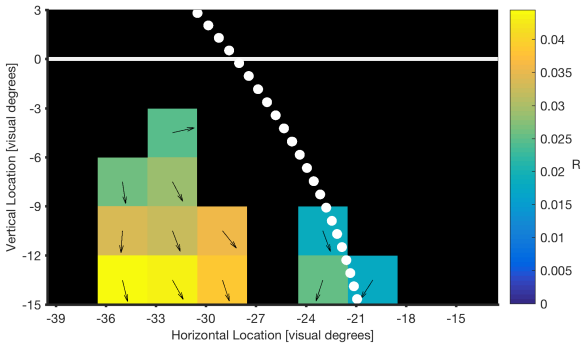

(d) Cell nr.172: 20181003_sun_129.1, Monkey I-right

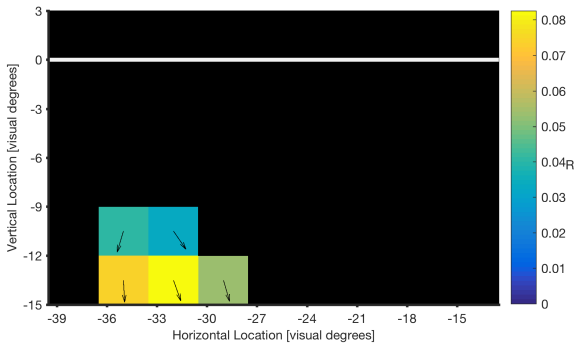

(e) Cell nr.173: 20181003_sun_129.2, Monkey I-right

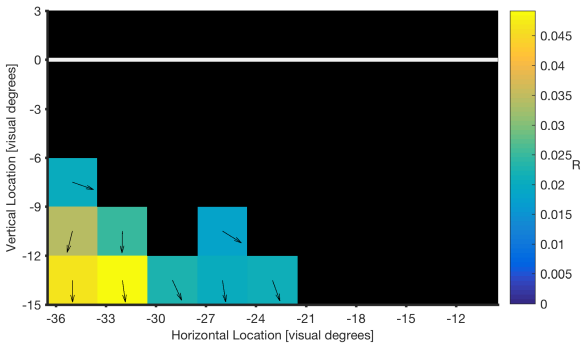

(f) Cell nr.175: 20181004_sun_129.1, Monkey I-right

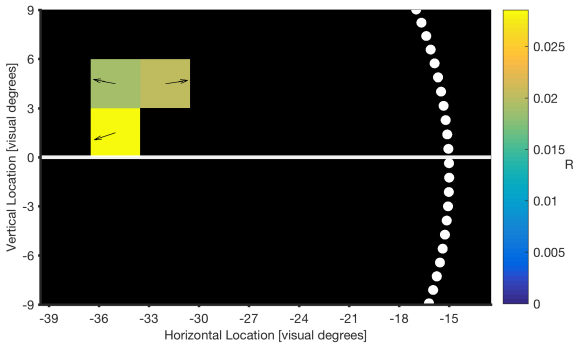

(g) Cell nr.177: 20181017_sun_131.1, Monkey I-right

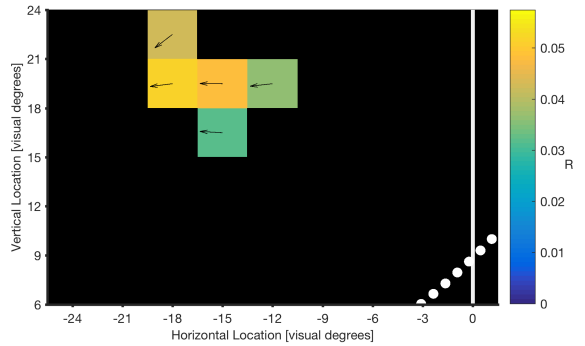

(h) Cell nr.181: 20181022_sun_129.1, Monkey I-right

Fig. 3.19 Compilation of all Reverse Correlation maps - part 5.

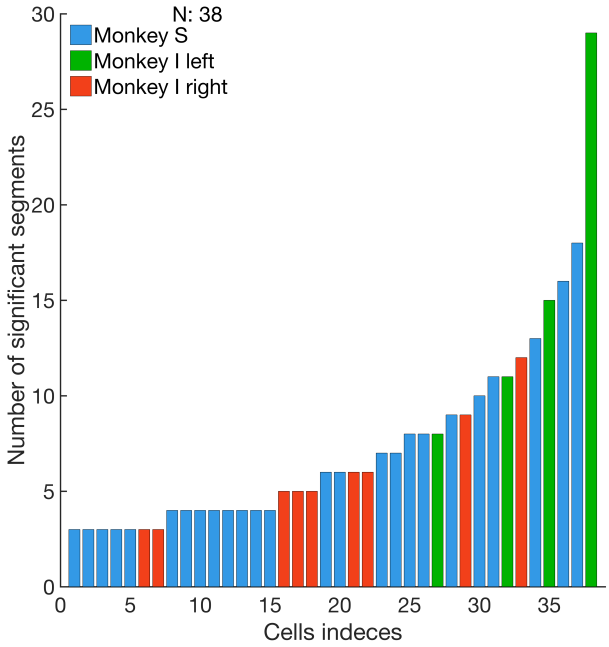

Fig. 3.20 Number of significant segments across cells with recovered RC maps.

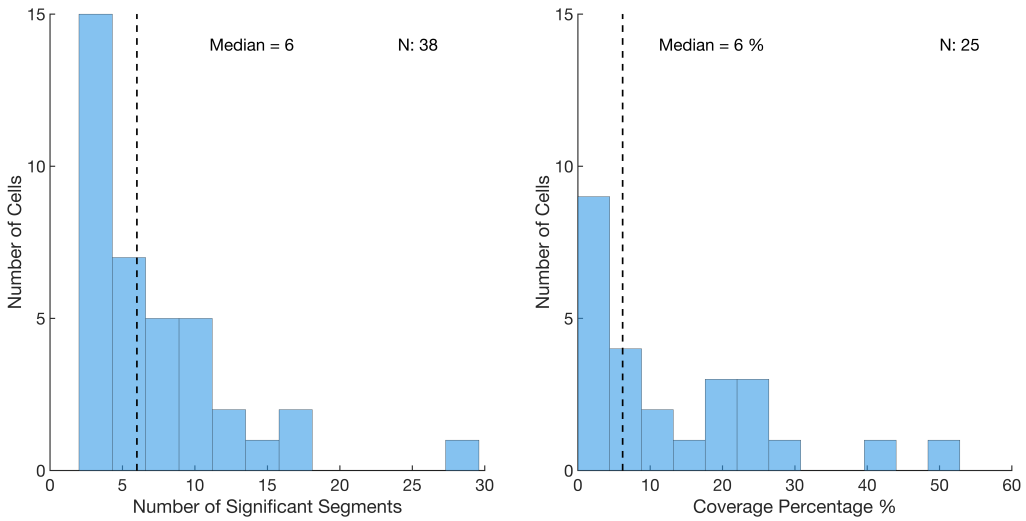

(a) (b)

Fig. 3.21 Distribution of significant segments numbers and receptive field coverage. A: Distribution of significant segments numbers across cells with recovered RC maps (N: 38 cells, median = 6 segments). B: Distribution of receptive fields coverage percentages numbers across cells with recovered RC maps and with acceptable Automatic Mapping fit (N: 125 cells, median = 6 %).

Interestingly there appears to be a relationship between how well a cell is directionally tuned to linear and spiral tuning stimuli and whether it can be successfully mapped using our method of reverse correlation. (Fig. 3.22) shows that those cells that were successfully mapped had clearly higher linear and spiral directionality index values in comparison to those cells with no significant RC maps. Specifically, by establishing an arbitrary threshold where spiral DI = 0.5 and linear DI = 0.5, distinguishing between well directional cells (with spiral and linear DI > 0.5) and those that are less clearly directional, we find that 52% of those cells that are better directional were successfully mapped with the method of reverse correlation.

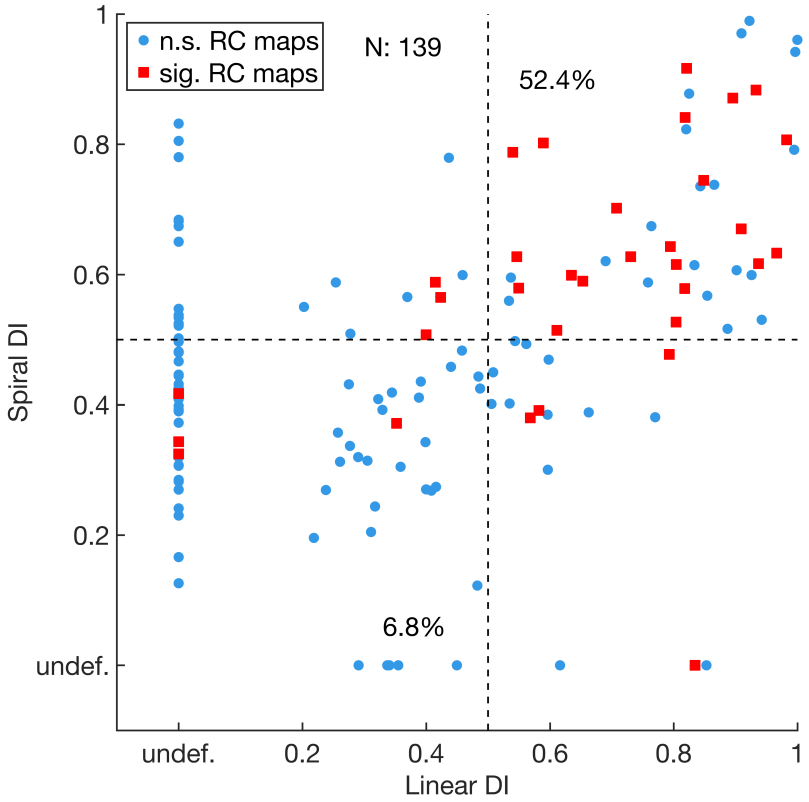

Fig. 3.22 Linear and spiral directionality scatter plot of all cells that participated in the Reverse Correlation task and Tuning. While 139 cells underwent both tasks (blue circles), we recovered significant RC maps for 33 cells (red squares). If the cell had non-significant or poor fitted linear (in central location at any speed) or spiral (in any location or any speed) tuning (r-square < 0.2 or ANNOVA p > 0.05), its DI was deemed as undefined.

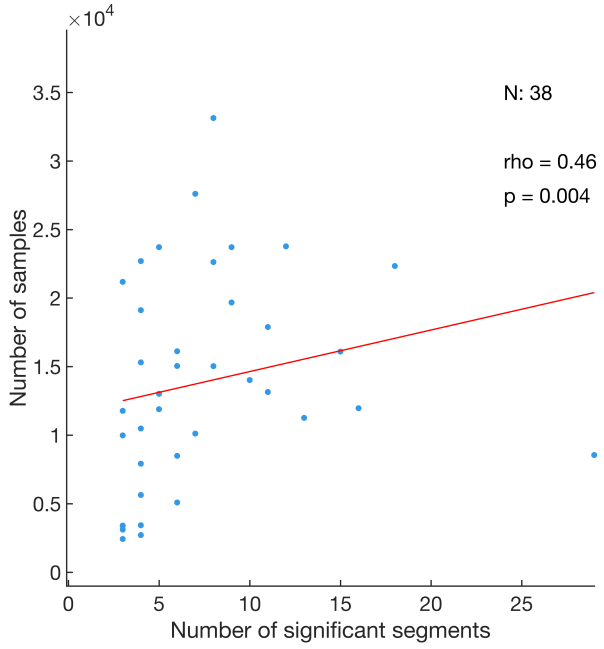

(a)

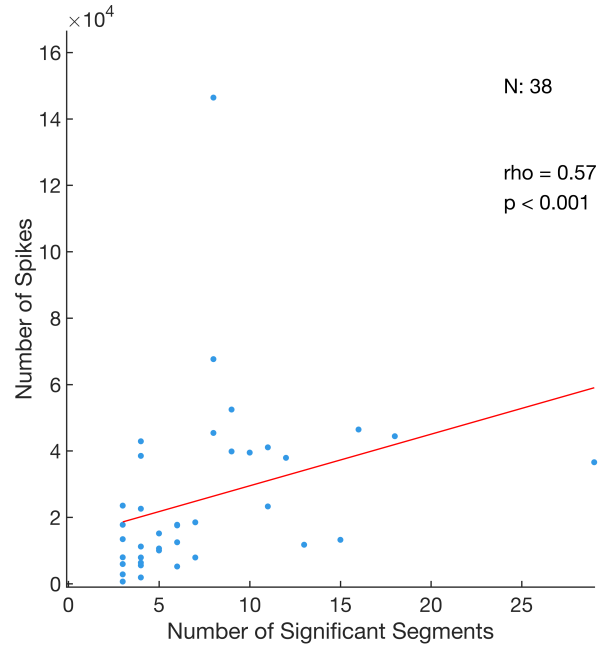

(b)

Fig. 3.23 Influencing factors and number of significant segments in the recovered RC maps. **a -** Total number of RC stimulus presentation samples is plotted against number significant segments; significant correlation is found (Spearmann's rank correlation test; coefficient = 0.46, p value < 0.01). **b -** Total number of spike number entering the reverse correlation analysis is plotted against number significant segments; significant correlation is found (Spearmann's rank correlation test; coefficient = 0.57, p value < 0.001). Linear regression model is fitted to the data to illustrate correlation.

We found there was a significant positive correlation between the number of sample presentations in a Reverse Correlation task and the number of significant segments in successfully mapped receptive fields (Spearmann's rank correlation test; coefficient = 0.46, p value < 0.01)(Fig. 3.23 a). Additionally, there was a significant positive correlation between the total number of spikes that a neuron emitted in response to the RC stimulus during the experiment and the number of significant segments (Spearmann's rank correlation test; coefficient = 0.57, p value < 0.001)(Fig. 3.23 b).

3.4.2 Preferred Motion Patterns

By studying the preferred motion patterns as revealed in the significant RC maps across 38 cells, we note that most of the RC maps share a mostly homogenous linear motion preference dominating across the map. To better assess this tendency, we conducted the following analysis: for every cell with a recovered RC map, we calculated an averaged motion direction across all local motion directions of significant segments. We then pooled the differences in motion direction between the calculated mean and the individual motion directions in all significant segments. And then we pooled again across cells the pooled differences into a cumulative distribution (Fig. 3.24).

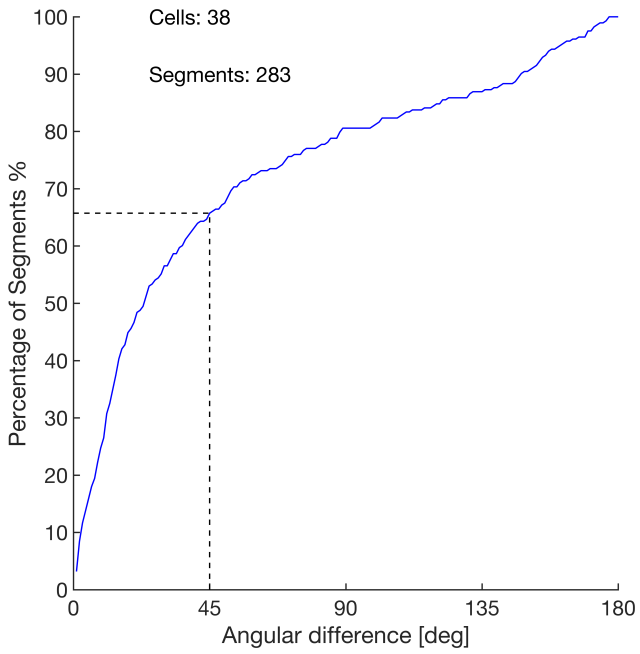

Fig. 3.24 Cumulative distribution of angular differences between preferred motion direction in individual segments and the mean motion direction of an RC map.

We can see that over 65% of all segments vary within 45° of the average motion direction of the map, confirming the general linear preferences as observed in the recovered RC maps. This contrasts sharply with known selectivity of MSTd cells to complex motion patterns such as radial and rotational motion.

3.4.3 Similarity Index

As mentioned earlier, at the heart of our method of reverse correlation is the assumption that the behavior of the neuron in response to a global form of motion can be explained through its responses to the local motion patterns. We then would expect that in those cells whose receptive fields were successfully recovered with reverse correlation, we would be able to explain the response of a cell to tuning stimuli using its responses to the local motion patterns that we used in the reverse correlation stimulus. Assuming a linearly integrating neuron that was successfully mapped by reverse correlation, the recovered RC map should theoretically indicate the optimal motion pattern that this given neuron prefers. The responses of such a neuron to different motion patterns could then be explained based on the motion similarity of such patterns to the 'optimal' motion pattern found in the recovered RC map.

We calculated the Similarity Index (SI) as outlined in the method section for all cells to better quantify the motion similarity of a given motion pattern (in a tuning stimulus) to the optimal motion pattern as found in an RC map. Out of 33 cells with significant maps and with an at least one overlapping spiral tuning configuration, we found 18 cells (54%) with a significant correlation between motion similarity as quantified by the similarity index and the response (Spearmann's rank test; p value < 0.001). Out of 28 cells with significant maps and with an overlapping linear tuning configuration, we found 19 cells (68%) with a significant correlation between motion similarity as quantified by the similarity index and the response (Spearmann's rank test; p value < 0.001)(Fig. 3.25).

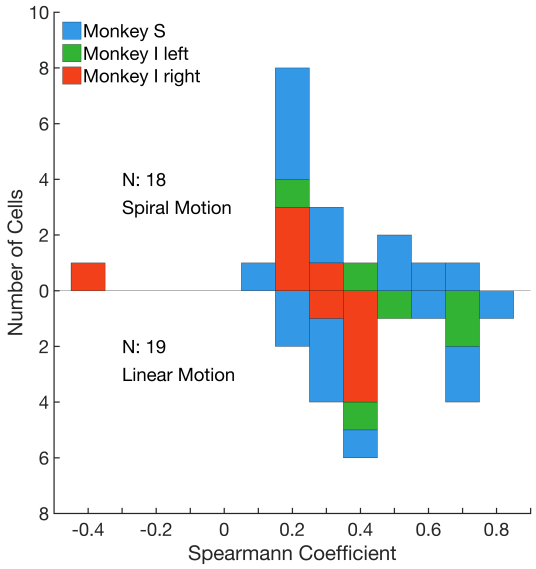

Fig. 3.25 Correlation of motion Similarity Index (SI) and neural responses across cells. In total number of 18/33 cells (54%) there was a significant correlation between SI and neural responses to spiral tuning stimuli, while in 19/28 cells (68%) there was a significant correlation between SI and neural responses to linear tuning stimuli.

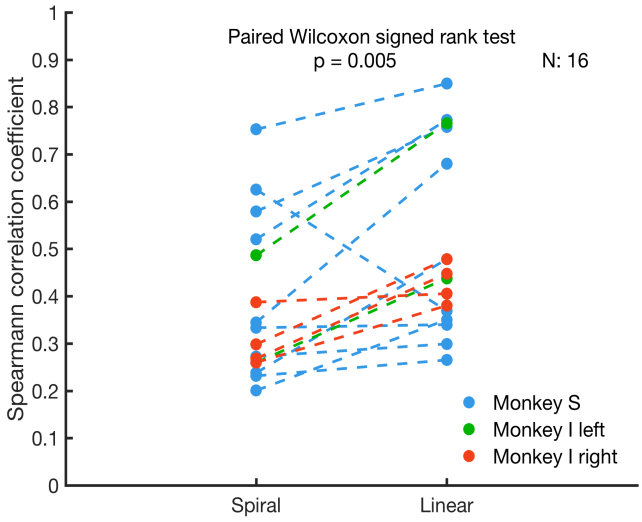

Fig. 3.26 Correlation of responses with motion similiarity to spiral and linear stimuli. In those cells where there was a significant correlation between neural responses and motion similarity to both spiral and linear motion 16/28 cells (57%), RC maps consistently explained responses to linear motion significantly more so than to spiral motion across cells (Wilcoxon signed rank test; p value < 0.01).

Out of 28 cells, where there was an overlap between the central tuning location and the recovered RC map, there were 16 cells (16/28, 57%) where there was a significant correlation between neural responses and motion similarity to both spiral and linear motion. The correlation with motion similarity to linear motion patterns was stronger than correlation with motion similarity to spiral motion patterns in almost every cell (Wilcoxon signed rank test; p value < 0.01) (Fig. 3.26); indicating that RC maps were significantly better able to explain linear rather than spiral global motion.

(Fig. 3.27 a) shows that there is no significant relationship between how well directional a cell is to spiral motion (defined through an average of its DI at spiral configurations at the respective preferred speeds) and how well the optimal motion pattern as recovered by the RC map can explain the response of the cell to the spiral stimuli (as we defined through the correlation between similarity index and response) (Spearmann's rank correlation test; p value > 0.05).

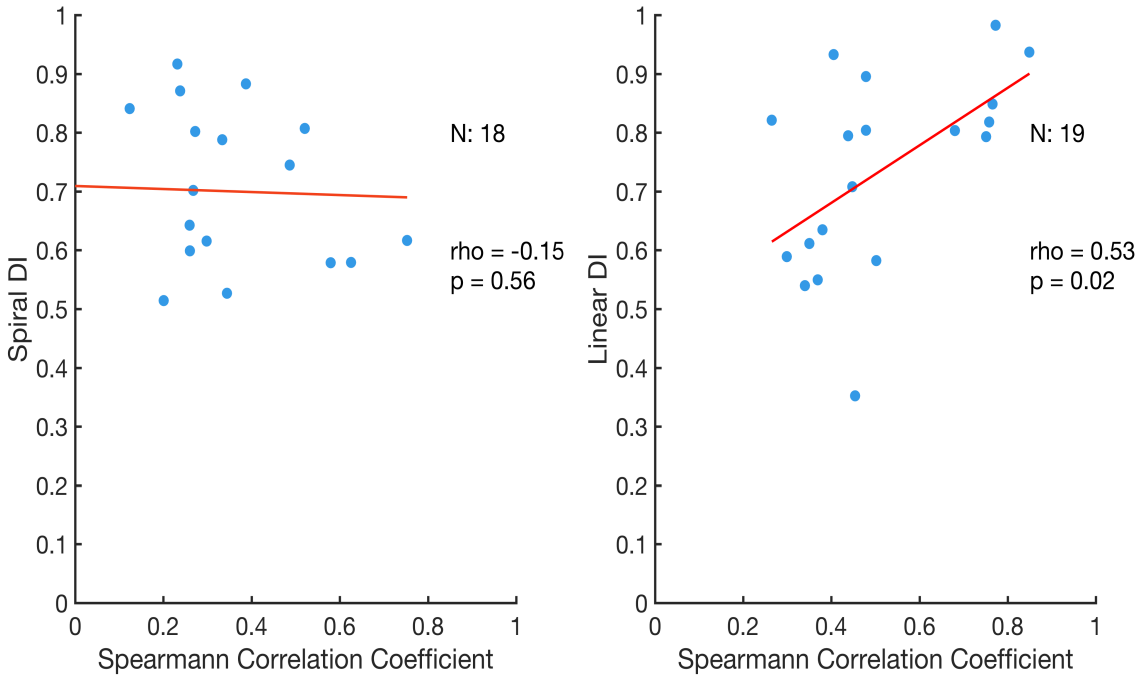

Fig. 3.27 Correlation of motion Similarity Index (SI) and neural responses across cells correlated with linear and spiral DI. **a -** No correlation exists between how well an RC map explains responses to spiral tuning stimuli and how well the cell is directional to spiral motion (Spearmann's rank correlation test; p value > 0.05). Linear regression model is fitted to the data (red line). **b -** Positive correlation exists between how well an RC map explains responses to linear tuning stimuli and how well the cell is directional to linear motion (Spearmann's rank correlation test; p value < 0.05). Linear regression model is fitted to the data to illustrate correlation (red line).

(Fig. 3.27 b) shows a significant relationship between how well directional a cell is to linear motion (through the DI at the linear configuration at the preferred speed) and how well the optimal motion pattern as recovered by the RC map can explain the response of the cell to the linear stimuli (Spearmann's rank correlation test; coefficient = 0.53, p value < 0.05). Indicating that the better directional a cell is to linear motion the better able the recovered RC map at explaining the response of the cell to the global linear motion pattern of a linear tuning stimulus. However the same does not seem to apply to spiral motion tuning stimuli.

The degree to which an RC map can explain the response of a cell to the global motion in linear and spiral tuning stimuli is marginally significantly correlated with the total spike number going into the reverse correlation analysis (Spearmann's rank correlation test; coefficient = 0.45, p value = 0.05) (Fig. 3.28 A), but not with the total number of presentation samples of the Reverse Correlation stimulus (Spearmann's rank correlation test; coefficient = 0.28, p value > 0.05) (Fig. 3.28 B). This suggests that a more lengthy recording session with a higher number of presentation samples may not necessarily yield an RC map that is more able to explain the motion preferences of the neuron.

Finally, we aimed to address the size aspect of the RC stimulus, i.e. the number of segments and thereby the number of parameters that are mapped with the method of reverse correlation. We investigated whether using a smaller number of parameters, i.e. a smaller stimulus, would result in a lower level of noise to which a neuron is subjected, and would perhaps reveal a larger number of local motion preferences inside the receptive field (higher number of significant RC segments in the recovered maps in those cells where the smaller stimulus was used). However, no such significant effect could be found (Mann-Whitney-Wilcoxon test, p > 0.05) (Fig. 3.29)s.

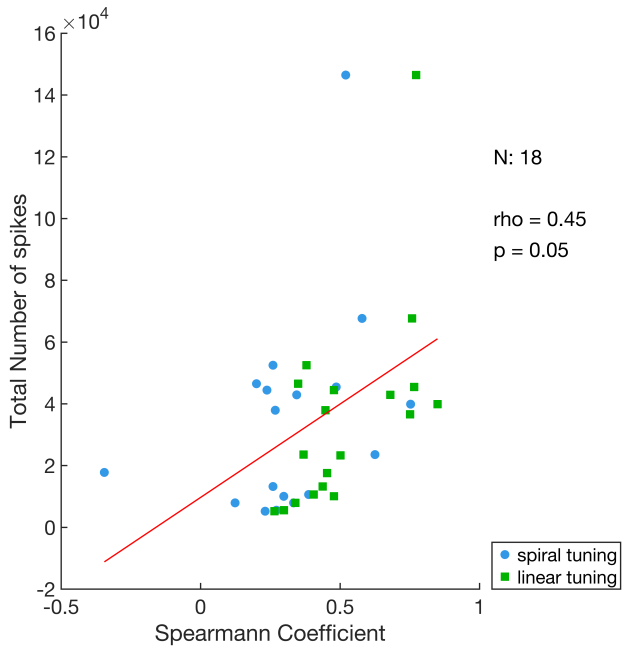

(a)

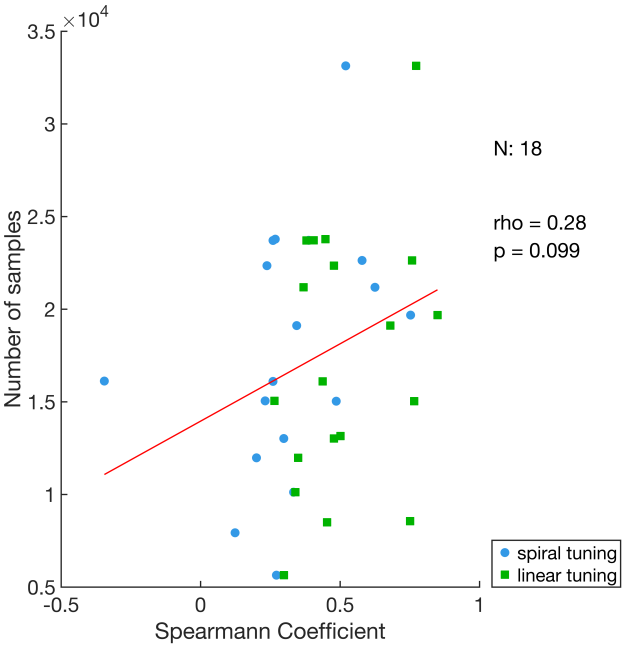

(b)

Fig. 3.28 Correlation of motion Similarity Index (SI) and neural responses across cells correlated with influencing factors. **a -** Marginal positive correlation exists between how well an RC map explains responses to linear tuning stimuli and total number of spikes entering the reverse correlation analysis (Spearmann's rank correlation test; p value = 0.05). Linear regression model is fitted to the data to illustrate correlation (red line). **b -** Positive correlation exists between how well an RC map explains responses to linear tuning stimuli and total number of RC stimulus samples presentation (Spearmann's rank correlation test; p value > 0.05). Linear regression model is fitted to the data to illustrate correlation (red line).

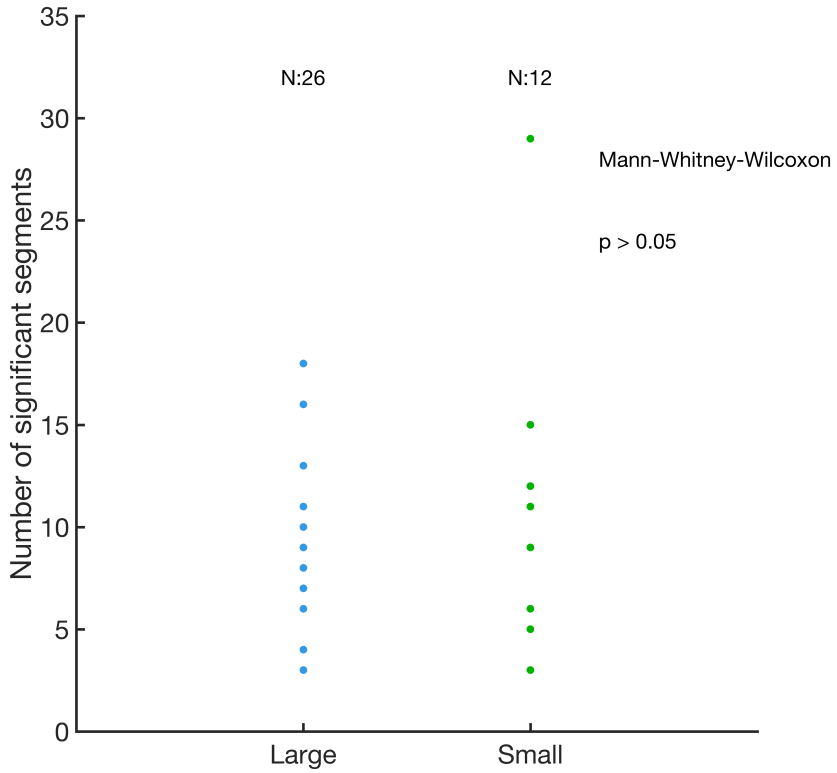

Fig. 3.29 Large RC stimulus configuration vs. small configuration. In the large configuration, 10 X 15 segments were shown, whereas in the small configuration, only 6 X 9 segments were shown. There is no significant difference between the two configurations as to the number of signficant RC segments recovered in the RC maps (Mann-Whitney-Wilcoxon test, $p > 0.05$).

Chapter 4

Discussion

4.1 Overview

We successfully used a reverse correlation approach to recover the detailed, yet partial local spatial and directional motion preferences in a number of MSTd neurons. The success of this method is clearly dependent on how well a given neuron is directional to classical linear and spiral motion stimuli. The recovered RC maps were mostly dominated by homogenous linear motion preferences; where the local motion preferences in these maps were able to significantly explain the responses of many neurons to the global motion in linear (in 68% of the cells) and spiral (in 54% of the cells) tuning stimuli, albeit significantly more so to linear motion than to spiral motion. Additionally, our analysis pointed to a prevalence of position invariance across MSTd neurons with a predominance in directional selectivity to expansion and contraction patterns, in accordance with previous evidence from literature (Graziano et al., 1994).

4.2 Position invariance

We reproduced population analysis results of position invariance as can be found by Graziano et al. (1994). We quantified up to 80% of recorded cells to be position invariant; i.e., they retain the preferred motion directions at the peripheral tuning locations within an interval of 90° of the preferred motion direction at the central location (lack of reversal in motion direction preference between the central and peripheral locations), with 77% of cells maintaining all preferred directions across locations within an angle interval of 90°, which points to a significant selectivity to the preferred spiral motion direction across tuning locations in MSTd cells. Furthermore, we found that the more strongly directional a cell is to spiral space stimuli in the

central location, the more likely for it to exhibit the feature of position invariance.
It is important to note here that a reversal in motion direction preference is not the only possible behavior of a cell with position variant responses. Positioning tuning stimuli displaying different spiral space directions in different locations within the boundaries of a large receptive field permeated by preference to one optic flow pattern (such as expansion), with well defined heading direction (i.e. well defined selectivity to a given location of the center of the motion pattern), might yield un-tuned/un-directional responses rather than a reversal in the selectivity to the preferred motion direction. In this work we are yet to quantify how prevalent the loss of tuning in some tuning locations across cells is. While such un-directional responses might depend on the placement of tuning stimuli within the receptive field, one could compare such responses to baseline firing rate of the neuron to better qualify whether such un-tuned responses result from local lack of motion sensitivity in a part of the receptive field, or betrays perhaps an improper placement of tuning stimuli within tuned regions of a receptive field characterized by position variant responses.
In addition, the occurrence of motion direction preference reversal might depend on the size of tuning stimuli. Lappe et al. (1996) suggested that a reversal in motion direction selectivity was more frequent when center of motion pattern was displaced by a large distance (40 - 80°) across tuning locations than when a smaller distance was used (15 - 30°), and that this issue might explain previous findings: Duffy & Wurtz (1991b) used a displacement distance of 66° resulting in 16 - 40% of cells reversing selectivity, Lagae et al. (1994) and Orban et al. (1992) used a distance of 40° resulting in 60% of cells reversing selectivity. Finally, Graziano et al. (1994) used a distance of 10° resulting in none of the cells reversing selectivity. Our usage of small sizes of tuning stimuli similar to the study of Graziano et al., with center of motion displaced by distances of 10 - 16° might explain our finding of position invariance predominance in area MSTd. To address this confounding issue, one could conduct an experiment with a large range of tuning stimuli sizes and varying displacement distances and can then confirm whether the existence of position invariance depends on such factors.
As suggested previously in the literature, our preliminary findings of position invariance stand in contradiction to the current view of individual MSTd neurons as encoding heading direction (Britten, 2008; Britten & van Wezel, 1998; Britten & Van Wezel, 2002; Celebrini & Newsome, 1994; Duffy & Wurtz, 1995; Gu et al., 2012, 2006; Lappe et al., 1996; Takahashi et al., 2007), and suggests a scheme of population encoding of heading direction as suggested by Graziano et al. (1994). Additionally, the prevalence of position invariance seems to preclude the notion of a linear-summation integration model in MSTd, and emphasizes the non-linear nature of these neurons. One can

expect then the method of reverse correlation to fail in retrieving any significant receptive field structure, which however was not the case in our study.

4.3 Reverse Correlation in MSTd

The method of reverse correlation was successful in many cells (25%) in recovering significant receptive field maps, with significant RC maps recovered in more than one half of cells that are best directional to linear and spiral motion. Preliminary testing showed the structure of recovered maps to be quite robust, and not the result of random noise. However this method only recovered partial maps, with a median of only 6% of the receptive field mapped. We propose that in at least 25% of MSTd cells, receptive fields contain regions of visual field that can be successfully mapped using a simple linear method of reverse correlation, perhaps due to a linear integration scheme for input coming from those regions. This suggests that MSTd neurons must possess non-linear processing mechanisms that are able to encode position invariance.
This view of MSTd neuron as being able to perform linear and non-linear processing is in line with results found in a previous study (Mineault et al., 2012): a linear integration model could effectively characterize many MSTd neurons, however the addition of a non-linear integration component significantly enhanced the power of the model. This proposition might also explain why the motion similarity of tuning stimuli with the optimal motion pattern as recovered in the RC maps in our study was correlated with neural responses in only 54-68% of the cells, as the similarity analysis relies on the notion of linear-integration of local motion directions, which appears to be only partially present in a subset of MSTd neurons. Additionally, the direction tuning in the recovered regions of receptive fields using reverse correlation was significantly better able to explain neural responses to linear than to spiral motion, a finding echoing the notion that a linear-integration model could better explain linear motion preferences rather than more complex optic flow motion patterns (Mineault et al., 2012). This relationship between a linear integration scheme and preference to linear motion can be found further in our results where ability of recovered RC maps to explain motion is correlated to how well a cell is directional to linear motion (linear DI), but not to spiral motion (spiral DI).
This line of argument leads to the conclusion, that the method of reverse correlation is not sufficient to completely characterize the receptive field of MSTd neurons, and that other non-linear mapping methods should be used to complement this method. The inability of reverse correlation to recover any meaningful data for many MSTd

neurons can have several explanations: the lack of a linear processing component or an overpowering and strong non-linear integration component in those neurons, weak tuning of such neurons to optic flow motion, inefficient stimulation, or a sub-optimal experimental design.

4.4 Design and Analysis Consideration

Our method of reverse correlation recovered only partial maps of MSTd receptive fields, with a median of only 6% of receptive field surface mapped. This limited success could be attributed to several design and analysis considerations that we address here.

4.4.1 Inhibitory Surrounds

One issue that we are yet to address in our reverse correlation analysis is the inhibitory responses of the cell to local motion directions. By correlating the time bins where no spikes were emitted with the different motion directions presented in local segments we can recover regions of the receptive field where specific local motion directions leads to an inhibitory response of the cell. This could shed light on the extent of inhibitory surrounds in MSTd neurons. It might as well explain our peculiar finding that while tuning responses of neurons were positively correlated with how well tuning stimuli were positioned centrally within the receptive field, tuning strength of these responses was negatively correlated with goodness of placement, indicating stronger tuned responses to stimuli placed off-center in the receptive field in comparison to stimuli placed exactly at the center of the receptive field.

4.4.2 Second Order Analysis

One could perform a second order level of reverse correlation analysis, specifically looking into how neural responses are correlated to a combination of motion directions in two different adjacent or distant segments, an analysis that might reveal non-linear interactions between the neural responses to local motion directions. One could even conduct an analysis of a third order, a fourth order, and so on. However the number of presentation samples might not be sufficient to retrieve significant and structured tuning in a second order or more complex analysis, as the number of direction combinations to be mapped increases exponentially with the analysis order. For example in the case of first order analysis (as performed in this study), n total number of samples can

be used to study the response of a cell to 12 motion directions (we consider in this example only 12 discrete motion directions for simplification) presented to a given segment. In case of second order analysis however, the same n total number of samples is used to study the responses of a cell to 12×12 motion direction combinations in a pair of segments, yielding a severe reduction in the power of the results.

4.4.3 Analysis of Speed Parameters

As we did not include speed parameters in our reverse correlation analysis, it might be possible that the consideration of speed parameters can enable us to reveal local speed preferences of the receptive field. This might also improve the ability of RC maps to explain the behavior of MSTd neurons to Tuning stimuli.

4.4.4 Stimulus Duration

Similar to a previous study where reverse correlation analysis was conducted in area MSTd (Chen et al., 2008) (where significant structured maps were recovered for 64% of cells), an individual presentation of the Reverse Correlation stimulus lasts for only 100ms, and this could be problematic: by investigating the temporal response properties of MSTd neurons (Duffy & Wurtz, 1991a, 1997b), it was suggested that there exists an early response period lasting from 60 - 100ms to 100 - 250ms after stimulus onset, where neural responses of up to two thirds of MSTd neurons are not selective to any particular optic flow motion pattern. This may not only be problematic for our Reverse Correlation stimulus, but also for Tuning and Automatic Mapping stimuli, which had stimulus duration of 100ms and 50ms, respectively.
Given however that we were successful in recovering Automatic Mapping data for almost all cells, it is clear at least that a stimulus duration of 50ms is enough to obtain spatial tuning properties independently of motion direction. Additionally, we were able to recover significantly tuned data in the majority of cells (with 156/169 cells with significant spiral tuning in at least one location, and 116/169 cells with significant linear tuning in the central location), further indicating that stimulus-duration of 100ms was adequate in a majority of cells to study directional tuning properties. Whether the same conclusion applies to a complex stimulus such as the Reverse Correlation stimulus in all cells is not clear. It is possible that a more optimal stimulus duration could yield better-tuned responses in the Tuning and Reverse Correlation task.
It is worth noting that with a stimulus duration of 100ms, as used in the Reverse Correlation task, a severe temporal smoothening of the neural responses resulted, and

we were not able to accurately study the temporal evolution of tuning properties in local segments using reverse correlation. A similar problem was encountered in another reverse correlation study focusing on MT (Richert et al., 2013). Shorter stimulus duration such as 20ms, might be more useful to study those temporal properties (Borghuis et al., 2003).

4.4.5 Sub-optimal Stimulation

Several additional design factors could have led to limited success of our reverse correlation approach: The number of parameters which were mapped in our Reverse Correlation stimulus in most of the cells was large (most importantly: 10 $\times$ 15 direction parameters in addition to 10 $\times$ 15 speed parameters), and this could have led to a decrease in the signal to noise ratio and reduced the efficiency of the method. Perhaps this a reason why a similar study employing reverse correlation in MSTd using only 4 $\times$ 4 direction parameters was up to one fold more successful in recovering significant RC maps (Chen et al., 2008). This is however not supported by our finding that using a smaller stimulus did not lead to significant increase in the success in recovering the local motion preferences in RC maps.

It might be possible that the range of motion speeds used in our study succeeded sufficiently yet not optimally in driving MSTd neurons. According to one study, the range of motion speed capable to drive MSTd neuron was 10-80°/s (Duffy & Wurtz, 1997a). In our study, the speed range was (0 – 20°/s) in the Reverse Correlation stimulus, a range that perhaps failed to maximally drive all of the neurons.

One design issue to consider is the direction and speed gradient used in the Reverse Correlation stimulus, which we introduced to keep the complex motion pattern presented to a neuron relatively smooth, based on previous findings from literature citing a higher neural response of MSTd neurons to stimuli with a direction and speed gradient (Tanaka et al., 1989). We are not certain how these gradients influenced our results, whether they were beneficial at all or if they introduced an unnecessary level of noise in the stimulus.

Adding depth information to stimuli should lead to better neural responses (Upadhyay et al., 2007). However this dramatically increases the number of required trials to map this additional dimension and its interaction with speed and direction. This issue can be considered across all tasks in this study.

The sizes of our tuning stimuli could have been less than optimal in driving MSTd cells properly, as larger sized stimuli appear to drive these neurons better, while retaining their directional selectivity (Duffy & Wurtz, 1991b). Furthermore, our choice of dot

sizes as used in the experiment might not have been optimal, where a 5 fold increase in dot size (although impractical in the Reverse Correlation and Automatic Mapping tasks) might have led to significantly better neural responses (Tanaka & Saito, 1989). Finally, the luminance's values of the stimuli used could influence the neural responses, with luminance values resulting in low contrast values leading to decreased firing rates.

4.4.6 Existing Anatomical Damage

The animals used in this experiment were not naïve to electrophysiological recordings, and had contributed to different experiments. Monkeys S and E previously underwent an experiment were MT of the left hemisphere was targeted for electrophysiological recording, and monkey I had been involved in an experiment were left MSTd was targeted. At the moment we cannot assess the extent to which these experiments had affected the integrity of area MT, damaged the anatomical connection from MT to MSTd, damaged MSTd cells, or rendered some neurons un-tuned to motion direction.

4.4.7 Sub-regions in MSTd

Our finding of a positive correlation between size and eccentricity of MSTd receptive fields is in line with some evidence from literature (Desimone & Ungerleider, 1986), yet is contradictory to several other studies that found no significant correlation (Raiguel et al., 1997; Tanaka et al., 1986), and yet others that found a significant negative correlation (Celebrini & Newsome, 1994). These discrepancies might be rooted in sampling two different sub-regions of MSTd neurons with different receptive field sizes and size to eccentricity ratios. This might explain the difference in size to eccentricity ratio profiles between the two hemispheres of monkey I.

4.5 Further steps

How do we reconcile the large body of evidence of heading direction tuning and the clear position invariance properties in MSTd neurons? We propose that to answer this question we need to apply a more efficient mapping method to characterize the receptive fields of MSTd neurons. We suggest applying a method that could overcome the reported non-linear properties of MSTd neurons that might have hindered the success of reverse correlation.

In essence this is a mathematical optimization problem. Using a stimulus similar to our reverse correlation stimulus that covers as much as possible of the receptive field,

there is a large set of parameters that determine the exact motion pattern produced by the stimulus. The basic approach would then be to optimize these parameters online (based on the responses of the neuron: a closed-loop system), to eventually reach a theoretical hotspot in the space defined by the stimulus parameters, a hotspot that generates the maximum response from the neuron. In case of a neuron which favors one specific motion pattern and that is tuned to all stimulus parameters in a symmetric uni-modal fashion, one could use reverse correlation/spike triggered average to identify the hotspot, i.e. that ideal set of values for all stimulus parameters which generate the best response of the neuron. However if a neuron has some non-linear properties, this concept of a singular hotspot might not apply. For example, a position invariant neuron would have a manifold (a subspace), or a set of local maxima that generate the best responses of the neuron. To recover the ideal parameters values one can apply an optimization method, some examples are: gradient descent algorithm similar to that used in machine learning, genetic algorithm or simplex (Nelder–Mead) method (Benda et al., 2007; DiMattina & Zhang, 2013). Different forms of these optimization methods have been used successfully in characterizing receptive fields in several visual and auditory areas, in addition to ganglion neurons in the retina (Bölinger & Gollisch, 2012; Chambers et al., 2014; Connor et al., 2006; Hung et al., 2012; Potter et al., 2014). Of course, the number of mapped parameters needs to remain reasonably low to maintain a good signal to noise ratio (by adjusting the number of stimulus segments that are being mapped, adding or removing speed and potentially depth parameters to each segment) and to reduce the number of dimensions of the space within which the optimization algorithm will operate. Another issue is to select a starting point for optimization, where one could start from a random point in the multi-dimensional optimization space and converge onto the hotspot, which might not be straightforward and could be lengthy; or one can start from a linear or spiral motion pattern to which the neuron appears to be maximally responsive and optimize the motion pattern until maximal firing rate is reached.

One could then run such a method several times on the same neuron (requiring the ability to keep a neuron throughout a long recording session) to determine whether the neuron possesses one or several response maxima. By comparing the motion patterns resulting at the found maxima from the several iterations, it becomes clear whether a neuron is responsive to one motion pattern with motion center fixed to a certain location (neuron is tuned to one heading direction), or whether it is selective to one specific motion pattern irrespective of the location of the motion center (for example a cell tuned to an expansion pattern but irrespectively of the accurate heading direction). We propose that this can clarify the abovementioned discrepancy of MSTd neurons

being position invariant and tuned to heading directions.
Using an optimization method one can explain how to clarify a discrepancy regarding the motion patterns to which MSTd neurons are mostly selective: using the spiral space stimuli, we found a predominance of selectivity to expansion and contraction patterns (corresponding to a self-motion in a straightforward or backward direction), as was reported by Graziano et al. (1994). However, in several studies investigating heading direction tuning (Gu et al., 2006; Takahashi et al., 2007), a predominance for selectivity to lateral motion (self-motion towards the left or right) was found.
Finally, one needs to consider that whereas the method of reverse correlation is robust to fluctuations as well as to adaptation in neural responses over time, the efficiency of an online optimization method could be compromised by neural fluctuations and is severely dependent on clean and well-isolated neural signal.

4.6 Conclusions

Our findings point to the existence of regions within the receptive fields that can be successfully and robustly mapped using a linear method of reverse correlation in at least 25% of MSTd neurons, with the recovered local motion patterns being better able to explain the responses of neurons to simple linear translational motion than to complex spiral motion patterns. Interestingly, local motion directions of recovered maps were largely dominated by homogenous linear motion preferences, suggesting that reverse correlation method can only recover regions in the MSTd receptive fields that are tuned to linear motion, but not to more complex forms of motion. It is important to note here that reverse correlation was clearly more successful in cells well tuned/directional to classical tuning stimuli, which might explain the limited success of the method in recovering significantly structured maps across cells.
Additionally, we confirmed that MSTd neurons are significantly position invariant in their responses to spiral space motion patterns, a finding that seemingly is contradictory to findings from literature regarding predominance of heading direction tuning in MSTd neurons, and further highlights the non-linear processing nature of this area. We suggest that the application of an online closed-loop optimization method in MSTd might be more suitable to explain position invariance, clarify the interaction of position invariance with heading direction tuning, and can shed further light on the exact complex motion patterns to which MSTd neurons are selectively responsive, which might explain the known tuning properties of MSTd neuron to different types of motion patterns.

Bibliography

Albright, T. D. (1993). Cortical processing of visual motion. *Reviews of oculomotor research*, 5:177–201.

a.M. van Gisbergen, J., Grashuis, J. L., Johannesma, P. I., and Vendrik, a. J. (1975). Neurons in the cochlear nucleus investigated with tone and noise stimuli. *Experimental Brain Research*, 23(4):387–406.

Andersen, R. a., Snowden, R. J., Treue, S., and Graziano, M. (1990). Hierarchical processing of motion in the visual cortex of monkey. *Cold Spring Harbor Symposia on Quantitative Biology*, 55:741–748.

Anderson, K. C. and Siegel, R. M. (2005). Three-dimensional structure-from-motion selectivity in the anterior superior temporal polysensory area, STPa, of the behaving monkey. *Cerebral Cortex*, 15(9):1299–1307.

Batschelet, E. (1981). Circular statistics in biology. *ACADEMIC PRESS, 111 FIFTH AVE., NEW YORK, NY 10003, 1981, 388*.

Benda, J., Gollisch, T., Machens, C. K., and Herz, A. V. (2007). From response to stimulus: adaptive sampling in sensory physiology. *Current Opinion in Neurobiology*, 17(4):430–436.

Berens, P. (2009). CircStat: A MATLAB toolbox for circular statistics. *Journal of Statistical Software*, 31(10):1–21.

Bölinger, D. and Gollisch, T. (2012). Closed-Loop Measurements of Iso-Response Stimuli Reveal Dynamic Nonlinear Stimulus Integration in the Retina. *Neuron*, 73(2):333–346.

Borghuis, B. G., Perge, J. a., Vajda, I., Van Wezel, R. J. a., Van De Grind, W. a., and Lankheet, M. J. M. (2003). The motion reverse correlation (MRC) method:: A linear systems approach in the motion domain. *Journal of Neuroscience Methods*, 123(2):153–166.

Bremmer, F., Kubischik, M., Pekel, M., Lappe, M., and Hoffmann, K. P. (1999). Linear vestibular self-motion signals in monkey medial superior temporal area. *Annals of the New York Academy of Sciences*, 871:272–281.

Britten, K. H. (2008). Mechanisms of self-motion perception. *Annual review of neuroscience*, 31:389–410.

Britten, K. H. and Heuer, H. W. (1999). Spatial summation in the receptive fields of MT neurons. *The Journal of neuroscience : the official journal of the Society for Neuroscience*, 19(12):5074–5084.

Britten, K. H. and van Wezel, R. J. (1998). Electrical microstimulation of cortical area MST biases heading perception in monkeys. *Nature neuroscience*, 1(1):59–63.

Britten, K. H. and Van Wezel, R. J. a. (2002). Area MST and heading perception in macaque monkeys. *Cerebral cortex (New York, N.Y. : 1991)*, 12(7):692–701.

Celebrini, S. and Newsome, T. (1994). Neuronal and Psychophysical Sensitivity to Motion Signals in Extrastriate Area MST of the Macaque Monkey. *The Journal of neuroscience*, 74(July).

Chambers, a. R., Hancock, K. E., Sen, K., and Polley, D. B. (2014). Online Stimulus Optimization Rapidly Reveals Multidimensional Selectivity in Auditory Cortical Neurons. *Journal of Neuroscience*, 34(27):8963–8975.

Chen, A., Deangelis, G. C., and Angelaki, D. E. (2011). Representation of vestibular and visual cues to self-motion in ventral intraparietal cortex. *The Journal of neuroscience : the official journal of the Society for Neuroscience*, 31(33):12036–12052.

Chen, a., Gu, Y., Takahashi, K., Angelaki, D. E., and DeAngelis, G. C. (2008). Clustering of Self-Motion Selectivity and Visual Response Properties in Macaque Area MSTd. *Journal of Neurophysiology*, 100(5):2669–2683.

Connor, K. N. O., Petkov, C. I., Sutter, M. L., Connor, O., N, K., and L, M. (2006). Adaptive Stimulus Optimization for Auditory Cortical Neurons Adaptive Stimulus Optimization for Auditory Cortical Neurons. *Journal of Neurophysiology*, (August 2005):4051–4067.

Crowell, J. a. and Banks, M. S. (1993). Perceiving heading with different retinal regions and types of optic flow. *Perception & Psychophysics*, 53(3):325–337.

De Valois, R. L., Cottaris, N. P., Mahon, L. E., Elfar, S. D., and Wilson, J. A. (2000). Spatial and temporal receptive fields of geniculate and cortical cells and directional selectivity. *Vision research*, 40(27):3685–3702.

DeAngelis, G. C., Ohzawa, I., and Freeman, R. D. (1995). Receptive-field dynamics in the central visual pathways. *Trends Neurosci.*, 18(10):451–458.

Deangelis, G. C., Ohzawa, I., Freeman, R. D., Tao, X., Zhang, B., Shen, G., Wensveen, J., and Smith, E. L. (1993). Spatiotemporal organization of simple-cell receptive fields in the cat ' s striate cortex . II . Linearity of temporal and spatial summation Spatiotemporal Organization of Simple-Cell Receptive Fields in the Cat ' s Striate Cortex . II . Linearity of Temp. 69(4):1118–1135.

Desimone, R. and Ungerleider, L. G. (1986). Multiple visual areas in the caudal superior temporal sulcus of the macaque. *Journal of Comparative Neurology*, 248(2):164–189.

DiMattina, C. and Zhang, K. (2013). Adaptive stimulus optimization for sensory systems neuroscience. *Frontiers in Neural Circuits*, 7(June):1–16.

Duffy, C. J. (1998). MST neurons respond to optic flow and translational movement. *Journal of neurophysiology*, 80(4):1816–1827.

Duffy, C. J. and Wurtz, H. (1995). Response of Monkey MST Neurons Shifted Centers of Motion to Optic Flow Stimuli with. 15(July):5192–5208.

Duffy, C. J. and Wurtz, R. H. (1991a). Sensitivity of MST neurons to optic flow stimuli. I. A continuum of response selectivity to large-field stimuli. *Journal of neurophysiology*, 65(6):1329–45.

Duffy, C. J. and Wurtz, R. H. (1991b). Sensitivity of MST neurons to optic flow stimuli. II. Mechanisms of response selectivity revealed by small-field stimuli. *Journal of neurophysiology*, 65(6):1346–59.

Duffy, C. J. and Wurtz, R. H. (1997a). Medial superior temporal area neurons respond to speed patterns in optic flow. *The Journal of neuroscience : the official journal of the Society for Neuroscience*, 17(8):2839–51.

Duffy, C. J. and Wurtz, R. H. (1997b). Multiple temporal components of optic flow responses in MST neurons. *Experimental brain research*, 114(3):472–82.

Duijnhouwer, J., Noest, A. J., Lankheet, M. J. M., van den Berg, A. V., and van Wezel, R. J. a. (2013). Speed and direction response profiles of neurons in macaque MT and MST show modest constraint line tuning. *Frontiers in Behavioral Neuroscience*, 7(April):1–11.

Eggermont, J. J., Johannesma, P. I. M., and Aertsen, a. M. H. (1983). Reverse correlation methods in auditory research. *Quarterly Reviews of Biophysics*, 16(3):341–414.

Fetsch, C. R., Deangelis, G. C., and Angelaki, D. E. (2010). Visual-vestibular cue integration for heading perception: Applications of optimal cue integration theory. *European Journal of Neuroscience*, 31(10):1721–1729.

Fetsch, C. R., Wang, S., Gu, Y., DeAngelis, G. C., and Angelaki, D. E. (2007). Spatial Reference Frames of Visual, Vestibular, and Multimodal Heading Signals in the Dorsal Subdivision of the Medial Superior Temporal Area. *Journal of Neuroscience*, 27(3):700–712.

Froehler, M. T. and Duffy, C. J. (2002). Cortical Neurons Encoding Path and Place: Where You Go Is Where You Are. *Science*, 295(5564):2462–2465.

Gattass, R. and Gross, C. G. (1981). Visual topography of striate projection zone (MT) in posterior superior temporal sulcus of the macaque. *Journal of neurophysiology*, 46(3):621–638.

Geesaman, B. J. and Andersen, R. a. (1996). The analysis of complex motion patterns by form/cue invariant MSTd neurons. *Journal of Neuroscience*, 16(15):4716–4732.

Graziano, M. S., Andersen, R. a., and Snowden, R. J. (1994). Tuning of MST neurons to spiral motions. *The Journal of neuroscience : the official journal of the Society for Neuroscience*, 14(1):54–67.

Gu, Y., Angelaki, D. E., and DeAngelis, G. C. (2008). Neural correlates of multisensory cue integration in macaque MSTd. *Nature Neuroscience*, 11(10):1201–1210.

Gu, Y., DeAngelis, G. C., and Angelaki, D. E. (2012). Causal Links between Dorsal Medial Superior Temporal Area Neurons and Multisensory Heading Perception. *Journal of Neuroscience*, 32(7):2299–2313.

Gu, Y., Fetsch, C. R., Adeyemo, B., Deangelis, G. C., and Angelaki, D. E. (2010). Decoding of MSTd population activity accounts for variations in the precision of heading perception. *Neuron*, 66(4):596–609.

Gu, Y., Watkins, P. V., Angelaki, D. E., and DeAngelis, G. C. (2006). Visual and non-visual contributions to three-dimensional heading selectivity in the medial superior temporal area. *The Journal of neuroscience : the official journal of the Society for Neuroscience*, 26(1):73–85.

Heuer, H. W. and Britten, K. H. (2004). Optic flow signals in extrastriate area MST: comparison of perceptual and neuronal sensitivity. *Journal of neurophysiology*, 91(3):1314–26.

Hubel, D. and Wiesel, T. N. (1968). Receptive Fields and Functional Architecture of Monkey Striate Cortex. *J. Physiol.*, 195:215–243.

Hubel, D. H. and Wiesel, T. N. (1959). Receptive fields of single neurones in the cat's striate cortex. *The Journal of Physiology*, 148(3):574–591.

Huk, A. C., Dougherty, R. F., and Heeger, D. J. (2002). Retinotopy and functional subdivision of human areas MT and MST. *The Journal of neuroscience : the official journal of the Society for Neuroscience*, 22(16):7195–7205.

Hung, C. C., Carlson, E. T., and Connor, C. E. (2012). Medial Axis Shape Coding in Macaque Inferotemporal Cortex. *Neuron*, 74(6):1099–1113.

Ilg, U. J. (2008). The role of areas MT and MST in coding of visual motion underlying the execution of smooth pursuit. *Vision research*, 48(20):2062–9.

Jones, J. P. and Palmer, L. a. (1987). The two-dimensional spatial structure of simple receptive fields in cat striate cortex. *J Neurophysiol*, 58(6):1187–1211.

Klein, D. J., Simon, J. Z., Depireux, D. a., and Shamma, S. a. (2006). Stimulus-invariant processing and spectrotemporal reverse correlation in primary auditory cortex. *Journal of Computational Neuroscience*, 20(2):111–136.

Kleinschmidt, a. (2002). Neural Correlates of Visual-Motion Perception as Object- or Self-motion. *NeuroImage*, 16(4):873–882.

Komatsu, H. and Wurtz, R. H. (1988). Relation of Cortical Areas MT and MST to Pursuit Eye Movements. I. Localization and Visual Properties of Neurons. pages 580–603.

Kourtzi, Z., Bülthoff, H. H., Erb, M., and Grodd, W. (2002). Object-selective responses in the human motion area MT/MST. *Nature neuroscience*, 5(1):17–18.

Lagae, L., Maes, H., Raiguel, S., Xiao, D. K., and Orban, G. a. (1994). Responses of macaque STS neurons to optic flow components: a comparison of areas MT and MST. *Journal of neurophysiology*, 71(5):1597–626.

Lappe, M., Bremmer, F., Pekel, M., Thiele, a., and Hoffmann, K. P. (1996). Optic flow processing in monkey STS: a theoretical and experimental approach. *The Journal of neuroscience : the official journal of the Society for Neuroscience*, 16(19):6265–85.

Layton, O. W. and Fajen, B. R. (2016). Competitive Dynamics in MSTd: A Mechanism for Robust Heading Perception Based on Optic Flow. *PLoS Computational Biology*, 12(6).

Lee, B., Pesaran, B., and Andersen, R. a. (2011). Area MSTd neurons encode visual stimuli in eye coordinates during fixation and pursuit. *Journal of neurophysiology*, 105(1):60–8.

Livingstone, M. S., Pack, C. C., and Born, R. T. (2001). Two-dimensional substructure of MT receptive fields. *Neuron*, 30(3):781–793.

Logan, D. J. and Duffy, C. J. (2006). Cortical area MSTd combines visual cues to represent 3-D self-movement. *Cerebral cortex (New York, N.Y. : 1991)*, 16(10):1494–507.

Maunsell, J. H. and Van Essen, D. C. (1983). Functional properties of neurons in middle temporal visual area of the macaque monkey. I. Selectivity for stimulus direction, speed, and orientation. *Journal of neurophysiology*, 49(5):1127–1147.

Maunsell, J. H. and van Essen, D. C. (1983). The connections of the middle temporal visual area (MT) and their relationship to a cortical hierarchy in the macaque monkey. *The Journal of neuroscience : the official journal of the Society for Neuroscience*, 3(12):2563–2586.

Maunsell, J. H. R. and Newsome, W. T. (1987). Visual Processing in Monkey Extrastriate Cortex. *Ann. rev. Neurosci*.

Merchant, H., Battaglia-Mayer, a., and Georgopoulos, a. P. (2001). Effects of optic flow in motor cortex and area 7a. *Journal of Neurophysiology*, 86(4):1937–1954.

Mineault, P. J., Khawaja, F. a., Butts, D. a., and Pack, C. C. (2012). PNAS Plus: Hierarchical processing of complex motion along the primate dorsal visual pathway. *Proceedings of the National Academy of Sciences*, 109(16):E972–E980.

Mishkin, M., Ungerleider, L. G., and Macko, K. a. (1983). Object vision and spatial vision: two cortical pathways. *Trends in Neurosciences*, 6(C):414–417.

Morrone, M. C., Tosetti, M., Montanaro, D., Fiorentini, a., Cioni, G., and Burr, D. C. (2000). A cortical area that responds specifically to optic flow, revealed by fMRI. *Nature neuroscience*, 3(12):1322–1328.

Nelissen, K. (2006). Charting the Lower Superior Temporal Region, a New Motion-Sensitive Region in Monkey Superior Temporal Sulcus. *Journal of Neuroscience*, 26(22):5929–5947.

Orban, G. a. (2008). Higher order visual processing in macaque extrastriate cortex. *Physiological reviews*, 88(1):59–89.

Orban, G. a. and Callens, M. (1977). Receptive field types of area 18 neurones in the cat. *Experimental brain research. Experimentelle Hirnforschung. Experimentation cerebrale*, 30(1):107–123.

Orban, G. a., Lagae, L., Verri, a., Raiguel, S., Xiao, D., Maes, H., and Torre, V. (1992). First-order analysis of optical flow in monkey brain. *Proceedings of the National Academy of Sciences of the United States of America*, 89(7):2595–9.

Page, W. K. (2002). Heading Representation in MST: Sensory Interactions and Population Encoding. *Journal of Neurophysiology*, 89(4):1994–2013.

Page, W. K., Sato, N., Froehler, M. T., Vaughn, W., and Duffy, C. J. (2015). Navigational path integration by cortical neurons: origins in higher-order direction selectivity. *Journal of neurophysiology*, 113(6):1896–906.

Paolini, M., Distler, C., Bremmer, F., Lappe, M., and Hoffmann, K.-P. (2000). Responses to continuously changing optic flow in area MST. *Journal of Neurophysiology*, 84(2):730–743.

Potter, S. M., El Hady, A., and Fetz, E. E. (2014). Closed-loop neuroscience and neuroengineering. *Frontiers in Neural Circuits*, 8(September):2013–2015.

Raffi, M., Squatrito, S., and Maioli, M. G. (2002). Neuronal Responses to Optic Flow in the Monkey Parietal Area PEc. *Cerebral Cortex*, pages 639–646.

Raiguel, S., Van Hulle, M. M., Xiao, D. K., Marcar, V. L., Lagae, L., and Orban, G. a. (1997). Size and shape of receptive fields in the medial superior temporal area (MST) of the macaque. *Neuroreport*, 8(12):2803–8.

Reid, R. C. and Shapley, R. M. (2002). Space and time maps of cone photoreceptor signals in macaque lateral geniculate nucleus. *The Journal of neuroscience*, 22(14):6158–6175.

Richert, M., Albright, T. D., and Krekelberg, B. (2013). The complex structure of receptive fields in the middle temporal area. *Frontiers in systems neuroscience*, 7(March):2.

Ringach, D. and Shapley, R. (2004). Reverse correlation in neurophysiology. *Cognitive Science*, 28(2):147–166.

Saito, H., Yukie, M., Tanaka, K., Hikosaka, K., Fukada, Y., and Iwai, E. (1986). Integration of direction signals of image motion in the superior temporal sulcus of the macaque monkey. *The Journal of neuroscience : the official journal of the Society for Neuroscience*, 6(1):145–157.

Siegel, R. M. and Read, H. L. (1997). Analysis of optic flow in the monkey parietal area 7a. *Cerebral Cortex*, 7(4):327–346.

Sugihara, H., Murakami, I., Shenoy, K. V., Andersen, R. a., and Komatsu, H. (2002). Response of MSTd neurons to simulated 3D orientation of rotating planes. *Journal of neurophysiology*, 87(1):273–85.

Takahashi, K., Gu, Y., May, P. J., Newlands, S. D., DeAngelis, G. C., and Angelaki, D. E. (2007). Multimodal coding of three-dimensional rotation and translation in area MSTd: comparison of visual and vestibular selectivity. *The Journal of neuroscience : the official journal of the Society for Neuroscience*, 27(36):9742–56.

Tanaka, K., Fukada, Y., and Saito, H. a. (1989). Underlying mechanisms of the response specificity of expansion/contraction and rotation cells in the dorsal part of the medial superior temporal area of the macaque monkey. *Journal of neurophysiology*, 62(3):642–56.

Tanaka, K., Hikosaka, K., Saito, H., Yukie, M., Fukada, Y., and Iwai, E. (1986). Analysis of local and wide-field movements in the superior temporal visual areas of the macaque monkey. *Journal of Neuroscience*, 6(1):134–144.

Tanaka, K. and Saito, H. (1989). Analysis of motion of the visual field by direction, expansion/contraction, and rotation cells clustered in the dorsal part of the medial superior temporal area of the macaque monkey. *Journal of neurophysiology*, 62(3):626–41.

Treue, S. and Andersen, R. a. (1996). Neural responses to velocity gradients in macaque cortical area MT. *Visual neuroscience*, 13(4):797–804.

Ungerleider, L. G. and Desimone, R. (1986). Cortical connections of visual area MT in the macaque. *The Journal of comparative neurology*, 248(2):190–222.

Upadhyay, U. D., Page, W. K., Duffy, C. J., Upadhyay, U. D., Page, W. K., and Duffy, C. J. (2007). MST Responses to Pursuit Across Optic Flow With Motion Parallax MST Responses to Pursuit Across Optic Flow With Motion Parallax. 2000(November 1999):818–826.

Van Essen, D. C., Maunsell, J. H., and Bixby, J. L. (1981). The middle temporal visual area in the macaque: myeloarchitecture, connections, functional properties and topographic organization. *The Journal of comparative neurology*, 199(3):293–326.

Van Essen, D. C. and Newsome, W. T. (1984). The visual field representation in the striate cortex of the macaque monkey: Asymmetries, anisptropies, and indiviual variability. *Vision Research*, 24(5):429–448.

Wall, M. B. and Smith, A. T. (2008). The Representation of Egomotion in the Human Brain. *Current Biology*, 18(3):191–194.

Warren, W. H. and Hannon, D. J. (1990). Eye movements and optical flow. *Journal of the Optical Society of America. A, Optics and image science*, 7(1):160–169.

Yu, C. P., Page, W. K., Gaborski, R., and Duffy, C. J. (2010). Receptive Field Dynamics Underlying MST Neuronal Optic Flow Selectivity. *Journal of Neurophysiology*, 103(5):2794–2807.

Zeki, S., Watson, J. D., Lueck, C. J., Friston, K. J., Kennard, C., and Frackowiak, R. S. (1991). A direct demonstration of functional specialization in human visual cortex. *The Journal of Neuroscience*, 11(March):641–649.

Zeki, S. M. (1974). Functional organization of a visual area in the posterior bank of the superior temporal sulcus of the rhesus monkey. *The Journal of Physiology*, 236(3):549–573.

Appendix

Overview of Recorded Cells

What follows is an overview of pilot data files recorded for this project. These files were recorded as concept-proof for the experiment, and were recorded with the experiment in various stages of design, and so they do not contain complete data-sets as described in this manuscript. None of these files were used in the analysis described in this work, and are only mentioned here to completion. Entries are: **File name**, where abbreviated names for the individual animals used in the pilot experiments are included (*sun* stands for monkey S. **Date**, date of data recording. **X, Y** refer to the chamber placement coordinates as outlined in the Methods section (units in mm). **Z** indicates the recording depth (mm), where 0 defines the intial resting position of the electrodes prior to entering the dura. **Cell Indeces** refer to the cell ID as used in the analysis, where every cell is assigned a number throughout the analysis. **Experimenter** refers to the person conducting the experiment, with *amm* referring to the author of this work Amr Maamoun.

File name	Date	X	Y	Z	Experimenter
amm-MSTRC-sun-001-01+01	20150122	-2	-1	4647	amm
amm-MSTRC-sun-002-01+01	20150127	-2	-1	5261	amm
amm-MSTRC-sun-003-01+01	20150129	-2	-1	5182	amm
amm-MSTRC-sun-003-01+02	20150129	-2	-1	5182	amm
amm-MSTRC-sun-003-01+03	20150129	-2	-1	5182	amm
amm-MSTRC-sun-004-01+01	20150211	-2	-1	4678	amm
amm-MSTRC-sun-005-01+01	20150216	-1	-2	4246	amm
amm-MSTRC-sun-006-01+01	20150216	-1	-1	1888	amm
amm-MSTRC-sun-007-01+01	20150219	-1	-1	1159	amm
amm-MSTRC-sun-007-01+02	20150219	-1	-1	1159	amm
amm-MSTRC-sun-007-02+01	20150219	-1	-1	1437	amm
amm-MSTRC-sun-007-02+02	20150219	-1	-1	1437	amm
amm-MSTRC-sun-007-03+01	20150219	-1	-1	1181	amm
amm-MSTRC-sun-007-03+02	20150219	-1	-1	1181	amm
amm-MSTRC-sun-007-04+01	20150219	-1	-1	1181	amm
amm-MSTRC-sun-008-01+01	20150220	-1	-1	4412	amm
amm-MSTRC-sun-008-01+02	20150220	-1	-1	4412	amm
amm-MSTRC-sun-008-01+03	20150220	-1	-1	4412	amm
amm-MSTRC-sun-009-01+01	20150223	-1	-1	2799	amm
amm-MSTRC-sun-009-01+02	20150223	-1	-1	2799	amm
amm-MSTRC-sun-011-01+01	20150225	-1	-1	1596	amm

File name	Date	X	Y	Z	Experimenter
amm-MSTRC-sun-012-01+01	20150227	-1	-1	4568	amm
amm-MSTRC-sun-013-01+01	20150302	-1	-1	7596	amm
amm-MSTRC-sun-014-01+01	20150303	-1	-1	7000	amm
amm-MSTRC-sun-015-01+01	20150303	-1	-1	7000	amm
amm-MSTRC-sun-015-01+02	20150303	-1	-1	7250	amm
amm-MSTRC-sun-016-01+01	20150303	-1	-1	7650	amm
amm-MSTRC-sun-018-01+01	20150305	-2	-1	7535	amm
amm-MSTRC-sun-020-01+01	20150310	-2	-1	2302	amm
amm-MSTRC-sun-020-01+02	20150310	-2	-1	2302	amm
amm-MSTRC-sun-021-01+01	20150310	-2	-1	2302	amm
amm-MSTRC-sun-024-01+01	20150313	0	-2	2744	amm
amm-MSTRC-sun-025-01+01	20150313	0	-2	2770	amm
amm-MSTRC-sun-026-01+01	20150313	0	-2	2985	amm
amm-MSTRC-sun-026-01+02	20150313	0	-2	2985	amm
amm-MSTRC-sun-026-01+03	20150313	0	-2	2985	amm
amm-MSTRC-sun-027-01+01	20150428	-1	-1	2000	amm
amm-MSTRC-sun-028-01+01	20150511	-1	-1	1824	amm
amm-MSTRC-sun-029-01+01	20150513	-1	-1	1750	amm
amm-MSTRC-sun-030-01+01	20150513	-1	-1	2082	amm
amm-MSTRC-sun-030-01+02	20150513	-1	-1	2082	amm
amm-MSTRC-sun-031-01+01	20150515	-1	-0.6	1850	amm
amm-MSTRC-sun-032-01+02	20150519	-1	-1	1422	amm
amm-MSTRC-sun-033-01+02	20150519	-1	-1	1686	amm
amm-MSTRC-sun-034-01+02	20150519	-1	-1	6052	amm
amm-MSTRC-sun-035-01+01	20150520	-1	-1.1	5972	amm
amm-MSTRC-sun-036-01+01	20150520	-1	-1.1	5269	amm
amm-MSTRC-sun-037-01+01	20150521	-1	-1.5	7628	amm
amm-MSTRC-sun-038-01+01	20150521	-1	-1.5	5239	amm
amm-MSTRC-sun-039-01+01	20150522	-1	-1.5	6461	amm
amm-MSTRC-sun-040-01+01	20150522	-1	-1.5	8264	amm
amm-MSTRC-sun-041-01+01	20150522	-1	-1.5	8379	amm
amm-MSTRC-sun-042-01+01	20150529	-1	-2	4056	amm
amm-MSTRC-sun-043-01+01	20150602	-1	-2	6461	amm
amm-MSTRC-sun-044-01+01	20150603	-1	-2	6422	amm
amm-MSTRC-sun-045-01+01	20150604	-1	-2	5972	amm
amm-MSTRC-sun-046-01+01	20150610	-0.8	-2	3318	amm
amm-MSTRC-sun-047-01+01	20150611	-0.8	-2	2985	amm
amm-MSTRC-sun-048-01+01	20150612	-0.8	-2	7158	amm
amm-MSTRC-sun-049-01+01	20150626	-1	-1.5	4072	amm
amm-MSTRC-sun-050-01+01	20150629	-1	-1.5	3700	amm
amm-MSTRC-sun-051-01+01	20150630	-0.5	-2	3719	amm
amm-MSTRC-sun-051-01+02	20150630	-0.5	-2	3719	amm
amm-MSTRC-sun-052-01+01	20150702	-1	-1	4847	amm
amm-MSTRC-sun-053-01+01	20150703	-1.4	-1	5797	amm
amm-MSTRC-sun-054-01+01	20150804	-1.3	0.7	3321	amm
amm-MSTRC-sun-055-01+01	20150805	-1.4	0.7	2700	amm
amm-MSTRC-sun-056-01+01	20150805	-1.4	0.7	2907	amm
amm-MSTRC-sun-059-01+01	20150813	-1.5	1	3910	amm
amm-MSTRC-sun-060-01+01	20150814	-1.5	1	3855	amm
amm-MSTRC-sun-062-01+01	20150818	-1.5	0.8	3195	amm
amm-MSTRC-sun-063-01+01	20150818	-1.5	0.8	8331	amm

File name	Date	X	Y	Z	Experimenter
amm-MSTRC-sun-064-01+01	20150819	-1.25	1	7959	amm
amm-MSTRC-sun-067-01+01	20150821	-1.25	1	3480	amm
amm-MSTRC-sun-068-01+01	20150826	-1.25	0.8	3208	amm
amm-MSTRC-sun-070-01+01	20150903	-1	0.8	8060	amm
amm-MSTRC-sun-071-01+01	20150904	-1	0.8	7686	amm
amm-MSTRC-sun-071-01+02	20150904	-1	0.8	7686	amm
amm-MSTRC-sun-071-01+03	20150904	-1	0.8	7686	amm
amm-MSTRC-sun-072-01+01	20150907	-1	0.8	7656	amm
amm-MSTRC-sun-072-01+02	20150907	-1	0.8	7656	amm
amm-MSTRC-sun-076-01+01	20150910	-1.2	1	4866	amm
amm-MSTRC-sun-076-01+02	20150910	-1.2	1	4866	amm
amm-MSTRC-sun-077-01+01	20150911	-1.2	1	3970	amm
amm-MSTRC-sun-077-01+02	20150911	-1.2	1	3970	amm
amm-MSTRC-sun-078-01+01	20150915	-1	1	7870	amm
amm-MSTRC-sun-078-01+02	20150915	-1	1	7870	amm
amm-MSTRC-sun-079-01+01	20150915	-1	1	7667	amm
amm-MSTRC-sun-079-01+02	20150915	-1	1	7667	amm
amm-MSTRC-sun-081-01+01	20151118	-1.2	1	4208	amm

What follows is an overview of data files and cells recorded for this project. Entries are: **File name**, where abbreviated names for the individual animals used in the experiment are included (*sun* stands for monkey S, *igg* stands for monkey I, and *edg* stands for monkey E). Note that all *igg* cells recorded in 2018 belong to monkey I-right, with all *igg* cells recorded before 2018 belong to I-left. **Date**, date of data recording. **X, Y** refer to the chamber placement coordinates as outlined in the Methods section (units in mm). **Z** indicates the recording depth (mm), where 0 defines the intial resting position of the electrodes prior to entering the dura. **Cell Indeces** refer to the cell ID as used in the analysis, where every cell is assigned a number throughout the analysis. **Experimenter** refers to the person conducting the experiment, with *amm* referring to the author of this work Amr Maamoun, and *bew* referring to Bendict Wild. **Included** determines whether a given cell was included in the general analysis. And **Comments** indicate reasons for not including a cell. The term *incomplete data* designate cells that did not have recorded data in the Reverse Correlation task. *Unsortable* means we were not able to cleanly sort any of the recorded neurons during offline sorting.

File name	Date	X	Y	Z	Cell Indeces	Experimenter	Included	Comments
amm-MSTRC-sun-084-01+01	20151126	-1.6	1	7.698		amm	no	incomplete data
amm-MSTRC-sun-085-01+01	20151126	-1.6	1	7.443	1	amm	yes	
amm-MSTRC-sun-086-01+01	20151202	-1.6	1	8.521		amm	no	incomplete data
amm-MSTRC-sun-087-01+01	20151202	-1.6	1	9489		amm	no	unsortable
amm-MSTRC-sun-089-01+01	20151217	-1.25	1.25	4.593	2	amm	yes	
amm-MSTRC-sun-090-01+01	20160112	-1.6	1	8.954	3	amm	yes	
amm-MSTRC-sun-091-01+01	20160113	-1	1.25	3.660	4	amm	yes	
amm-MSTRC-sun-092-01+01	20160114	-1	1.25	5.004	5	amm	yes	
amm-MSTRC-sun-093-01+01	20160115	-1	1.25	4.256	6, ,7 ,8, 9, 10	amm	yes	
amm-MSTRC-sun-094-01+01	20160119	-1	1.25	8.750	11	amm	yes	
amm-MSTRC-sun-096-01+01	20160122	-1	1.25	8.645	12	amm	yes	
amm-MSTRC-sun-097-01+01	20160122	-0.8	1.25	8.730	13	amm	yes	
amm-MSTRC-sun-098-01+01	20160202	-1.4	1	8.700	14, 15	amm	yes	
amm-MSTRC-sun-099-01+01	20160204	-1.4	0.9	9.831		amm	no	incomplete data
amm-MSTRC-sun-100-01+01	20160204	-1.4	0.9	10.010	16, 17	amm	yes	
amm-MSTRC-sun-101-01+01	20160209	-1.4	0.9	10.131		amm	no	incomplete data
amm-MSTRC-sun-102-01+01	20160209	-1.4	0.9	10.012		amm	no	incomplete data
amm-MSTRC-sun-103-01+01	20160216	-1	0.9	7.559	18	amm	yes	
amm-MSTRC-sun-105-01+01	20160218	0	1	6.319	19	amm	yes	
amm-MSTRC-sun-106-01+01	20160219	0	1	8.551	20	amm	yes	
amm-MSTRC-sun-108-01+01	20160309	0	1.25	9.049	21, 22, 23	amm	yes	
amm-MSTRC-sun-111-01+01	20160330	0	1.25	4.607	24	amm	yes	
amm-MSTRC-sun-112-01+01	20160331	0	1.25	4.500	25	amm	yes	
amm-MSTRC-sun-113-01+01	20160413	0	1.25	4.350		amm	no	incomplete data
amm-MSTRC-sun-114-01+01	20160420	-1	2	6.109	26	amm	yes	
amm-MSTRC-sun-115-01+01	20160421	-1	2	6.050	27	amm	yes	
amm-MSTRC-sun-116-01+01	20160422	-1	2	5.559	28, 29	amm	yes	
amm-MSTRC-sun-117-01+01	20160426	-1	2	3.801	30	amm	yes	
amm-MSTRC-sun-118-01+01	20160428	-1	2	3.580	31, 32	amm	yes	
amm-MSTRC-sun-119-01+01	20160429	-1	2.15	7.100	33	amm	yes	
amm-MSTRC-sun-120-01+01	20160503	-1	2.15	6.500	34	amm	yes	
amm-MSTRC-sun-123-01+01	20160511	-1	2.15	5.044	35, 36	amm	yes	
amm-MSTRC-sun-124-01+01	20160526	-1	2	3634		amm	no	unsortable
amm-MSTRC-sun-125-01+01	20160601	-1.3	2	3.634	37	amm	yes	
amm-MSTRC-sun-126-01+01	20160602	-1.3	2	5.818		amm	no	incomplete data

File name	date	x	y	z	Cell Indeces	Experimenter	Included	Comments
amm-MSTRC-sun-127-01+01	20160602	-1.3	2	6.048	38, 39	amm	yes	
amm-MSTRC-sun-128-01+01	20160603	-1.3	2	5.818		amm	no	incomplete data
amm-MSTRC-sun-130-01+01	20160615	-1.3	2	6.294	40	amm	yes	
amm-MSTRC-sun-131-01+01	20160623	-1.3	2	7.100		amm	no	poor isolation
amm-MSTRC-sun-132-01+01	20160624	-2	2	4.835	41	amm	yes	
amm-MSTRC-sun-133-01+01	20160628	-2	2	5.027	42	amm	yes	
amm-MSTRC-sun-134-01+01	20160629	-2	2	3.788	43, 44	amm	yes	
amm-MSTRC-sun-135-01+01	20160630	-2	2	3.700	45	amm	yes	
amm-MSTRC-sun-136-01+01	20160701	-2	2	5.364	46, 47	amm	yes	
amm-MSTRC-sun-137-01+01	20160705	-2	2	6.431	48	amm	yes	
amm-MSTRC-sun-138-01+01	20160706	-2.3	2	5.364	49	amm	yes	
amm-MSTRC-igg-001-01+01	20160706	-2	-1	5.252		amm	no	incomplete data
amm-MSTRC-sun-139-01+01	20160707	-1.8	2.4	7.219	50, 51	amm	yes	
amm-MSTRC-sun-140-01+01	20160708	-1.8	2	5.423	52	amm	yes	
amm-MSTRC-igg-002-01+01	20160708	-3	-1	5.100		amm	no	incomplete data
amm-MSTRC-sun-141-01+01	20160712	-1.8	2	5.637	53	amm	yes	
amm-MSTRC-sun-142-01+01	20160713	-2	2.5	5.315	54, 55	amm	yes	
amm-MSTRC-sun-143-01+01	20160714	-2	2.5	6.136	56, 57	amm	yes	
amm-MSTRC-sun-144-01+01	20160715	-2	2.5	4.771	58	amm	yes	
amm-MSTRC-sun-145-01+01	20160719	-2	2.5	5.281		amm	no	incomplete data
amm-MSTRC-sun-146-01+01	20160720	-2	2.25	4.253	59	amm	yes	
amm-MSTRC-igg-003-01+01	20160726	-3	-1	5.252		amm	no	incomplete data
amm-MSTRC-igg-004-01+01	20160727	-3	-1	5.084	60	amm	yes	
amm-MSTRC-sun-147-01+01	20160727	-1.5	2.5	5.400	61	amm	yes	
amm-MSTRC-sun-148-01+01	20160728	-1	2.5	5.685	62	amm	yes	
amm-MSTRC-igg-005-01+01	20160729	-3	-1	11.323		amm	no	incomplete data
amm-MSTRC-sun-149-01+01	20160729	-2	3	5.179	63, 64	amm	yes	
amm-MSTRC-sun-150-01+01	20160802	-2	3	7.693	65	amm	yes	
amm-MSTRC-sun-151-01+01	20160803	-2	3	6.034	66, 67	amm	yes	
amm-MSTRC-igg-008-01+01	20160804	-3	0	10.396		amm	no	poor isolation
amm-MSTRC-sun-152-01+01	20160804	-2	3	5.503	68, 69	amm	yes	
amm-MSTRC-sun-153-01+01	20160805	-2	3	6.450	70	amm	yes	
amm-MSTRC-sun-154-01+01	20160809	-2	3	6.092	71	amm	yes	
amm-MSTRC-sun-155-01+01	20160811	-2	3	6.700	72	amm	yes	
amm-MSTRC-sun-156-01+01	20160812	-2.5	3	7.333	73	amm	yes	
amm-MSTRC-igg-010-01+01	20161020	-3	-1	3.478	74	amm	yes	
amm-MSTRC-igg-011-01+01	20161026	-3	-1	3.545	75	amm	yes	
amm-MSTRC-sun-157-01+01	20161026	-2	3	5.800		amm	no	incomplete data
amm-MSTRC-sun-158-01+01	20161026	-2	3	6.000		amm	no	incomplete data
amm-MSTRC-igg-012-01+01	20161027	-4	-1	5.479	76	amm	yes	
amm-MSTRC-sun-159-01+01	20161027	-2	3	8.130	77	amm	yes	
amm-MSTRC-igg-014-01+01	20161104	-3	+1	6.839	78	amm	yes	
amm-MSTRC-igg-015-01+01	20161108	-4	+1	10.796	79	amm	yes	
amm-MSTRC-sun-160-01+01	20161108	-2	3	6.170	80	bew	yes	
amm-MSTRC-sun-161-01+01	20161109	-2	3	6.830	81, 82	bew	yes	
amm-MSTRC-igg-016-01+01	20161110	-4	+1	8.716	83	amm	yes	
amm-MSTRC-sun-162-01+01	20161111	-2	3	6.614	84	bew	yes	
amm-MSTRC-sun-163-01+01	20161115	-3	3	8.050	85	bew	yes	
amm-MSTRC-sun-164-01+01	20161117	-2.5	3	8.350	86	bew	yes	
amm-MSTRC-igg-017-01+01	20161122	-2	1	8.100		amm	no	incomplete data
amm-MSTRC-igg-018-01+01	20161122	-2	1	9.563	87	amm	yes	
amm-MSTRC-sun-165-01+01	20161123	-2	2.5	7.200	88, 89	bew	yes	

File name	date	x	y	z	Cell Indeces	Experimenter	Included	Comments
amm-MSTRC-igg-019-01+01	20161124	-2	1	1.800	90	amm	yes	
amm-MSTRC-sun-167-01+01	20161129	-3	2	5.551	91, 92	bew	yes	
amm-MSTRC-sun-168-01+01	20161130	-3	2	5.600	93	bew	yes	
amm-MSTRC-igg-023-01+01	20161201	-3	1	7.008	94	amm	yes	
amm-MSTRC-sun-169-01+01	20161201	-3	2	6.100		bew	no	incomplete data
amm-MSTRC-sun-170-01+01	20161202	-3	2	5.700		bew	no	incomplete data
amm-MSTRC-sun-171-01+01	20161202	-3	2	5.400	95	bew	yes	
amm-MSTRC-sun-172-01+01	20161206	-3	2	5.900	96	bew	yes	
amm-MSTRC-sun-174-01+01	20161206	-3	2	6.280	97, 98	bew	yes	
amm-MSTRC-sun-175-01+02	20161209	-3	2	6.080	99, 100	bew	yes	
amm-MSTRC-sun-177-01+01	20161213	-3	2	7.800	101, 102	bew	yes	
amm-MSTRC-sun-178-01+01	20161214	-3	2	5.926	103	bew	yes	
amm-MSTRC-sun-179-01+01	20161215	-3	2	5.642	104	bew	yes	
amm-MSTRC-sun-180-01+01	20161216	-3	2	6.900	105	bew	yes	
amm-MSTRC-sun-181-01+01	20161221	-3	2	4.200	106	bew	yes	
amm-MSTRC-sun-182-01+01	20161222	-3	2	6.217	107	bew	yes	
amm-MSTRC-igg-025-01+01	20161222	-2	1	8.735	108	amm	yes	
amm-MSTRC-sun-183-01+01	20170112	-1.5	3	7.874		bew	no	incomplete data
amm-MSTRC-sun-184-01+01	20170113	-1.5	3	7.206	109	bew	yes	
amm-MSTRC-sun-185-01+01	20170117	-1.5	3	7.330	110	bew	yes	
amm-MSTRC-igg-026-01+01	20170119	-1	1	6.364	111	amm	yes	
amm-MSTRC-sun-186-01+01	20170120	-2	2	6.800	112	bew	yes	
amm-MSTRC-sun-187-01+01	20170124	-2	2	7.115		bew	no	incomplete data
amm-MSTRC-sun-188-01+01	20170124	-2	2	7.060	113, 114	bew	yes	
amm-MSTRC-sun-189-01+01	20170125	-2	2	6.908	115	bew	yes	
amm-MSTRC-igg-027-01+01	20170125	0	1	4.341	116	amm	yes	
amm-MSTRC-sun-190-01+01	20170126	-2	2	8.025		bew	no	incomplete data
amm-MSTRC-sun-191-01+01	20170126	-2	2	6.793	117	bew	yes	
amm-MSTRC-sun-192-01+01	20170127	-2	2	7.931	118, 119	bew	yes	
amm-MSTRC-sun-193-01+01	20170131	-2	2	7.000	120	bew	yes	
amm-MSTRC-igg-028-01+01	20170131	-1	1	8.148	121	amm	yes	
amm-MSTRC-sun-194-01+01	20170201	-2	2	8.250		bew	no	incomplete data
amm-MSTRC-sun-195-01+01	20170201	-2	2	7.432	122	bew	yes	
amm-MSTRC-sun-196-01+01	20170203	-2	2	7.666	123	bew	yes	
amm-MSTRC-sun-197-01+01	20170209	-2.5	2	8.130	124, 125	bew	yes	
amm-MSTRC-sun-199-01+01	20170210	-3	2	8.150	126	bew	yes	
amm-MSTRC-igg-030-01+01	20170214	0	1	5.999	127	amm	yes	
amm-MSTRC-igg-031-01+01	20170221	0	1	6.938	128	amm	yes	
amm-MSTRC-sun-201-01+01	20170221	-1.5	1	3.100	129, 130, 131	bew	yes	
amm-MSTRC-sun-202-01+01	20170222	-2	1	5.922	132	bew	yes	
amm-MSTRC-igg-032-01+01	20170302	0	1	6.269	133	amm	yes	
amm-MSTRC-igg-033-01+01	20170303	-1	1	4.555	134	amm	yes	
amm-MSTRC-igg-034-01+01	20170315	0	1	5.858	135	amm	yes	
amm-MSTRC-igg-035-01+01	20170316	0	1	5.108	136	amm	yes	
amm-MSTRC-igg-036-01+01	20170331	0	1	3.771	137	amm	yes	
amm-MSTRC-igg-038-01+01	20170406	0	1	3.284	138	amm	yes	
bew-MSTRC-edg-004-01+01	20170504	0	-3	6.527	139	bew	yes	
bew-MSTRC-edg-005-01+01	20170505	-1	-3	7.856	140	bew	yes	
bew-MSTRC-edg-009-01+01	20170512	-1	-4	5.381		bew	no	incomplete data
bew-MSTRC-edg-010-01+01	20170517	-1	-4	5.110		bew	no	incomplete data
bew-MSTRC-edg-011-01+01	20170519	-0.5	-4	5.300		bew	no	incomplete data

File name	date	x	y	z	Cell Indeces	Experimenter	Included	Comments
bew-MSTRC-igg-039-01+01	20170719	-3	2	3.916		bew	no	incomplete data
bew-MSTRC-igg-040-01+01	20170726	-3	1	10.300		bew	no	incomplete data
bew-MSTRC-igg-041-01+01	20170726	-3	1	9.238	141	bew	yes	
bew-MSTRC-igg-042-01+01	20170802	-1	0	2.571	142	bew	yes	
bew-MSTRC-igg-043-01+01	20170803	-1	0	4.200		bew	no	incomplete data
bew-MSTRC-igg-044-01+01	20170803	-1	0	3.510	143	bew	yes	
bew-MSTRC-igg-045-01+01	20170804	-1	1	3.921		bew	no	incomplete data
bew-MSTRC-igg-046-01+01	20170810	-1	0	7389	144	bew	yes	
bew-MSTRC-igg-075-01+02	20180621	1	1	9670	145	bew	yes	
bew-MSTRC-igg-076-01+02	20180622	1	1	9021	146, 147	bew	yes	
bew-MSTRC-igg-077-01+02	20180712	1	1	10206	148	bew	yes	
bew-MSTRC-igg-078-01+02	20180717	1.5	1	10001	149	bew	yes	
bew-MSTRC-igg-081-01+01	20180720	1	1	9571	150	bew	yes	
bew-MSTRC-igg-082-01+01	20180724	1	1	10050	151	bew	yes	
bew-MSTRC-igg-083-01+01	20180725	1	1	10019	152	bew	yes	
bew-MSTRC-igg-085-01+01	20180727	1	1	9600	153	bew	yes	
bew-MSTRC-igg-086-01+01	20180730	1	1	9746	154	bew	yes	
amm-MSTRC-igg-091-01+02	20180829	1	0.5	9207	155, 156	amm	yes	
bew-MSTRC-igg-092-01+03	20180830	1	0.5	9850	157	bew	yes	
amm-MSTRC-igg-093-01+01	20180831	1	0.5	10538	158, 159	amm	yes	
amm-MSTRC-igg-098-01+01	20180911	0.5	0	9899	160	amm	yes	
amm-MSTRC-igg-099-01+01	20180912	0.5	0	10476	161	amm	yes	
amm-MSTRC-igg-100-01+01	20180913	0.5	0	10670	162, 163	amm	yes	
bew-MSTRC-igg-101-01+02	20180914	0.5	0	11620	164	bew	yes	
amm-MSTRC-igg-102-01+01	20180918	0.5	0	10238	165	amm	yes	
amm-MSTRC-igg-104-01+01	20180920	0.5	0.5	10400	166	amm	yes	
amm-MSTRC-igg-106-01+01	20180924	0.5	0.5	11117	167, 168	amm	yes	
amm-MSTRC-igg-108-01+01	20180926	1	0.5	9949	169	amm	yes	
amm-MSTRC-igg-109-01+01	20180927	1	0.5	11346	170	amm	yes	
amm-MSTRC-igg-112-01+01	20181002	1	1	10721	171	amm	yes	
bew-MSTRC-igg-113-01+01	20181003	1	1	10118	172, 173, 174	bew	yes	
amm-MSTRC-igg-114-01+01	20181004	1	1	10540	175	amm	yes	
bew-MSTRC-igg-118-01+01	20181010	0.5	0.5	9797	176	bew	yes	
bew-MSTRC-igg-122-01+01	20181017	1.5	0.5	10321	177	bew	yes	
amm-MSTRC-igg-123-01+01	20181018	1.5	0.5	10941	178, 179	amm	yes	
amm-MSTRC-igg-124-01+01	20181019	1.5	0.5	11181	180	amm	yes	
amm-MSTRC-igg-125-01+01	20181022	1.5	0.5	8920	181	amm	yes	

What follows is an overview of included cells and which experimental task they underwent. Entries are: **A - Cell Indeces** refers to the cell ID as used in the analysis, where every cell is assigned a number throughout the analysis. **B - Automatic Mapping** refers to the task of Automatic Mapping, where **data** indicates whether any data were recorded in this task (+ data present, - not present), where **included** indicates whether the data were included in further analysis involving Automatic Mapping task (+ included, - not included), and where **comments** lists any other reason for exclusion [*Low spk nr.*: spike number in this task < 100 spikes in total; $r^2 < 0.2$: receptive field fit of R squared < 0.2; *excluded fit*: excluded data, as the fitted center of the receptive field lies 10 degrees outside of the stimulated visual field; *hand excluded*: cells that were hand excluded (see method section)]. **C - Tuning** refers to the task of Tuning, where **data** indicates whether any data were recorded in this task (+ data present, - not present), where **included** indicate whether the data were included in further analysis involving Tuning task (+ included, - not included), and where **comments** lists any other reason for exclusion [*Low spk nr.*: spike number in this task < 800 spikes in total]. **D- Reverse Correlation** refers to the task of Reverse Correlation, where **data** indicates whether any data were recorded in this task (+ data present, - not present), where **included** indicates whether the data were included in further analysis involving Tuning task (+ included, - not included), where **recovered** indicate whether a reverse correlation map was recovered for this cell (+ map recovered, - not recovered), and where **comments** lists any other reason for exclusion [*Low spk nr.*: spike number in this task < 658 spikes in total; *Low sample nr.*: sample number in this task < 2430 samples in total (see Materials and Methods)].

Cell Indeces	Automatic Mapping			Tuning			Reverse Correlation			
	data	included	comments	data	included	comments	data	included	recovered	comments
1	+	+		+	+		+	+	+	
2	+	-	excluded fit	+	+		+	+	-	
3	+	+		+	+		+	+	+	
4	+	-	$r^2 < 0.2$	+	+		+	+	-	
5	+	-	excluded fit	+	+		+	+	-	
6	+	-	excluded fit	+	+		+	-	-	Low spk nr.
7	+	+		+	+		+	-	-	Low spk nr.
8	+	-	$r^2 < 0.2$	+	+		+	-	-	Low spk nr.
9	+	-	hand excluded	+	+		+	+	-	
10	-	-		+	-	Low spk nr.	+	+	+	
11	+	+		+	+		+	+	+	
12	+	+		+	+		+	+	-	
13	+	-	$r^2 < 0.2$	+	+		+	+	-	
14	+	+		+	+		+	+	+	
15	+	-	hand excluded	+	+		+	+	-	
16	+	+		+	+		+	+	+	
17	+	+		+	+		+	+	+	
18	+	+		+	+		+	+	-	
19	+	+		+	+		+	+	+	
20	+	+		+	+		+	+	+	
21	+	+		+	+		+	+	-	
22	+	+		+	+		+	+	+	
23	-	-		+	-	Low spk nr.	+	+	+	

Cell Indeces	Automatic Mapping			Tuning			Reverse Correlation			
	data	included	comments	data	included	comments	data	included	recovered	comments
24	+	-	excluded fit	+	+		+	+	-	
25	+	-	$r^2 < 0.2$	+	+		+	+	-	
26	+	-	excluded fit	+	+		+	+	-	
27	+	-	$r^2 < 0.2$	+	+		+	+	+	
28	+	+		+	+		+	+	-	
29	+	-	$r^2 < 0.2$	+	+		+	+	-	
30	+	-	$r^2 < 0.2$	+	+		+	+	+	
31	+	-	$r^2 < 0.2$	+	+		+	+	-	
32	+	-	$r^2 < 0.2$	+	+		+	+	+	
33	+	+		+	+		+	+	-	
34	+	+		+	+		+	+	+	
35	+	+		+	+		+	+	-	
36	+	+		+	+		+	+	-	
37	+	-	$r^2 < 0.2$	+	+		-	-	-	Low spk nr.
38	+	+		+	+		+	+	+	
39	+	-	excluded fit	+	+		+	-	-	Low spk nr.
40	+	-	excluded fit	+	+		+	+	-	
41	+	-	excluded fit	+	+		+	+	-	
42	+	+		+	+		+	+	-	
43	+	-	excluded fit	+	+		+	+	-	
44	+	-	excluded fit	+	+		+	+	-	
45	+	-	excluded fit	+	+		+	+	+	
46	+	-	excluded fit	+	+		+	+	-	
47	+	+		+	+		+	+	-	
48	+	-	excluded fit	+	+		+	-	-	Low spk nr.
49	+	-	$r^2 < 0.2$	+	+		+	+	-	
50	+	+		+	+		+	+	-	
51	+	+		+	+		+	+	+	
52	+	-	$r^2 < 0.2$	+	+		+	+	-	
53	+	-	$r^2 < 0.2$	+	-	Low spk nr.	+	+	+	
54	+	-	$r^2 < 0.2$	+	+		+	-	-	Low sample nr.
55	+	-	$r^2 < 0.2$	+	+		-	-	-	Low spk nr.
56	+	+		+	+		+	+	+	
57	-	-		+	-	Low spk nr.	+	+	+	
58	+	+		+	+		+	+	+	
59	+	-	excluded fit	+	+		+	+	+	
60	+	+		+	+		-	-	-	Low spk nr.
61	+	-	$r^2 < 0.2$	+	-	Low spk nr.	+	-	-	Low spk nr.
62	+	-	$r^2 < 0.2$	+	+		+	+	-	
63	+	+		+	+		+	+	-	
64	+	-	hand excluded	+	+		+	+	-	
65	+	+		+	+		+	+	-	
66	+	+		+	+		+	+	-	
67	+	+		+	+		+	+	-	
68	+	+		+	+		+	+	-	
69	+	-	$r^2 < 0.2$	+	+		+	+	-	
70	+	-	excluded fit	+	+		-	-	-	Low spk nr.
71	+	+		+	+		+	+	-	
72	+	-	excluded fit	+	+		+	+	+	
73	+	-	$r^2 < 0.2$	+	+		+	+	-	
74	+	+		+	+		-	-	-	Low spk nr.

Cell Indeces	Automatic Mapping			Tuning			Reverse Correlation			
	data	included	comments	data	included	comments	data	included	recovered	comments
75	+	+		+	+		-	-	-	Low spk nr.
76	+	+		+	+		-	-	-	Low spk nr.
77	+	-	excluded fit	+	+		+	-	-	Low spk nr.
78	+	+		+	+		-	-	-	Low spk nr.
79	+	+		+	+		-	-	-	Low spk nr.
80	+	-	excluded fit	+	+		-	-	-	Low spk nr.
81	+	+		+	+		-	-	-	Low spk nr.
82	+	+		+	+		-	-	-	Low spk nr.
83	+	+		+	-	Low spk nr.	-	-	-	Low spk nr.
84	+	-	hand excluded	+	+		-	-	-	Low spk nr.
85	+	+		+	+		+	+	+	
86	+	-	$r^2 < 0.2$	+	+		+	+	-	
87	+	+		+	+		-	-	-	Low spk nr.
88	+	+		+	+		+	+	-	
89	+	+		+	+		+	+	-	
90	+	+		+	+		-	-	-	Low spk nr.
91	+	-	excluded fit	+	+		+	+	-	
92	+	-	Low spk nr.	+	+		+	+	-	
93	+	-	excluded fit	+	+		+	+	-	
94	+	-	$r^2 < 0.2$	+	+		-	-	-	Low spk nr.
95	+	-	$r^2 < 0.2$	+	+		+	+	-	
96	+	-	$r^2 < 0.2$	+	+		+	+	-	
97	+	+		+	+		+	+	-	
98	+	+		+	+		+	+	-	
99	+	+		+	+		+	+	-	
100	+	+		+	+		+	+	-	
101	+	-	excluded fit	+	+		+	+	-	
102	+	-	$r^2 < 0.2$	+	+		+	+	-	
103	+	+		+	+		+	+	-	
104	+	+		+	+		+	+	-	
105	+	+		+	+		+	+	-	
106	+	+		+	+		+	-	-	Low sample nr.
107	+	+		+	+		+	+	-	
108	+	+		+	+		-	-	-	Low spk nr.
109	+	-	excluded fit	+	+		+	+	-	
110	+	+		+	+		+	+	-	
111	+	+		+	+		-	-	-	Low spk nr.
112	+	+		+	+		+	+	-	
113	+	+		+	+		+	+	-	
114	+	+		+	+		+	+	-	
115	+	+		+	+		+	+	-	
116	+	+		+	+		-	-	-	Low spk nr.
117	+	+		+	+		+	+	-	
118	+	+		+	+		+	+	-	
119	+	+		+	+		+	+	-	
120	+	-	excluded fit	+	+		+	+	-	
121	+	+		+	-	Low spk nr.	-	-	-	Low spk nr.
122	+	+		+	+		+	+	-	
123	+	+		+	+		+	+	-	
124	+	+		+	+		+	+	-	

Cell Indeces	Automatic Mapping			Tuning			Reverse Correlation			
	data	included	comments	data	included	comments	data	included	recovered	comments
125	+	+		+	+		+	+	-	
126	+	+		+	+		+	+	-	
127	+	+		+	+		+	+	-	Low sample nr.
128	+	+		+	+		+	+	-	Low spk nr.
129	+	-	$r^2 < 0.2$	+	+		+	+	-	
130	+	-	$r^2 < 0.2$	+	+		+	+	-	Low spk nr.
131	+	-	$r^2 < 0.2$	+	+		+	+	-	Low sample nr.
132	+	-	excluded fit	+	+		+	+	-	
133	+	+		+	+		+	+	+	
134	+	+		+	+		+	+	-	
135	+	+		+	+		+	+	+	
136	+	+		+	+		+	+	+	
137	+	+		+	+		+	+	-	
138	+	+		+	+		+	+	-	
139	+	-	excluded fit	+	+		+	+	-	
140	+	+		+	+		+	-	-	Low spk nr.
141	+	+		+	+		+	+	+	
142	+	+		+	+		+	+	-	
143	+	-	hand excluded	+	+		+	-	-	Low spk nr.
144	+	+		+	+		+	+	-	
145	+	+		+	+		+	+	+	
146	+	+		+	+		+	+	-	
147	+	-	$r^2 < 0.2$	+	+		+	-	-	Low spk nr.
148	+	+		+	+		+	+	-	
149	+	+		+	+		+	+	-	
150	+	+		+	+		+	+	-	
151	+	+		+	+		+	+	-	
152	+	+		+	+		+	+	+	
153	+	+		+	+		+	+	-	
154	+	+		+	+		+	+	+	
155	+	-	excluded fit	+	+		+	+	+	
156	+	+		+	+		+	+	-	
157	+	-	excluded fit	+	+		+	+	-	
158	+	-	excluded fit	+	-	Low spk nr.	+	+	-	
159	+	-	Low spk nr.	+	-	Low spk nr.	+	+	-	
160	+	-	excluded fit	+	+		+	+	-	
161	+	+		+	+		+	+	-	
162	+	+		+	+		+	+	-	
163	+	-	$r^2 < 0.2$	+	+		+	+	-	
164	+	-	excluded fit	+	+		+	+	-	
165	+	-	$r^2 < 0.2$	+	+		+	+	-	
166	+	-	Low spk nr.	+	+		+	+	-	
167	+	+		+	+		+	+	-	
168	+	+		+	+		+	+	-	
169	+	+		+	+		+	+	-	
170	+	+		+	+		+	+	-	
171	+	+		+	+		+	+	-	
172	+	+		+	+		+	+	+	
173	+	-	$r^2 < 0.2$	+	+		+	+	+	
174	+	-	$r^2 < 0.2$	+	+		+	+	-	

Cell Indeces	Automatic Mapping			Tuning			Reverse Correlation			
	data	included	comments	data	included	comments	data	included	recovered	comments
175	+	-	excluded fit	+	+		+	+	+	
176	+	+		+	+		+	+	-	
177	+	+		+	+		+	+	+	
178	+	-	excluded fit	+	+		+	+	-	
179	+	-	excluded fit	+	+		+	+	-	
180	+	-	excluded fit	+	+		+	+	-	
181	+	+		+	+		+	+	+	

What follows is an overview of included cells and specific experimental settings. experimental task they underwent. Entries are: **Cell Indeces** refers to the cell ID as used in the analysis, where every cell is assigned a number throughout the analysis. **Pos. Inv. Arrang.** refers to the arrangment of stimuli in the Tuning task, where a *minus sign* - under the heading *Concentric* indicates that stimuli were positioned in a 5 concentric circles scheme (cloverleaf arrangment) within the receptive field, whereas a *plus sign* + indicates that they were positioned without specific arrangment to cover as much as possible of the receptive field, or were not even placed inside the offline-uncovered receptive fields (*Spread*). **RC. Stim. Arrang.** refers to the arrangment of the Reverse Correlation stimulus, where *15 X 10* indicates that the stimulus contained 15 X 10 segments, whereas *9 X 6* indicates that the stimulus contained 9 X 6 segments. **Blanks** refers to the existence of blanks in the Automatic Mapping and Tuning tasks (see method section) (+ present, - not present).

Cell Indeces	Pos. Inv. Arrang.		RC. Stim. Arrang.		Blanks	Setup
	Concentric 5	Spread	15 X 10	9 X 6		
1	+		+		-	A
2		+	+		-	A
3		+	+		-	A
4		+	+		-	A
5		+	+		-	A
6		+	+		-	A
7		+	+		-	A
8		+	+		-	A
9		+	+		-	A
10		+	+		-	A
11		+	+		-	A
12		+	+		-	A
13		+	+		-	A
14	+		+		-	A
15		+	+		-	A
16	+		+		-	A
17	+		+		-	A
18		+	+		-	A
19	+		+		-	A
20	+		+		-	A
21		+	+		-	A
22		+	+		-	A
23		+	+		-	A
24		+	+		-	A
25		+	+		-	A
26		+	+		-	A
27	+		+		-	A
28	+		+		-	A
29	+		+		-	A
30	+		+		-	A

Cell Indeces	Pos. Inv. Arrang.		RC. Stim. Arrang.		Blanks	Setup
	Concentric 5	Spread	15 X 10	9 X 6		
31	+		+		-	A
32	+		+		-	A
33	+		+		-	A
34	+		+		-	A
35	+		+		-	A
36	+		+		-	A
37	+		+		-	A
38	+		+		-	A
39	+		+		-	A
40	+		+		-	A
41	+		+		-	A
42	+		+		-	A
43	+		+		-	A
44	+		+		-	A
45	+		+		-	A
46		+	+		-	A
47		+	+		-	A
48	+		+		-	A
49		+	+		-	A
50	+		+		-	A
51	+		+		-	A
52		+	+		-	A
53	+		+		-	A
54	+		+		-	A
55	+		+		-	A
56	+		+		-	A
57	+		+		-	A
58	+		+		-	A
59	+		+		-	A
60	+		+		-	B
61	+		+		-	A
62	+		+		-	A
63	+		+		-	A
64	+		+		-	A
65	+		+		-	A
66	+		+		-	A
67	+		+		-	A
68		+	+		-	A
69		+	+		-	A
70	+		+		-	A
71	+		+		-	A

Cell Indeces	Pos. Inv. Arrang.		RC. Stim. Arrang.		Blanks	Setup
	Concentric 5	Spread	15 X 10	9 X 6		
72	+		+		-	A
73	+		+		-	A
74	+		+		-	B
75	+		+		-	B
76	+		+		-	B
77	+		+		-	A
78	+		+		-	B
79	+		+		-	B
80		+	+		-	A
81	+		+		-	A
82	+		+		-	A
83	+		+		-	B
84	+		+		-	A
85	+		+		-	A
86	+		+		-	A
87	+		+		-	B
88	+		+		-	A
89	+		+		-	A
90	+		+		-	B
91	+		+		-	A
92	+		+		-	A
93	+		+		-	A
94	+		+		-	B
95	+		+		-	A
96	+		+		-	A
97	+		+		-	A
98	+		+		-	A
99	+		+		-	A
100	+		+		-	A
101	+		+		-	A
102	+		+		-	A
103	+		+		-	A
104	+		+		-	A
105	+		+		-	A
106		+	+		+	A
107	+		+		+	A
108	+		+		+	B
109	+		+		+	A
110	+		+		+	A
111	+		+		+	B
112	+		+		+	A

Cell Indeces	Pos. Inv. Arrang.		RC. Stim. Arrang.		Blanks	Setup
	Concentric 5	Spread	15 X 10	9 X 6		
113	+		+		+	A
114	+		+		+	A
115	+		+		+	A
116	+		+		+	B
117	+		+		+	A
118	+		+		+	A
119	+		+		+	A
120	+		+		+	A
121	+		+		+	B
122	+		+		+	A
123	+		+		+	A
124	+		+		+	A
125	+		+		+	A
126	+		+		+	A
127	+		+		+	B
128	+		+		+	B
129	+		+		+	A
130	+		+		+	A
131	+		+		+	A
132	+		+		+	A
133	+		+		+	B
134	+		+		+	B
135	+			+	+	B
136	+			+	+	B
137	+			+	+	B
138	+			+	+	B
139	+			+	+	A
140	+			+	+	A
141	+			+	+	B
142	+			+	+	B
143	+			+	+	B
144	+			+	+	B
145	+			+	+	B
146	+			+	+	B
147	+			+	+	B
148	+			+	+	B
149	+			+	+	B
150	+			+	+	B
151	+			+	+	B
152	+			+	+	B

Cell Indeces	Pos. Inv. Arrang.		RC. Stim. Arrang.		Blanks	Setup
	Concentric 5	Spread	15 X 10	9 X 6		
153	+			+	+	B
154	+			+	+	B
155	+			+	+	C
156	+			+	+	C
157	+			+	+	C
158	+			+	+	C
159	+			+	+	C
160	+			+	+	C
161		+		+	+	C
162	+			+	+	C
163		+		+	+	C
164	+			+	+	C
165	+			+	+	C
166	+			+	+	C
167	+			+	+	C
168	+			+	+	C
169	+			+	+	C
170	+			+	+	C
171	+			+	+	C
172	+			+	+	C
173	+			+	+	C
174		+		+	+	C
175	+			+	+	C
176	+			+	+	C
177	+			+	+	B
178	+			+	+	B
179	+			+	+	B
180	+			+	+	B
181	+			+	+	B

Amr Maamoun - MD

Address: Zimmermannstr.11 app.393 , 37075 Göttingen

E-Mail: amaamoun@protonmail.com

Mobile: +49 162 4971743

Born on the 17.06.1987 in Damascus

Education

01/2018 – Today

Postgraduate Scientist/Data Analyst

Department of Cognitive Neurosciences, German Primate Center (DPZ), Göttingen, Germany

10/2013 – 01/2018

PhD Study: Göttingen Graduate School for Neurosciences, Biophysics, and Molecular Biosciences (GGNB)

Georg-August Universität, Göttingen, Germany

Department of Cognitive Neurosciences, German Primate Center (DPZ), Göttingen, Germany

Project's title: Receptive Field Characterization in MSTd Neurons

Supervisor: Prof. Dr. Stefan Treue

Focus & Responsibilities:

- **Software development** of a multi-dimensional visual stimulus plugin with a realtime feedback loop in C++ (relying on o**ptimization methods**, including genetic algorithm and gradient descent algorithm)
- **Electrophysiological data acquisition** in the visual area MSTd of the Macaque monkey brain
- Writing and implementing **mathematical and statistical analyses** (eg. reverse correlation) on the collected data using MATLAB
- Uncovering and **visualizing** significant **trends** in data

- **Developing and managing database** containing project relevant neural data
- Internal **project presentation**, and poster presentation at international scientific conferences
- Extensive **Teamwork** to guarantee sufficient data acquisition
- **Collaboration** with fellow lab scientists in creating standardized programming functions in MATLAB to evaluate psychophysical data
- **Teaching** and **supervising** graduate students during lab rotation, with emphasis on **meeting deadlines**
- **Time** and **project management**

Graduation January 2018 **– Title: Doctor Rerum Naturalium - Dr. rer. nat.** (to be awarded early 2019)

10/2012 – 10/2013

Neuroscience Masters/PhD Programm

International Max Planck Research School (IMPRS)

Georg-August Universität, Göttingen, Germany

Award **Stipend:** „The Excellence Foundation for the Promotion of the Max Planck Society“

01/2012 – 06/2012

Assistant Doctor - Pathology department, Mouassat hospital

Damascus University, Medical Faculty

08/2010 – 05/2011

Practical medical internship year – in the frame of medical studies

Damascus University Hospital, Medical Faculty

09/2005 – 09/2011

Medical School

Damascus University, Medical Faculty

Graduation December 2011 **– Title: Medical Doctor M.D.**

09/1992 – 7/2005

Primary, Secondary, and High School

Lycée Laïque De Damas, Damascus

Graduation note: 236/240

Skills

Languages:

- English – Fluent in speech and writing
- German – Fluent in speech and writing
  Goethe-Zertifikat C1 (Note: 88/100)
- Arabic – Native language
- French – Beginner/Intermediate level

Programming Languages:

- Matlab & C++: Advanced level
- Python: Intermediate level
- LaTeX: Intermediate level

Softwares:

- Xcode, Pages, Keynote
- Microsoft Office Programs (PowerPoint, Word)

Communication:

- Project and poster presentation skills
- Long-term teamwork
- Intercultural communication
- Teaching and supervision of undergraduate students

Tests

Goethe-Zertifikat C1 - 03.05.2018 - Note: 88%

TOEFL Paper-based - 10.08.2010 - Note: 657/677

GRE General - 20.10.2010 - Note:

Verbal 630 /91%, Quantitative 750/82%

GRE Subject - Biology - 11.12.2010 - Note: 880/97%

Göttingen, the 24.09.2018 Amr Maamoun